

**NUMERICAL ANALYSIS OF CONJUGATE HEAT
TRANSFER IN THE PRESENCE OF POROUS
MEDIUM**

Thesis

Submitted in partial fulfillment of the requirements for the degree of

DOCTOR OF PHILOSOPHY

by

PRAKASH HEERASING JADHAV



DEPARTMENT OF MECHANICAL ENGINEERING
NATIONAL INSTITUTE OF TECHNOLOGY KARNATAKA,
SURATHKAL, MANGALORE - 575025

DECEMBER, 2022

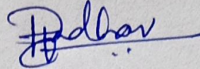
DECLARATION

I hereby declare that the Research Thesis entitled “**Numerical Analysis of Conjugate Heat Transfer in the Presence of Porous Medium**” which is being submitted to the **National Institute of Technology Karnataka, Surathkal** in partial fulfilment of the requirements for the award of the Degree of **Doctor of Philosophy in Mechanical Engineering** is a *bonafide report of the research work carried out by me*. The material contained in this Research Thesis has not been submitted to any other Universities or Institutes for the award of any degree.

Register Number: **187039ME011**

Name of the Research Scholar: **Prakash Heerasing Jadhav**

Signature of the Research Scholar:



Department of Mechanical Engineering

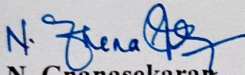
Place: NITK, Surathkal

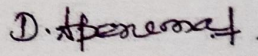
Date: **27-12-2022**

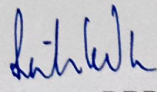
CERTIFICATE

This is to certify that the Research Thesis entitled "Numerical Analysis of Conjugate Heat Transfer in the Presence of Porous Medium" submitted by Mr. Prakash Heerasing Jadhav (Register Number: 187039ME011) as the record of the research work carried out by him, *is accepted as the Research Thesis submission* in partial fulfilment of the requirements for the award of the degree of **Doctor of Philosophy**.

Research Guides


Dr. N. Gnanasekarar
Assistant Professor
Department of Mechanical Engineering
NITK, Surathkal


Dr. Arumuga Perumal D
Assistant Professor
Department of Mechanical Engineering
NITK, Surathkal


Chairman-DRPC 29.12.2022

Department of Mechanical Engineering
National Institute of Technology Karnataka, Surathkal



ACKNOWLEDGMENT

"The real guru is the pure intellect within; and the purified, deeply aspiring mind is the disciple." The Guru is the remover of darkness: Gu means darkness, and Ru means remover. Darkness refers to what obscures the light of awareness. The guru removes *avidya*, or ignorance, which is a case of mistaken identity. Foremost, I would like express my sincere gratitude to my research guides **Dr. N. Gnanasekaran** and **Dr. Arumuga Perumal D** for providing me wonderful opportunity and continuous support of my Ph.D study and research, for their patience, motivation, enthusiasm, and immense knowledge. Their guidance helped me in all the time of research and writing of this thesis to complete the fulfilment. I could not have imagined having a better guides and mentor for my Ph.D study and general things as well.

I am extremely grateful to our honourable director **Prof. Prasad Krishna** and former director's **Prof. Udaykumar R. Yaragatti** and **Prof. Karanam Umamaheshwar Rao** for creating such assertiveness approach towards research for students. I sincerely thank our HOD, **Prof. Ravikiran Kadoli** and former HOD, **Prof. Shrikantha S Rao** for making available all the facilities needed for the smooth progress of my research work. I would like to thank **Dr. Kumar G N**, **Dr. Parthasarathy P** and **Dr. Balan A S S** for their constant support and guidance during my research tenure. My special thanks to **Prof. Gangadharan K V** for providing DAQ facilities to conduct the experiments. I am also thankful to my RPAC committee members **Dr. Ranjith M** and **Dr. Vishwanath K P** for their guidance during my presentation. I express my earnest thanks to **Prof. Moghtada Mobedi**, Shizuoka University Japan for his valuable collaborative work and motivation during my research work.

I feel happy to thank **Dr. Harsha Kumar, Dr. Banjara Kotresha, Dr. Vishweshwara P S, Dr. Narendran G, Muthamil Selvan N, G Venkatapathy, Trilok G, Diganjit Rawal, Aditya N, Dr. Anil Kadam, Dr. Sashikumar, Dr. Santosh Chavan, Dr. Kalinga T, Madhu, Vashista, Rakesh L, Neeraj M P** and list seems to be endless. I am extremely thankful to the Department of Mechanical Engineering, NITK, Faculty and non-teaching staff for providing all the facilities to carry out my research work.

I bow down the feet of my parents **Shri. Heerasing Jadhav** and **Smt. Saroja Jadhav** and my father-in-law **Shri. Vasudev Rathod** and my mother-in-law **Smt. Mangala Rathod** for their continuous support for furnishing the needs to fulfil my wishes to achieve them. I would extremely to thank my younger brothers **Mr. Santosh** and **Mr. Mohan** for their valuable support during my research work. I feel happy to thank to my brother-in-law **Dr. Pritam Rathod** and sister **Mrs. Shilpa Rathod** for their valuable continuous support with lots of joy, love showed to my kids so that I could concentrate towards my research study. I would like to thank my elder sister **Mrs. Savitra Rathod**, brother-in-law **Shri. Vinod Rathod** and younger sister **Mrs. Shilpa Rathod**, brother-in-law **Shri. Arvind Rathod** for their continuous support to furnish and fulfil my research. Also, I would like to thank my sister kids **Sanjana, Ritika** and **Ritesh**. Last but not the least, I would like to thank to **Ms. Ritu Rathod** for supporting my wife and love showed towards my kids has been never forgettable.

My special thanks to my beloved wife **Mrs. Priyanka Jadhav** for her valuable patience and constant support during my research time and lots of love to my kids **Vedika Jadhav** and **Vedant Jadhav**.

I would like to thank all my teachers, relatives and friends who have been supported me in one way or the other way and their best wishes were always for me.

PRAKASH HEERASING JADHAV

ABSTRACT

The intent of the current research is to emphasize the computational modelling of forced convection heat dissipation in the presence of high porosity and high thermal conductivity metallic foam in a circular pipe for different regimes of fluid flow for a range of Reynolds number. For a constant heat flux condition, the goal is to find out the efficient metal foam and configurations when air is considered as a working fluid. Flow dynamics and heat transport phenomenon are captured using Darcy Extended Forchheimer (DEF) flow and local thermal non-equilibrium (LTNE) models within the porous filled region of the pipe. The numerical results are initially matched with experimental and analytical results for the purpose of validation. Initially, the effect of fully filled foam (i.e., $L_f = 0.6L$ (i.e., 60% L), $0.8L$ (i.e., 80% L) and L (i.e., 100% L), i.e., $L_f =$ length of the foam, $L =$ length of test section), and discrete filled foam (i.e., $L_f = 0.6L$ (i.e., 60% L) and $0.8L$ (i.e., 80% L)), in a pipe is accomplished to decrease and increase the pressure drop and heat transfer rate, respectively. The average Nusselt number for fully filled foam ($L_f = L$) is found to be higher compared to other filling rate of metallic foams and the clear pipe at the cost of pressure drop. Further, in the presence of discrete filled foam ($L_f = 0.8L$), the heat transfer rate deteriorates significantly while increases considerably for fully filled foam ($L_f = 0.8L$) accompanied with the same pressure drop. As an important finding, it has been observed that the laminar and transition flow gives higher heat transfer enhancement ratio and thermal performance factor compared to turbulent flow. This work resembles numerous industrial applications such as solar collectors, heat exchangers, electronic cooling, and microporous heat exchangers. The novelty of the work is the selection of suitable flow and thermal models in order to clearly assimilate the flow and heat transfer in metallic foam. The parametric study proposed in this work surrogates the complexity and cost involved in developing an expensive experimental setup.

Further in this contemporary research, a parametric analysis of partially filled high porosity metallic foams in a horizontal pipe is performed to augment heat transfer with reasonable

pressure drop. The investigation includes six different models filled partially with aluminium foam by varying internal diameter of foams from the wall side and external diameter of foam from the core of the pipe. The pore density of the foam ranges from 10 to 45 PPI (pores per inch) and their porosity varies from 0.90 to 0.95. The results showed that the thermal performance factor of 10 PPI aluminium foam performs close to the 10 PPI expensive copper foam. The performance factor is found to be higher for 30 PPI aluminium foam amongst the PPI's of the foam considered. However, the performance factor is found to be 2.93, 2.22 and 1.73 for 30PPI, 45 PPI and 20PPI with their porosities of 0.92, 0.90 and 0.90, respectively for the model 1, model 2 and model 3 at lower Reynolds number of 4500 and then it decreases progressively with increasing flow rates of the fluid.

Further, optimization study is proposed to optimize for various (six) filling rate of the metallic foam in a horizontal circular pipe. Optimization study in flow through metal foams for heat exchanging applications is very much essential as it involves variety of fluid flow and structural properties. Moreover, the identification of best combinations of structural parameters of metal foams for simultaneous improvement of heat transfer and pressure drop is a pressing situation. In this work, six different metal foam configurations are considered for the enhancement of heat transfer in a circular pipe. The foam is aluminium with PPI varying from 10 to 45 and almost the same porosity (0.90-0.95). The aluminium foams are chosen from the available literature and they are partially filled in the pipe to reduce the pressure drop. A special attention is paid to the preference between pressure drop and heat transfer enhancements. Hence, Technique for Order Preference by Similarity to Ideal Solution (TOPSIS) optimization techniques with five different criteria (contains the combination of the weightage/priority of heat transfer and pressure drop) is used. Based on the numerical results of heat and fluid flow in pipe, it is found that when an equal importance is given to both heat transfer and friction effect, 30 PPI aluminium foam with 80% filling on the inner lateral of the pipe provides the best score as 0.8197.

Keywords: – Forced convection, Pipe, Metal foam, LTNE, DEF, TOPSIS

CONTENTS

CONTENTS	i
LIST OF FIGURES.....	vi
LIST OF TABLES.....	x
ABBREVIATIONS.....	xi
NOMENCLATURE	xiii
GREEK LETTERS	xvii
1 INTRODUCTION.....	1
1.1 BACKGROUND OF STUDY	1
1.2 POROUS MEDIUM	4
1.2.1 Applications of Porous Medium	4
1.3 POROUS METAL FOAM	5
1.3.1 Advantages of Porous Metal Foams	9
1.3.2 Applications of Porous Metal Foams.....	9
1.4 LOCAL THERMAL EQUILIBRIUM (LTE) MODEL	10
1.5 LOCAL THERMAL NON EQUILIBRIUM (LTNE) MODEL .	10
1.6 ORGANIZATION OF THESIS	11
2 LITERATURE REVIEW.....	13
2.1 INTRODUCTION	13
2.2 FULLY FILLED POROUS MEDIUM IN A CONDUIT/CHANNEL	14
2.3 PARTIALLY FILLED POROUS MEDIUM IN A CONDUIT/CHANNEL	22

2.4	REVIEW ON OPTIMIZATION WITH/WITHOUT POROUS MEDIUM.....	28
2.5	SUMMARY OF LITERATURE AND RESEARCH GAPS	31
2.6	MOTIVE AND SCOPE FOR THE PRESENT WORK.....	33
2.7	OBJECTIVES OF THE WORK	34
2.8	CLOSURE.....	34
3	NUMERICAL SIMULATION OF FORCED CONVECTION HEAT TRANSFER IN THE PRESENCE OF FULLY AND DISCRETE FILLED ALUMINIUM METAL FOAM IN A PIPE....	35
3.1	INTRODUCTION.....	35
3.2	PROBLEM GEOMETRY	35
3.3	PROBLEM STATEMENT	36
3.4	BOUNDARY CONDITIONS.....	38
3.5	DETAILS OF NUMERICAL SIMULATION	39
3.6	GRID INDEPENDENCE STUDY	44
3.7	VALIDATION OF THE NUMERICAL RESULTS.....	45
3.7.1	Temperature on Top Surface Validation.....	45
3.7.2	Pressure Drop Study	46
3.7.3	Velocity Distribution for Fully and Partially Filled Foams	47
3.7.4	Comparison of Wall Temperature	48
3.8	RESULTS AND DISCUSSION	50
3.8.1	Solid-Fluid Temperature and Velocity Profile	50
3.8.2	Wall Temperature of Pipe.....	51
3.8.3	Convective Heat Transfer Coefficient	53

3.8.4	Average Nusselt Number	56
3.8.5	Pressure Drop Study	60
3.8.6	Friction Coefficient (f) Study	62
3.8.7	Heat Transfer Enhancement Ratio (Nu_{ER}).....	63
3.8.8	Performance Factor (η_p)	65
3.9	SUMMARY	66
3.10	CLOSURE	67

4 PERFORMANCE EVALUATION OF PARTIALLY FILLED HIGH POROSITY METAL FOAM CONFIGURATIONS IN A PIPE

69

4.1	INTRODUCTION	69
4.2	PROBLEM STATEMENT	69
4.3	NUMERICAL DOMAIN AND BOUNDARY CONDITIONS .	71
4.4	DETAILS OF NUMERICAL COMPUTATION.....	73
4.5	GRID INDEPENDENCE STUDY	75
4.6	VALIDATION OF NUMERICAL MODEL	76
4.7	RESULTS AND DISCUSSION.....	77
4.7.1	Velocity and Temperature Distributions.....	77
4.7.2	Average Wall Temperature ($\overline{T_w}$)	81
4.7.3	Forced Convection Coefficient.....	83
4.7.4	Average Nusselt Number (\overline{Nu}).....	85
4.7.5	Pressure Drop.....	89
4.7.6	Friction Coefficient (f)	91
4.7.7	Heat transfer Enhancement Ratio (Nu_{ER})	93

4.7.8	Colburn j Factor (j) and Performance Factor (η_p).....	95
4.8	SUMMARY	97
4.9	CLOSURE.....	98
5	PERFORMANCE SCORE BASED MULTI-OBJECTIVE OPTIMIZATION FOR THERMAL DESIGN OF PARTIALLY FILLED HIGH POROSITY METAL FOAM PIPES UNDER FORCED CONVECTION.....	101
5.1	INTRODUCTION.....	101
5.2	PROBLEM STATEMENT	101
5.3	GOVERNING EQUATIONS AND BOUNDARY CONDITIONS	106
5.4	TOPSIS METHOD FOR MULTI – OBJECTIVE FUNCTIONS	108
5.4.1	Step I: Computation of Normalized Matrix.....	108
5.4.2	Step II: Computation Weight Assigned Normalized Matrix	109
5.4.3	Step III: Compute Ideal Worst Values of V^- –and Ideal Best Values of V^+ Among Weighted Normalized Matrix of Nu and f	109
5.4.4	Step IV: Compute Euclidean Distance from Weighted Resultant Ideal Best Value	110
5.4.5	Step V: Compute Euclidean Distance from Weighted Resultant Ideal Worst Value.....	110
5.4.6	Step VI: Compute the Performance Score.....	110
5.5	COMPUTATIONAL DETAILS, GRID SENSITIVITY ANALYSIS AND VALIDATION STUDY.....	112
5.6	RESULTS AND DISCUSSION	112

5.6.1	Velocity Distribution at Different Locations of Pipe.....	112
5.6.2	Fluid-Solid Temperature Distribution at Different Locations of Pipe.	113
5.6.3	Friction Coefficient.....	114
5.6.4	Average Nusselt Number.....	116
5.7	PERFORMANCE INVESTIGATION OF MULTI-OBJECTIVE FUNCTIONS.....	119
5.7.1	Criteria I $(f)_{\min}:(Nu)_{\max} = 0.0:1.0$	119
5.7.2	Criteria II $(f)_{\min} : (Nu)_{\max} = 0.25 : 0.75$	120
5.7.3	Criteria III $(f)_{\min} : (Nu)_{\max} = 0.50 : 0.50$	121
5.7.4	Criteria IV $(f)_{\min}:(Nu)_{\max} = 0.75:0.25$	122
5.7.5	Criteria V $(f)_{\min} : (Nu)_{\max} = 1.0:0.0$	124
5.8	SUMMARY	125
5.9	CLOSURE	126
6	CONCLUSIONS.....	127
6.1	SCOPE FOR FUTURE WORK.....	130
	REFERENCES	131
	LIST OF PUBLICATIONS	145
	BIODATA.....	149

LIST OF FIGURES

Figure 1.1 Passive method for heat transfer augmentation.....	2
Figure 1.2 Active method to augment heat transfer.....	3
Figure 1.3 Compound method of enhancing heat transfer rate.....	3
Figure 1.4 Few applications of porous medium.....	5
Figure 1.5 Metal foams (a) Open cell (b) Closed cell.....	6
Figure 3.1 Illustration of the circular pipe.	36
Figure 3.2 Illustration of numerical domain for 0.6L m fully filled foam.....	38
Figure 3.3 Variation of temperature on the top surface ($x = 0.5 h$) of aluminium metallic foam.	46
Figure 3.4 Variation of pressure drop through aluminium metal foam ($l = 0.1524$ m) with mean velocity of fluid.....	46
Figure 3.5 (a) Variation of velocity profile for fully/partly filled aluminium metal foam with (Lu et al. (2016)) and (b) validation of velocity profile for fully filled metal foam with (Xu et al. (2011)).	47
Figure 3.6 Comparison average Nusselt number for the present study with (Hamadouche et al. 2015) and (Zhao et al. 2001).....	48
Figure 3.7 Wall temperature of the present study is compared with experimental results of (Baragh et al. (2018)) (a) $Re = 1125$, (b) $Re = 3500$	49
Figure 3.8 Solid-fluid temperature variation along the length of pipe in radial direction (a) $L_f = L$ m and (b) $L_f = 0.6L$ m. (c) Velocity distribution for $L_f = L$ m at different Re	51
Figure 3.9 Changes in wall temperature along the pipe length of 0.6L m filled foam for (a) laminar $Re = 1125$ (b) transition $Re = 3500$ and (c) turbulent flow $Re = 6437$	53
Figure 3.10 Illustration of convection coefficient for 0.6L m filled foam with various PPI of metallic foam for (a-c), (a) laminar, (b) transition, (c) turbulent flows and (d) Average convection coefficient for different filling rate of metallic foam.....	55
Figure 3.11 Average Nusselt number of 0.6L m fully filled foam for (a-c), (a) varying porosities (b) varying PPI (c) varying Re for 0.6L m fully filled foam and clear pipe and (d) Average Nusselt number of various filling rate of metallic foams with Re	58

Figure 3.12 Comparison of mean Nusselt number for different PPI, (a) comparative results (b) porosity 0.95, with (Baragh et al. 2018).	60
Figure 3.13 (a) Pressure drop for varying PPI and clear pipe, (b) changes in pressure drop for various filling rate of metallic foams and (c) comparisons of pressure drop results.	61
Figure 3.14 (a) Friction coefficient for varying PPI and clear pipe and (b) Friction coefficient for various filling rate of metallic foams.	63
Figure 3.15 Nu_{ER} with varying Re (a) For 0.6L m fully filled foam varying PPI of metal foam and (b) various filling rate of metal foam.	64
Figure 3.16 Variation of ηp for various filling rate of metallic foams with Re for (a) 30 PPI metallic foam (b) 40 PPI metallic foam.	66
Figure 4.1 Representation of computational domain.	71
Figure 4.2 The variation of (a) temperature on the top surface with (Garrity and Klausner (2015)) and (b) pressure drop with (Kamath et al. (2013)).	76
Figure 4.3 Variation in dimensionless velocity versus dimensionless height.	77
Figure 4.4 Velocity distribution at exit of the conduit along the radius for model 2 and model 5.	78
Figure 4.5 Temperature distribution at exit of pipe along the radius for model 2 and model 5.	79
Figure 4.6 Velocity distribution for (a) Model 6 with varying PPI, (b) Model 1 – Model 6 for 30 PPI and (c) velocity contours for Model 1 – Model 6 for 30 PPI.	80
Figure 4.7 Temperature distribution along radius of the pipe (a) model 6 and (b) comparative results of all models.	81
Figure 4.8 Variation in (a-e) the T_w with respect to velocity of air for model 1-model 5 and (f) comparative study of T_w for all the six models.	83
Figure 4.9 Variation of (a-c) h vs. Re for model 1-model 3 and (d) comparative study of h for all six models.	85
Figure 4.10 Changes in (a-b) average Nusselt number vs. Re for model 2 and model 6 and (c-d) comparative results of average Nusselt number for all six models filled with 45 PPI aluminium and 10 PPI copper foams respectively.	87

Figure 4.11 Changes in pressure drop for (a) contour plots for model 1 – model 6, (b-c) comparative study for model 1 and model 4 (d-e) comparative study of model 1 – model 6 for 30 PPI and 45 PPI partly filled foam and clear pipe.	91
Figure 4.12 Changes in (a-b) friction coefficient vs. velocity of air for model 1 and model 4 and (c-d) comparative study of pressure drop for 30 PPI and 45 PPI partly filled foam and clear pipe.	92
Figure 4.13 Nu_{ER} vs. flow Re for (a-c) model 1- model 3 and (d) comparative results for 30 PPI aluminium foam.....	94
Figure 4.14 Colburn j factor vs. Re for (a) model 1 and (b) comparative results of 30 PPI aluminium foam for all six models.	96
Figure 4.15 Performance factor versus Re for (a) model 1 and (b) comparative results for 30 PPI aluminium foam for all six models.....	97
Figure 5.1 Schematic of computing domain.	104
Figure 5.2 Flowchart representing the steps involved in numerical simulation.	107
Figure 5.3 Flowchart that represents the steps involved in TOPSIS methodology. .	111
Figure 5.4 Fluid velocity variation in the pipe for model 2 when $Re = 6500$ (a) PPI = 10, $\varepsilon = 0.95$ and (b) PPI = 45, $\varepsilon = 0.90$	113
Figure 5.5 Fluid and solid temperature variation for Model 2 when $Re = 6500$ (a) PPI = 10, $\varepsilon = 0.95$ and (b) PPI = 45, $\varepsilon = 0.90$	114
Figure 5.6 The change of friction coefficient with Reynolds number based on permeability for different models and PPI (a) model 1, (b) comparative study of all models for 10 PPI and (c) comparative study of all models for 45 PPI.....	116
Figure 5.7 The variation of average Nu with Re_k , (a) for model 1, (b) for all models when PPI = 10, (c) for all models when PPI = 45.	118
Figure 5.8 Performance score of 6 Models for <i>Criteria I</i> (f) _{min} : (Nu) _{max} = 0.0 : 1.0, (a) $Re = 6500$ and (b) $Re = 16500$	120
Figure 5.9 Performance score of 6 models for <i>Criteria II</i> (f) _{min} : (Nu) _{max} = 0.25 : 0.75, (a) $Re = 6500$ and (b) $Re = 16500$	121
Figure 5.10 Performance score of 6 models for <i>Criteria III</i> (f) _{min} : (Nu) _{max} = 0.50 : 0.50, (a) $Re = 6500$ and (b) $Re = 16500$	122
Figure 5.11 Performance score of 6 models for <i>Criteria III</i> (f) _{min} : (Nu) _{max} = 0.75 : 0.25, (a) $Re = 6500$ and (b) $Re = 16500$	123

Figure 5.12 Performance score of 6 models for *Criteria III* $(f)_{min} : (Nu)_{max} = 1.0 : 0.0$,
(a) $Re = 6500$ and (b) $Re = 16500$124

LIST OF TABLES

Table 3.1	Various computational domains considered for present study.	37
Table 3.2	Boundary conditions used for the computational domain.....	39
Table 3.3	Correlation used to compute the properties of metallic foam.	44
Table 3.4	Grid independence analysis for 0.6L fully filled foam.	45
Table 4.1	Schematic of the various models considered for the present study.	70
Table 4.2	Dimensions of the partially filling metallic foams.....	70
Table 4.3	Boundary conditions imposed for the numerical investigation.....	72
Table 4.4	The interface coupling conditions at porous medium and the clear fluid. ..	73
Table 4.5	Properties of aluminium and copper metallic foams (Kamath et al. (2011 & 2013); Kotresha and Gnanasekaran (2018)).	74
Table 4.6	Superficial surface area of aluminium and copper metallic foams.	75
Table 4.7	Grid independence study for 10 PPI, $\varepsilon = 0.95$ at $Re = 5000$ for model 3. ..	75
Table 4.8	Percentage increase in average Nu for 20 PPI and 45 PPI with porosity of 0.90 compared to Baragh et al. (2018).....	88
Table 5.1	Numerical domains considered for all six models.	102
Table 5.2	Details of the dimensions of all six models.	102
Table 5.3	Properties of aluminium metallic foams Aluminium (Kamath et al. (2011 & 2013); Kotresha and Gnanasekaran (2018)).	104
Table 5.4	Superficial surface area of aluminium metallic foam.	104

ABBREVIATIONS

AI	- Artificial Intelligence
ANN	- Artificial Neural Network
ATEG	- Annular Thermoelectric Generator
CMF	- Composite Metal Foam
CSA	- Continuum Scale Approach
CFD	- Computational Fluid Dynamics
DEF	- Darcy Extended Forchheimer Flow
DSA	- Discrete Scale Approach
ERT	- Enhanced Receiver Tube
ETfHE	- Enhanced Tube for Heat Exchanger
FEM	- Finite Element Method
FVM	- Finite Volume Method
GA	- Genetic Algorithm
GAFIS	- Genetic Algorithm Based Fuzzy Inference System
GMF	- Graded Metal Foam
GPM	- Graded Porous Medium
HG	- Helical Groove
HTER	- Heat Transfer Enhancement Ratio
HPR	- Heat pipe radiator
HVAC	- Heating, Ventilation and Air Conditioning
LCS	- Lost Carbonate Sintering
LTE	- Local Thermal Equilibrium
LTNE	- Local Thermal Non-Equilibrium
MCDM	- Multiple Criteria Decision Making
MCPM	- Multi-Layered Porous Medium
MHP	- Micro Heat Pipe
MFHPR	- Metal Foam Heat Pipe Radiator
NSGA	- Non-Dominated Sorting Genetic Algorithm
PCM	- Phase Change Material
PEC	- Performance Evaluation Criteria

- PF - Performance Factor
- PPI - Pores Per Inch
- RSM - Response Surface Method
- SSA - Specific Surface Area
- TFHPR - Traditional Fin Heat Pipe Radiator
- TKE - Turbulent Kinetic Energy
- TOPSIS - Technique for Order Preference by Similarity to Ideal Solution
- TREC - Thermally Regenerative Electrochemical Cycle
- WHRS - Waste Heat Recovery System

NOMENCLATURE

A	- Cross section area of pipe (m^2)
A_o	- Dimensionless amplitude flow displacement
a_{sf}	- Interfacial surface area (m^{-1})
Br	- Brinkman number
C	- Form drag coefficient (m^{-1})
C_p	- Specific heat of fluid ($J/(kg.K)$)
D	- Diameter of pipe (m)
D_o	- External diameter of foam (m)
D_h	- Hydraulic diameter of pipe (m)
d_o	- Outer diameter of inner layer foam (m)
d_i	- Internal diameter of foam (m)
d_f	- Fiber diameter (m)
d_p	- Pore diameter (m)
Da	- Darcy number
D_{tp}	- Heat exchanger tube pitch (m)
f	- Friction coefficient
G_k	- Turbulent kinetic energy generation (m^2/s^3)
G_ω	- Generation due to ω (m^2/s^3)
H	- Height of channel (m)
h	- Local or heat transfer coefficient ($W/(m^2.K)$)
\bar{h}	- Average heat transfer coefficient ($W/(m^2.K)$)
h_{sf}	- Interfacial heat transfer coefficient ($W/(m^2.K)$)
j	- Colburn j factor = $St. (Pr)^{\frac{2}{3}}$
K	- Permeability (m^2)
k	- Turbulent kinetic energy (m^2/s^2)
k'	- Surface curvature (m)
L	- Length of the pipe (m)
L_f	- Length of foam (m)
M1	- Model 1

M2	- Model 2
M3	- Model 3
M4	- Model 4
M5	- Model 5
M6	- Model 6
M_{opt}	- Optimal level charge
μm	- Micron meter
Nu	- Nusselt number
\overline{Nu}	- Average surface Nusselt number
\overline{Nu}_ϕ	- Average Nusselt number of empty pipe
Nu_{ER}	- Heat transfer enhancement ratio
P	- Perimeter of pipe (m)
P_i	- Performance index/score
P_{in}	- Pressure inlet (Pa)
P_{out}	- Pressure outlet (Pa)
Pr	- Prandtl number
q''_w	- Heat flux (W/m ²)
R	- Fixed radius of pipe (m)
R	- Dimensionless height of parallel plate
r	- Radial coordinate
r'	- Variable radius from center of pipe (m)
Ra	- Rayleigh number
R_{rad}	- Porous radius ratio
Re	- Reynolds number
Re_D	- Darcy Reynolds number
Re_{TD}	- Transition to Darcy Reynolds number
Re_{TN}	- Transition to Non-Darcy Reynolds number
Re_{ND}	- Non-Darcy Reynolds number
R_i	- Richardson number
Re_{df}	- Reynolds number based fiber diameter
Re_H	- Hydraulic Reynolds number

Re_k	- Permeability based Reynolds number
Re_p	- Reynolds number based porous medium
Re_ω	- Kinetic Reynolds number
S	- Euclidean distance
S_i^+	- Positive Euclidean distance
S_i^-	- Negative Euclidean distance
St	- Stanton number = $\frac{h}{\rho_f u_{in} c_p}$
T	- Temperature (°K or °C)
T_{mf}	- Mean fluid temperature (°K or °C)
T_w	- Wall temperature (°K or °C)
U	- Dimensionless velocity of fluid
$u = u_{in}$	- Inlet velocity of fluid (m/s)
u_p	- Seeping/Superficial/Darcy velocity (m/s)
V	- Normalized weighted matrix
V_i^+	- Ideal best magnitude
V_i^-	- Ideal worst magnitude
W	- Weights assigned
X	- Matrix
\bar{X}	- Normalized matrix
Z	- $z/4.5L$ = Dimensionless length of conduit
z	- Axial coordinate

Subscript

eff	- Effective
ER	- Enhancement ratio
f	- Fluid
i	- Row of matrix
j	- Column of matrix
n	- Normalized
s	- Solid

s_e - Solid effective

w - Wall

Symbols

+ - To specify ideal best value

- - To specify ideal worst value

$\langle \rangle$ - Volume average porous medium

GREEK LETTERS

- ρ_f - Density of fluid (kg/m³)
- μ_f - Dynamic viscosity of fluid (N.s/m²)
- μ_t - Turbulent viscosity (N.s/m²)
- μ_{eff} - Effective viscosity (N.s/m²)
- ν - Kinematic viscosity of fluid (m²/s)
- ε - Porosity
- λ - Thermal conductivity (W/m.K)
- λ_f - Thermal conductivity of fluid (W/m.K)
- λ_s - Thermal conductivity of solid (W/m.K)
- λ_r - Thermal conductivity ratio
- δ - Distance between pitch (m)
- φ - Tilt angle in deg.
- σ_ω - Turbulent Prandtl number for ω
- σ_k - Turbulent Prandtl number for k
- ω - Turbulent specific dissipation rate (m²/s²)

CHAPTER 1

INTRODUCTION

1.1 BACKGROUND OF STUDY

In today's scenario, due to increased demand of heat removal in applications like electronic cooling, industry, geothermal, solar applications etc. the performance of the thermal system needs to be improved. The development comprising heat dissipation is addressed in numerous areas including electronic industry (Ahammed et al. (2016); Asirvatham et al. (2015); Brusly Solomon et al. (2013)), automotive areas specially in radiators (Zhao et al. (2016)), di-icing systems involved in wind turbine and aerospace applications (Sabatier et al. (2016)), cooling of electronic circuit board (Hunt et al. (2017)), waste heat recovery systems and chemical handling industries. Heat transfer enhancement with optimal pressure drop in heat exchanger devices is a critical phenomenon with numerous applications in heat exchangers and process industries. The fundamental issue in the thermal device is overheating which leads to system failure and other heat losses which reduces the efficiency of the system greatly. As a result, effective cooling is a major demand of today's industry. The main device required for cooling is a heat exchanger which is used to transfer heat from hot to cold fluid. Henceforth, the heat transfer enhancement by convection is a very important for the existing thermal systems. Heat exchangers are used for a variety of purposes including cooling and increasing system efficiency. For example, in a thermal power plant, heat exchangers such as super heaters, condensers, feed water heaters, and air pre-heaters are used. The two important primary parameters in a heat exchangers are heat transfer rate and the pressure drop across the heat exchanger. As a result, improving heat transfer while taking into account the pressure drop in heat exchanger device is currently a highly important task. Thereby, several researchers have devised strategies to enhance heat transfer rates in a heat exchanger. The conventional techniques involved like finned systems, heat sinks, cooling of thermoelectric systems etc. do not achieve the required cooling effect (Angeline et al. (2018) and Godson et al.

(2010)). It is well familiar that the augment of heat transfer is possible with increase in the surface area (Manova et al. (2020a & b); Nimmagadda et al. (2019); Tharayil et al. (2016 & 2018); Tomy et al. (2016)). Different techniques are involved for the enhancement of heat transfer called passive technique, active technique and the combinations of both according to (Bodade (2013); Gugulothu et al. (2017); Mousa et al. (2021)).

Figure 1.1 represents the passive method used for improving heat transfer. The passive technique is a very basic approach that is based on surface treatment. Due to simple approach, this method does not require any additional power and has a lower operating cost than the active method. Various surface treatment procedures such as the use of a baffle, adding surface roughness, modifying the geometry of the pipe/channel, inserting the tape etc. are used in this approach. The concept behind this is when the flow is restricted for example by employing baffles the flow separates and recirculates near the channel walls causing increased mixing and turbulence. This leads to improved heat transfer rate. Generally, natural convection would be most effective for cooling electronic equipment by using air as the working fluid which would be more affordable owing to little maintenance and faster cooling; however, natural convection is insufficient to cool such systems in some circumstances due to higher heat flux. Therefore, at higher flux situations the active method is more affordable for the heat dissipation.

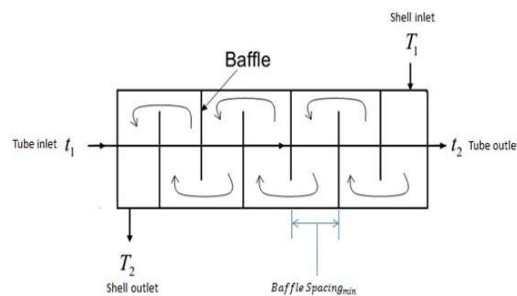


Figure 1.1 Passive method for heat transfer augmentation.

(<http://processprinciples.com/2012/06/shell-and-tube-hx-baffles/>)

Figure 1.2 presents the active method for improving heat transfer rate. The active technique works on the principle of forced convection. It means that by employing

some external devices such as fans, blowers, pumps, vibrating the fluid with a magnetic field, pulsating flow etc., the fluid is agitated to increase the heat transfer rate. At higher heat flux situations, the forced convection can promote better heat transfer but it takes more pumping power.

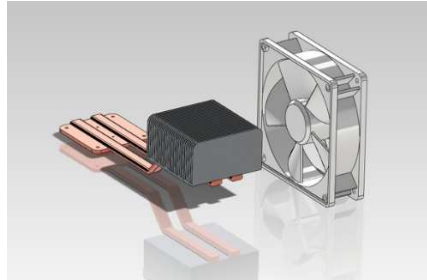


Figure 1.2 Active method to augment heat transfer.

(<http://www.norenproducts.com/forced-convection-cooling>)

The combination of passive and active methods is given in Figure 1.3. This method is widely used in all types of heat exchanger applications since it boosts heat transfer rate allowing the heat exchanger to be smaller. As a result, we observe this technology in current heat exchangers which are often small and utilised to cool small electronic devices like laptops, micro heat exchangers, computers and other electronic instruments. However, this work is solely done on the passive technique for enhancement of heat transfer.

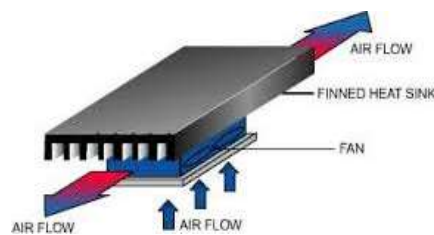


Figure 1.3 Compound method of enhancing heat transfer rate.

(<https://thermal.ferrotec.com/technology/thermoelectric/thermalRef05>)

From the above discussion, it is understood that the augment of heat transfer is possible with increase in the surface area. Therefore, the use of porous media method has gained more attentions by the researchers for augment of heat transfer in many other applications. Fluid flow and heat transfer through porous media is a novel branch of

fluid mechanics and heat transfer that is gaining more popularity among the researchers. The researchers have been paying close attention to the use of porous media in industrial applications to improve heat transfer. In numerous engineering applications, porous materials such as perforated plates, wire meshes and metal foams are also extensively examined for improving heat transfer.

1.2 POROUS MEDIUM

Porous medium means a material consisting of a solid matrix with an interconnected void (pore) (Kaviany (1991); Neild and Bejan (2006)). The solid matrix may either be rigid or it may undergo a little deformation. The fluid stream is allowed to flow through the pores in a single-phase flow; the interconnected void is saturated by a single fluid. In naturally available porous medium, the distribution (scattered) of void (pore) with respect to size and shape is irregular. Some of the examples of naturally available porous media are: beach sand, human lungs, wood, limestone, sandstone, bread slice etc. However, in the present scenario, the porous metal foam has been gaining more attention by the researchers since porous metal foam has many advantages over other types of porous medium which are available in the market (Zhao (2012); Zhao et al. (2001)).

1.2.1 Applications of Porous Medium

Various engineering disciplines such as mechanical, geological, chemical, environmental, petroleum and others, are interested in fluid flow and heat transfer through porous media (Kaviany (1991)). Figure 1.4 presents some of the applications of porous medium. Porous media is also good candidate for enhancing the combustion efficiency in order to minimize the pollution formation, such as soot, CO and NO_x detailed in (Devi et al. (2023)). Further, it is possible to exploit porous medium in domestic heaters, gas turbine combustion chambers, vehicle heaters, fuel cells and energy managements in many industrial processes, such as furnaces and cogeneration systems. Such porous media are vast in nature and have different fields of engineering applications (e.g. groundwater flow, catalytic converters, porous burners, filters (Deb et al. (2021)) and (Devi et al. (2023))).

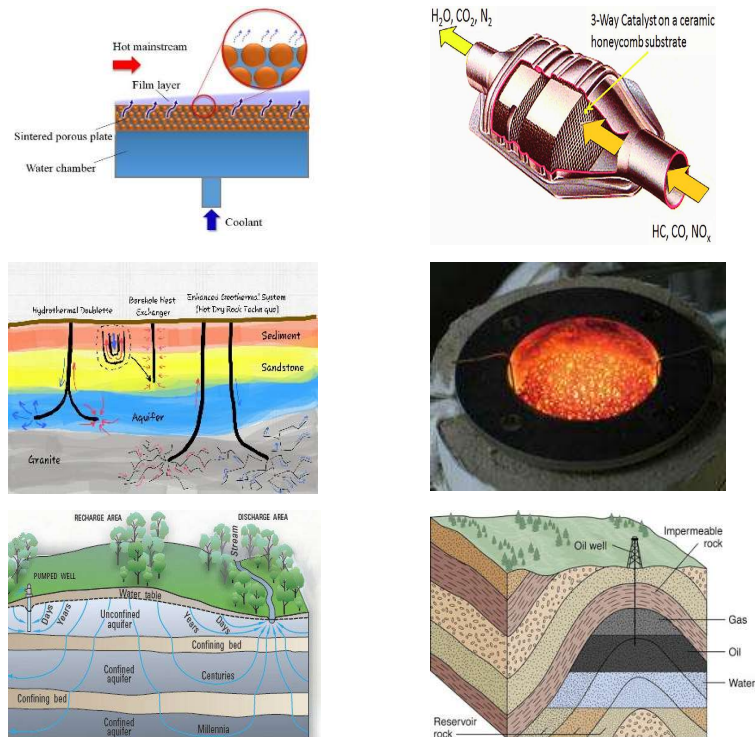


Figure 1.4 Few applications of porous medium.

(<https://www.ebz-dresden.de/process-technology/burner/>)

(<https://www.iitg.ac.in/pmkumar/greencombustion.html>)

1.3 POROUS METAL FOAM

In many engineering applications, it is appealing to design a primary mechanical structure to fulfil other functions such as heat transfer/dissipation. A reliable methodology that allows the mechanical performance (strength, weight, stiffness) and thermal qualities (heat dissipation, pumping power) to be adjusted simultaneously is desirable for such multifunctional structures. On the other hand, it is acknowledged that thermal management concerns are diverse. The increasing demand for speed in modern computers has resulted in enormous heat fluxes ($> 100 \text{ W/cm}^2$) at the chip level (Zhao et al. (2001)). The enormous heat fluxes present a challenge when it comes to eliminating heat from power electronics connections. As a result, one of the most promising cooling approaches is the use of porous metals as effective compact heat exchangers for heat removal. This is due to high surface-area-to-volume ratio in these materials which result in improved heat transport and thermal system miniaturisation.

Metal foams are the new emerging class of porous medium that contains voids usually filled with fluid. The metal foam structure forms a network that contains struts and ligaments to form a metal matrix. The void volume consists of pores that can be interconnected by fibres (open-cell foams) or which can be closed (closed-cell foams) (Banhart (2001); Kopanidis et al. (2010); Mendes et al. (2014); Paul and Ramamurty (2000); Ranut et al. (2014); Solórzano et al. (2008)). The voids in open foams are connected by open pores called open-celled foam, whereas the voids in closed cellular foams are connected by open channels but divided by a solid wall called closed-celled foam. The open-celled metallic foams comprise reticulate cellular structure which is similar to sponges. As a result, they are frequently referred to as metal sponges (Banhart (2001)). Metal foams are divided into various groups based on their microstructure: closed-cell, semi-open, open-cell and fibre arrangement (Banhart (2001); Kopanidis et al. (2010); Mendes et al. (2014); Paul and Ramamurty (2000); Ranut et al. (2014); Solórzano et al. (2008)). The shape of open celled metal sponges gives a high specific surface area which provides a tortuous form that allows for better mixing to augment heat exchange. Based on solid phase material, both types are electrically and thermally conductive, as well as light weight, relative strength and high porosity (Paul and Ramamurty (2000) and Solórzano et al. (2008)). Metal foams can have high porosity values of up to 0.99. The number of pores per inch (PPI) can range from 5 to 100 (Kaviani (1991)). Figure 1.5 depicts open cell and closed metal foams.

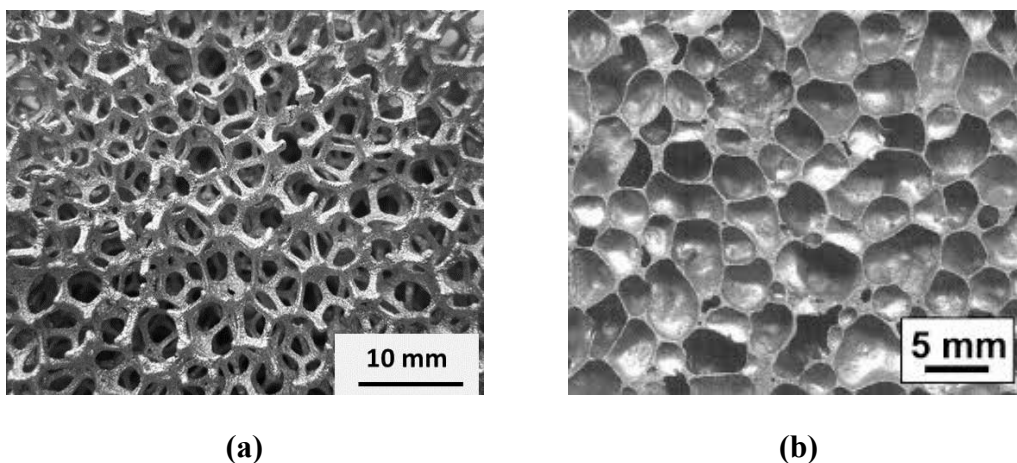


Figure 1.5 Metal foams (a) Open cell (b) Closed cell.

(<https://ultramet.com/refractory-open-cell-foams/reticulated-vitreous-metal-foam>).

A fast-emerging topic of thermal science is forced convective heat transport in porous materials. Numerous thermal engineering applications such as heat exchangers, thermal insulations, geothermal systems, filtering devices, microelectronic cooling systems and chemical industry goods, can benefit from a better understanding of convection through porous materials. The first study of fluid flow through a porous material was conducted in the nineteenth century. Darcy (Darcy (1856)) was the first to conduct experiments and formulate porous medium compositions. He established that the area-averaged fluid velocity in a porous material column is proportional to the pressure gradient and inversely related to the dynamic viscosity (μ) of the fluid seeping through the porous material, as shown by the Darcy flow law.

$$u_p = \frac{K}{\mu} \left(-\frac{dP}{dx} \right) = \frac{K}{\mu} (-\nabla P) \quad (1.1)$$

where u_p is the seeping/superficial/Darcy velocity of the porous medium which is smaller than the real/actual velocity. K is a constant called material permeability. It is responsible for the amount of fluid flow to pass through the porous material. The permeability depends on the shape and porosity of the porous material.

Following that, the Darcy flow model has been used in a variety of engineering applications involving fluid flow and heat transfer in porous materials. Although the Darcy model is widely used in porous media convective heat transfer research, it ignores a number of important physical aspects in channel/conduit flows. For example, Darcy flow model does not fulfil no-slip condition on a solid surface boundary because it ignores friction owing to macroscopic shear and inertial forces, which are important for moderately fast flows. Hence, Darcy law is applicable only for very smaller velocity of isothermal and incompressible flows. Also, when the Reynolds number based on pore or particle diameter grows in the range of 1 to 10, the linearity collapses due to form drag caused by the porous medium solid phase (Neild and Bejan (2006)). Therefore, in this situation the Darcy law is not applicable. In order to account the shear and inertial forces the Darcy law is extended to a Darcy extended Forchheimer law that defines inertial effects against motion of fluid flow which accounts in the form of inertial resistance or form drag coefficient depicted in Eq. (1.2). The form drag

coefficient is basically depending on the internal structural of porous ligaments, pore size and porosity of the porous medium.

$$-\nabla P = \frac{\mu u_p}{K} + \frac{\rho C_F}{\sqrt{K}} |u_p| u_p \quad (1.2)$$

The modified Darcy law shown in Eq. (1.1) is originally signified by (Dupuit (1863)). and (Forchheimer (1901)). The second term of Eq. (1.2) in the right hand side is called as Forchheimer term where, C_F is called Forchheimer constant. The transition flow within the porous medium is possible only when the permeability Reynolds number is greater than 150 (Neild and Bejan (2006)).

It is difficult to fully comprehend the fluid flow and heat transfer characteristics of porous media. The complicated microscopic transport phenomena at the pore level is crucial in this regard because they determine macroscopic phenomena like heat transfer enhancement and pressure loss. However, due to the complexity of the cellular morphology present in commercial porous metals, a full microscopic analysis of the transport events at the pore level is usually not possible. As a result, the general transport equations are frequently integrated over a representative elementary volume that encompasses both the fluid and solid states within a porous structure. Though the integrated quantities, in combination with a set of proper constitutive equations representing the effects of microscopic interactions on the integrated quantities, provide a rigorous and effective basis for analysing the transport phenomena in porous materials, the loss of information with respect to microscopic transport phenomena is unavoidable with this approach.

The volume-averaging approach for heat transport exploration can be applied in two ways: one is to average over a representative elementary volume containing both the fluid and solid phases, and the other is to average individually over each phase, resulting in a different energy equation for each phase (Neild and Bejan (2006); Kambiz Vafai (2005); Zhao et al. (2001)). The one-equation model and the two-equation model are the names given to these two models. The one-equation model is valid when thermal transmission is adequate enough that the local difference in temperature between the fluid and solid phases is negligible (Neild and Bejan (2006); Kambiz Vafai (2005); Zhao et al. (2001)). Temperature changes between phases, on the other hand, cannot be

ignored in some applications. Heat transfer enrichment in porous materials is caused by the impacts of the interfacial surface and interstitial heat transfer coefficients, which are connected to the internal heat exchange between the solid and fluid phases. In these situations, the two-equation model must be used (Neild and Bejan (2006); Xu et al. (2011b); Zhao et al. (2001)). The heat transport thermal model for the analysis within the porous medium are discussed detailed in next section 1.4 and 1.5.

1.3.1 Advantages of Porous Metal Foams

The advantages of metal foams are as follows (Zhao (2012) and Zhao et al. (2001)).

- Light weight
- High contact surface area
- Excellent stiffness to weight ratio
- High porosity
- Ability to increase the turbulence
- High thermal conductivity
- Damping factor is larger than the solid metals (order of 10)
- Low density with good shear and fracture strength

1.3.2 Applications of Porous Metal Foams

Metal foams have unique qualities that allow them to be used in a wide range of thermal applications. Metal foams with a high porosity are more common and are employed as a good candidate for heat dissipation in the heat exchanger, electronic industries and more others (Xu et al. (2011b); Zhao et al. (2001)). Metal foams are used in the following applications.

- Compact heat exchanger
- Electronic cooling
- Geothermal application
- Filters
- Automotive applications
- Aerospace applications

1.4 LOCAL THERMAL EQUILIBRIUM (LTE) MODEL

The LTE model assumes that the solid and fluid phases in the porous medium are in thermal equilibrium such that $T_s = T_f = T$. Since, heat conduction in both the phases occurs concurrently, therefore, the net/total heat transfer between the phases of the porous medium is zero (Neild and Bejan (2006)). Both the phases of the porous media are subjected to energy conservation as shown in Eqs. (1.3) and (1.4).

$$\text{For solid} \quad (1 - \varepsilon)(\rho c)_s \frac{\partial T_s}{\partial t} = (1 - \varepsilon)\nabla \cdot (k_s \nabla T_s) + (1 - \varepsilon) q_s''' \quad (1.3)$$

$$\text{For fluid} \quad \varepsilon(\rho c_p)_f \frac{\partial T_f}{\partial t} + (\rho c_p)_f u_p \cdot \nabla T_f = \varepsilon \nabla \cdot (k_f \nabla T_f) + \varepsilon q_f''' \quad (1.4)$$

Adding Eqn. (1.3) and (1.4)

$$(\rho c)_{eff} \frac{\partial T}{\partial t} + (\rho c)_f u_p \cdot \nabla T = \nabla \cdot (k_{eff} \nabla T) + q_{eff}''' \quad (1.5)$$

$$\text{where} \quad (\rho c)_{eff} = (1 - \varepsilon)(\rho c)_s + \varepsilon (\rho c_p)_f \quad (1.6)$$

$$k_{eff} = (1 - \varepsilon) k_s + \varepsilon k_f \quad (1.7)$$

$$q_{eff}''' = (1 - \varepsilon)q_s''' + \varepsilon q_f''' \quad (1.8)$$

Where, $u_p = \varepsilon V$. The u_p is velocity average taken with respect to a volume element of the medium consisting of both fluid and solid material called the Darcy or superficial or seepage or volumetric flux density. The V average velocity taken over the volume element of fluid only. Here in Eqs. (1.6)–(1.8) characterizes the effective heat capacity, thermal conductivity and heat generations respectively.

1.5 LOCAL THERMAL NON EQUILIBRIUM (LTNE) MODEL

The LTNE model assumes that the porous mediums solid and fluid phases are not in thermal equilibrium such that $T_s \neq T_f \neq T$ due to existence of the temperature gradient between the solid and fluid phases of the interface. The convection term accounts for heat transport between the solid and fluid sections and is expressed in Eqs. (1.9) and

(1.10) according to (Neild and Bejan (2006)). Therefore, the energy equations between solid and fluid phases of the porous medium are presented in Eqs. (1.9) and (1.10).

$$\begin{aligned} \text{For solid} \quad (1 - \varepsilon)(\rho c)_s \frac{\partial T_s}{\partial t} &= (1 - \varepsilon)\nabla \cdot (k_s \nabla T_s) + (1 - \varepsilon) q_s''' \\ &+ h_{sf} a_{sf} (T_f - T_s) \end{aligned} \quad (1.9)$$

$$\begin{aligned} \text{For fluid} \quad \varepsilon(\rho c_p)_f \frac{\partial T_f}{\partial t} + (\rho c_p)_f u_p \cdot \nabla T_f &= \varepsilon \nabla \cdot (k_f \nabla T_f) + \varepsilon q_f''' + h_{sf} a_{sf} (T_s - T_f) \end{aligned} \quad (1.10)$$

Where, a_{sf} is the specific surface density presented for simple case

$$a_{sf} = 6(1 - \varepsilon)/d_p \quad (1.11)$$

Interfacial heat transfer coefficient correlation reported by (Wakao et al. (1979)).

$$h_{sf} = 2.0 + 1.1 Pr^{1/3} Re_p^{0.6} \left(\frac{\varepsilon d_p}{d_h} \right)^{0.6} \quad (1.12)$$

where d_h is called hydraulic pore scale diameter.

According to (Wakao et al. (1979)), the above Eq. (1.12) is valid for $Re = 15$ to 8500 and $Pr = 0.7$. Based on kind of porous medium, different correlations exist for estimating specific surface area and interfacial heat transfer coefficient (Wakao et al. (1979)); (Calmidi and Mahajan (2000)); (Tian et al. (2004)); (Zukauskas (1987)).

1.6 ORGANIZATION OF THESIS

Chapter 1 describes the brief introduction about background, porous medium, metal foam, application of porous medium, application of metal foam and the advantages of metal foam.

Chapter 2 presents the critical literature on the previous and recent studies on fully and partially filled foam in a conduit/channel. Also, the literature review is extended to optimization study with and without presence of metal porous foam. The same chapter highlights the summary of the literature and research gaps, motive and scope of the present work and objective of the work.

Chapter 3 presents the details of numerical consideration of local thermal non-equilibrium (LTNE) and Darcy extended Forchheimer (DEF) models for the analysis of forced convection in a horizontal pipe in the presence of discrete and completely (different lengths) filled metal foams. This chapter also provides fluid flow distributions as well as solid-fluid temperature distributions of completely filled porous region of the conduit. Performance factor of discrete and completely filled metal foam is also examined in account of laminar, transition and turbulent flow regimes.

Chapter 4 explores the numerical investigation of partially filled high porosity metal foam in a pipe imposed with uniform heat flux. The numerical investigation includes six different models (numerical domain) with varying metal foam layer thickness from the conduit wall side and from core of the pipe. The fluid flow and temperature distributions are presented between porous and non-porous region of the pipe for various inlet velocity of air. Also, the results of Nusselt number, heat transfer enhancement ratio and thermo-hydrodynamic performance of partially filled foam pipe are plotted and discussed.

Chapter 5 is a continuation of chapter 4. Optimization study is proposed for the multi-objective optimization trade-off between heat transfer and the pressure drop. The TOPSIS (Technique for Order Preference by Similarity to Ideal Solution) method is applied for low and high Reynolds number to determine the optimum porous layer thickness for the maximization of heat transfer and minimization of pressure drop. This chapter provides the best configuration (model) of pipe/conduit to determine the location, PPI (Pores Per Inch) and porous layer thickness based on the requirement of thermal designer for weight of heat transfer and friction resistance.

Chapter 6 highlights an overview of major conclusions of the work as well as a description of the specific contribution made. There is also a special mention of the scope of future work.

CHAPTER 2

LITERATURE REVIEW

2.1 INTRODUCTION

In any commercial, industrial and domestic application, a heat exchanger system is necessary for energy usage, recovery and conversion. The thermal efficiency of any thermal system can be improved by optimising the heat exchange mechanism, which lowers the overall system cost. It is critical to design the thermal systems used in engineering applications to maximise efficiency and ensure smooth operation. Heat transfer can be improved using a variety of ways across a wide range of technical applications. Some few examples are heat sinks, micro-channel, extended fin surfaces, nanofluid, phase change materials, porous media etc.

In the recent times, heat transport phenomenon through high thermal conductive porous media is one of the most prominent processes in several engineering applications in the past decades. The motive of many reported heat management studies is to ensure the augment of heat dissipation in many engineering applications like heat exchangers, heat pipes, nuclear cooling, and solar collectors. Hence, more high performance cooling techniques are necessary to avoid the problems of conventional cooling devices. The use of high thermal conductive porous media has advantages to enhance heat transfer. The open-celled foam is one of the most promising used enhancer due to high heat transfer area between the fluid and solid phases of the foam, mixing the fluid flow in the pores, enhancement of convective heat transfer coefficient and finally the increase of the thermal conductivity of flow field (i.e. effective thermal conductivity). These effects promote the thermal performance or efficiency of the system, considerably. However, the use of open cell metal foam has a significant disadvantage and that is the increase of pressure drop (or flow resistance) causing the increase of fan or pump power.

2.2 FULLY FILLED POROUS MEDIUM IN A CONDUIT/CHANNEL

Many researchers have reported the thermo-hydrodynamic behaviour of heat and fluid flow through forced convection heat transfer in a tubes or channels filled with porous medium. The numerical investigation was examined through the forced convection channel occupied with aluminium metal foam in account of local thermal equilibrium (LTE) and local thermal non equilibrium (LTNE) thermal models (Lin et al. (2016)). In comparison with average Nusselt number, the LTE and LTNE thermal models confirm similar results when the velocity of fluid is high. Since, the LTE model used to envisage thermal performance of metal foam at high velocity flow and has large height, the state of thermal equilibrium is achieved. Further, at the state of equilibrium, the interfacial heat transfer coefficient does not show any significant effect on the heat transfer performance.

Xu et al. (2015) explored the numerical computations on convection heat transfer performance using metal foam in consideration with LTE and LTNE models. It is concluded that the use of porous metal foam conductivity and porosity play a significant role in the evaluation of heat dissipation rate with LTNE model.

Kuwahara et al. (2011) explored the analytical investigation of effective porosity on saturated porous media fully filled in a channel in account of LTNE model. In this study, an effective porosity concept addressed the effects of thermal dispersion as well as the tortuosity on specific effective heat conductivity of fluid and solid phases in the saturated porous medium. Further, metal foam with air combinations showed that the LTE assumptions could hold good for isothermal hot and cold walls, but it can fail in account of uniform heat flow walls.

Yang et al. (2015) accomplished the LTNE model for fully developed forced convective heat flow through the tube filled with porous foam where constant heat flux boundary conditions is incorporated. The exact solution obtained for the combined metal foam and air predict that the LTE assumptions may fail for the case of uniform heat flux assigned at the wall. This is because of the volume averaged temperature for aluminium

foam is significantly higher than those of air temperature. Finally, the obtained solution is fairly well agreeing with exact solution.

Nakayama (2011) numerically examined the LTNE forced convection air flow through the annulus fully filled with porous medium where the inner wall is heated with a uniform heat flux and outer wall is made an adiabatic boundary conditions, respectively. For local thermal constant heat input boundary condition at inner wall, the temperature gradient of fluid near the wall becomes very high in order to develop required constant heat input adjacent to the wall.

Gangapatnam and Kurian (2018) numerically examined the forced convection heat dissipation rate with the effect of foam thickness filled inside the vertical channel. They reported that, the convection coefficient deteriorates for the foam thicknesses of 10 mm to 20 mm and 20 mm to 30 mm where the enhancement in convection coefficient was observed only of 12% and 5.35% respectively.

Calmidi and Mahajan (2002) experimentally and numerically studied forced convection heat transfer through the channel completely filled with high porosity metallic foam. They considered various pore density of aluminium porous foams with their porosity changes from 0.89 to 0.97. Results revealed that, for foam-air combinations showed lesser influence on thermal dispersion effect since high heat conductivity of solid porous foam.

Wang and Guo (2019) carried out numerical investigation with completely cubic metal foam filled inside the channel. The model called volumetric convection heat dissipation coefficient for porous metallic foam was developed while considering the convection heat dissipation and heat conduction with the attached foam ligaments. From the results, foam filled near the wall of the channel, the velocity gradient is larger than in an empty channel, and the boundary layer at the wall becomes thinner.

Li et al. (2018b) applied discrete scale approach (DSA) versus continuum scale approach (CSA) with convection and coupled radiation in rectangular four – sided channel filled with porous metal foam. The LTNE model with Monte Carlo method was employed to compute the radiation heat emission rate. For the studied cases, the

CSA and DSA can predict constantly the temperature field whereas the inconsistency among them is relatively higher for the LTNE region.

Nazari et al. (2015) conducted experimental study on forced convection heat dissipation using nano-fluid in a circular pipe filled with metallic foam heat exchanger. The mass flow rate of the experimental study was varied in the range between $Re = 500$ to 5000 , while the temperature of pipe wall is kept constant. The maximum advancement in the Nusselt number was found to be 57% at Re equal to 3704 for Al_2O_3 inside the pipe filled with metallic foam. Further, the pumping power was increased by 39% for Al_2O_3 nano-fluid with volume fraction of 1.5% at $Re = 3704$.

Baragh et al. (2018) performed forced convection analysis in a single-phase flow through circular pipe with different arrangement of porous medium heat exchanger. They considered six different arrangement of porous medium for various flow regimes like laminar ($Re = 1125$), transition ($Re = 3500$) and turbulent ($Re = 6437$) inside the conduit. When the diameter of the porous medium is equal to the diameter of the pipe, it is found that the rate of heat dissipation as well as enhancement ratio is higher compared to other configurations considered in the study of laminar and turbulent flows.

Pavel and Mohamad (2004) experimentally and numerically examined augment of heat removal rate for gas heat exchanger fitted with various configurations of porous inserts. They reported that, for larger value of porous radius ratio in combinations with lower porosity leads to maximum fluid velocity shifted much nearly to the pipe wall, subsequently maximum heat transfer. When porous radius ratio is equal to one (fully filled pipe), develops constant velocity profile across the pipe diameter, therefore the heat removal rate reduces.

Abadi and Kim (2016) experimentally analysed heat dissipation rate and pressure drop in a tube heat exchanger filled with copper porous metallic foam. The R245fa (Pentafluoropropane) is considered as working fluid whose mass flux changes from 200 to $1000 \text{ kg/m}^2\text{s}$. Small copper tube filled with metallic foam enhances heat dissipation rate due to high superficial area to volume ratio exposed for heat dissipation. The heat

convection coefficient and the pressure drop showed strong dependent on Re number as well as the porous foam geometry.

Yang et al. (2022a) studied the coupling effects in a plate heat exchanger fully filled with porous media. The findings demonstrate that the thermal performance of one channel in a plate heat exchanger filled with porous media is influenced not only by this channel flow and heat transfer parameters, but also by the flow and heat transfer parameters of the plate heat exchangers of the other channel. When designing a plate heat exchanger with porous medium, this coupling effect should be taken into account.

Chen et al. (2019) considered the simulation of fluid flow and conjugate heat transport within the foam zones, the Darcy-extended Forchheimer equation and the LTNE model are used. When neglecting the heat radiation effects, the deviations of 18.5 percent in temperature and 13 percent in the performance factor were observed. However, with increasing length of the heat exchanger and ratio of annular dimension leads to enhance the performance factor as well as the effectiveness of heat exchanger.

Boyd and Hooman (2012) explored three-dimensional numerical investigation on metal porous foam heat exchanger for several cooling techniques such as water and air cooling. This study considered a graphite porous block with a thickness of 1 mm inserted among the cooling passage and the chamber of fuel cell system. Results demonstrates that, for the identical pressure drop the heat performance of water cooled heat exchanger was observed to be equal as that of air cooled foam heat exchanger.

Mancin et al. (2013) experimentally investigated forced convection through various copper and aluminium foam samples. The metal foam samples of pore density are varied from 5 PPI to 40 PPI and their porosity changing from 0.89 to 0.95. Two dissimilar thickness of porous foam such as 20 mm and 40 mm are considered for the experimental investigation. From the results, 20 mm thick foam sample obtained maximum efficiency even after 50% reduction in heat dissipation area relatively to 40 mm thick foam sample.

Kotresha and Gnanasekaran (2019) numerically investigated the effect of thermal conductivity and thickness of aluminium and copper metal foams filled through the vertical channel. Results reported that, the effect of variation in thermal conductivity of

foam does not showed any significant effect on heat transfer rate. But, in the variation of thickness of copper and aluminium foams, the copper metallic foam enhances only 4 percentage upsurge in heat dissipation rate than aluminium metallic foam.

Chumpia and Hooman (2014) investigated heat transfer and pressure drop characteristics of a metal foam-wrapped tubular heat exchanger. The thickness (or height) of the foam layer ranges from 5 mm to 20 mm. The results reveal that foam heat exchangers with a thicker foam layer operate better than those with a thinner foam layer within the specified air velocity range.

Zhao et al. (2006) employed Darcy Brinkman-extended equation and two-equation heat transfer models inside porous region to investigate heat transfer performance of a metal foam filled tube heat exchanger. The heat transfer capacity of a metal-foam filled tube heat exchanger increases with increasing pore density (PPI) or decreasing porosity.

Chen et al. (2022) performed numerical investigation of fluid flow and heat emission through wrapped metal foam heat exchanger. In this work, cold nitrogen flow through a tube to cool hot nitrogen running through a tube bank. They discovered that, as the nitrogen enters with a foam height of 2 mm, and that increasing Re number enhances outside heat transfer performance at the expense of external pressure drop.

Bagci and Dukhan (2018) experimentally studied the effect of oscillating water flow through high porous open-celled aluminium metal foam. The results showed that the PPI has appreciable repercussion on oscillating H_2O flow parameters counting entry pressure, friction factor and pressure losses. At lower frequencies 40 PPI foam showed similar results of friction factor for steady state as well as oscillating water flow.

Ghafarian et al. (2013) used computational fluid dynamics investigation in an oscillating flow through a channel fully filled with porous foam. The effects of foam porosity, Reynolds number, amplitude and frequency of oscillating air flow, λ_s (thermal conductivity of solid) on the surface temperature distribution, and the local Nusselt number of porous channel have all been studied. They reported that, the heat transfer augment of oscillating flow via metal porous foam filled channel is observed to growth with amplitude as well as the frequency of oscillating flow in an appropriate range.

Leong and Jin (2005) conducted the experimental study on the enhancement of heat emission of sinusoidal oscillation flow through the conduit/channel completely filled with pore density of 40 PPI aluminium metallic foam subjected steady uniform heat flux. From the results, the use of porous foam in a plate channel considerably improved heat emission with the oscillating flow. However, the kinetic Reynolds number Re_ω and dimensionless amplitude of flow displacement A_0 increases the cycle-averaged local Nusselt number.

Hutter et al. (2011) examined forced convection heat transfer through the tube inserted fully filled with designed metal foam. Reynolds numbers ranging from 600 to 7600 were considered. The geometry and structure of the metal foam has a significant impact. The increase in convective heat transfer with increased pore size attributed to the larger ligament thickness was seen in commercially available metal foam. When compared to sintered structure without a wall connection, the convective heat transfer rate of fully sintered device was found to be 30% higher.

Lu et al. (2006) explored the forced convection heat emission and pressure drop through the tube filled with porous metallic foam. They found that, in account of low conductivity foam, the influence of PPI is quite small and therefore the pressure drop can be reduced with use of high porosity foams. However, the heat transfer with use of porous metal foam can enhance significantly, up to 40-times higher comparatively to plain hollow tubes.

Boules et al. (2021) conducted experimental study on enhancement of heat dissipation through horizontal cylinder encased with fully and segmented layers of porous metallic foam. The constant heat input is imposed on the cylinder wall. The forced convection experiment was conducted for Re number range from 7500 – 18000. The segmented foam layer exhibited the best performance at largest diameter ratio, with 1.47 times the performance of bare cylinder at highest Re .

Alomar (2020) explored numerical examination and importance of non-Darcian flow and LTNE thermal model for two-phase flow in a horizontal porous channel evaporator with localised heating. Results reported that the growth of two-phase flow in axial direction is more significant influence than that in transverse direction. This statement

could be endorsed that the reduction in coefficient of effective diffusion in the region of two-phase which decreases the transport energy diffusion from superheated vapour region in axial direction.

Lu and Zhao (2019) explored the effect of various flow regimes on the forced convection heat dissipation through the manufactured copper foam by lost carbonate sintering (LCS) process. Five different flow regimes are identified by witnessing the variation in the slope of $\Delta P/LV - Re$ namely: (i) pre – Darcy, (ii) transition to Darcy (Re_{TD}), (iii) Darcy (Re_D), (iv) transition to non – Darcy (Re_{TN}) and (v) non-Darcy (Re_{ND}). In pre – Darcy regime the $Re < 10$. Therefore, the various regimes of flow are classified as; pre – Darcy ($Re < Re_{TD}$), transition to Darcy ($Re_{TD} < Re < Re_D$), Darcy ($Re_D < Re < Re_{TN}$), transition to non – Darcy ($Re_{TN} < Re < Re_{ND}$) and non – Darcy ($Re > Re_{ND}$).

Baloyo and Zhao (2021) explored the experimental study on structural effects of copper foam sample by lost carbonate sintering process. Various copper foam samples were fabricated with different porosity range from 0.5 to 0.8. The size of the pore is varied from 250 μm to 1500 μm . The K_2CO_3 (potassium carbonate) food grade powder particle (space holder) is used to interconnect the voids between the copper powder particles and which allows and enhances the permeability of fluid samples. Results reported that. The maximum convection coefficient was attained at an optimal porosity of 0.6.

Arbak et al. (2017) conducted the experimental study on the influence of PPI (pore density) on the thermal development with the use of open-celled porous foam. They noticed that, the thermal entry length for 10 PPI foam was around 2.9 pipe diameters (150 mm) and for 40 PPI foam was about 2.4 pipe diameters (122 mm); these values were consistent across Darcy and Forchheimer flow regimes and were unaffected by flow velocity.

Tio et al. (2000) examined analytical investigation of inclined micro heat pipe (MHP) filled with porous media. The Darcy equation incorporated for two-phase flow MHP porous media. At a given operating temperature of MHP, could exists a threshold value of heat transfer rate (Q_{max}), however; beyond which the micro heat pipe (MHP) cannot

function effectively due to flooding, dry-out or the mixtures of both will occur. Further, consistent to Q_{\max} also prevail an optimal level charge (M_{opt}), of MHP. Also, the gravity effect can also enhance the heat performance of MHP, and which is also depending on its orientation of the MHP.

Shen et al. (2021) performed the experimental study on fluid flow and thermal features of metallic porous foam heat pipe radiator (HPR). The pore density of 15 PPI copper metal foam is used in a heat pipe radiator to improve heat transfer between the ambient air and condensed part of the heat pipe. The results revealed that, the heat resistance of MFHPR (metal foam HPR) remains essentially stable when heating power increases, whereas the heat resistance of TFHPR (traditional finned HPR) declines as the heating power increases. Also, with the same pressure drop the heat resistance of MFHPR is still 5.6% lesser comparatively to TFHPR.

Edrisi et al. (2017) study mainly focused on heat removal rate in a ceramic heat insulator porous media. The self-consistent technique is adopted in order to accomplish effective heat conductivity of porous media. Here, the porous media is divided into discrete and the continuous phases. This process tends to an equation for effective convection coefficients and the porosity. They observed that, the chemical composition of porous matrix affects features of porous matrix such as size of the pores, spatial arrangements of pores, thermal and homogeneity characteristics of porous media.

Samudre and Kailas (2022) conducted experiments with use of open-pore celled metal foam and foam-fin heat sinks for the cooling applications in order to improve the performance of the system. The idea of current study is to minimize the thermal contact resistance by employing epoxy-gluing technique and fused-bonding approach. When compared to epoxy-gluing approach, fused bonding technique reduces the heat contact resistance by 19 times.

Celik et al. (2017) examined numerical investigation to determine the interfacial convection heat transfer coefficient for a thin periodic porous medium under mixed convection. For lower porosity values below 0.51, the average Nusselt number does not have any significant effect on Richardson (R_i) and Reynolds numbers (Re).

Furthermore, the interfacial convection heat transfer coefficient increases after Reynolds number exceeds 100, when Richardson number varies from 0.01 to 10.

Magyari and Storesletten (2008) reported the mixed convection flow in inclined porous channel considering effect of viscous dissipation. The balance governing equation evaluated analytically where the tilt angle of porous channel changes from $0 \leq \phi \leq 90^\circ$. They also observed that with vertical or inclined porous channel (i.e., inclination angle (ϕ) less than 90°), the velocity boundary value problem states or exists dual solutions for any given value of Ra number and dimensionless average velocity u_m , provided that $u_m \leq u_{m,max}$.

2.3 PARTIALLY FILLED POROUS MEDIUM IN A CONDUIT/CHANNEL

Partially filled tubes or channels with insertion of porous layer thickness can be alternate solution in order to minimize the pressure drop without heat transfer too much. Xu et al. (2011a) explored analytical investigation on heat transport through open celled metallic foam material partly filled in a parallel plate horizontal channel/conduit. The study concludes that the mass flow fraction in the porous medium is highly affected by the hallow ratio. The saturation hollow ratio exists where the mass flow fraction reduces to a level lesser than 10%.

Xu et al. (2011b) carried out analytical investigation in account of Darcy-Brinkman and two-equation models in order to compute the fluid flow and forced convective heat transfer through the tubes partially filled with open-celled high porosity metallic foam. It is stated that, at higher values of porosity the friction factor reduces and Nu number is found to be maximum at an optimal value of porosity.

Qu et al. (2012a) explored the partially filled porous foam inside annulus region and studied the effect of porosity, PPI and dimensionless porous thickness. The resistance due to fluid flow is reduced by reducing the pore density, increasing porosity and reducing the dimensionless thickness of the foam layer. The heterogeneity coefficient for the porosity values of 0.85, 0.90 and 0.95 is very close to each other, but significant changes appeared with increase of PPI of the porous foam.

Lu et al. (2016) explored analytical investigation on fluid and heat flow features of a fixed parallel plate partly filled with metallic foam. The temperature and velocity outlines are predicted for various pore densities of the metallic foam. The Nusselt number advanced marginally when dimensionless height of porous block is smaller (i.e., $H < 0.3$) then, Nusselt number increases considerably faster with increment in dimensionless height of the porous blocks accompanied with the cost of pumping power.

Ghorab (2015) explored partially filled foam channel being tested with two different heights of porous blocks (0.5 and 1) and bottom wall of the channel heated with four discrete uniform heat sources. When compared to non-foam channel, the Nusselt number for the partly filled foam convergent channel (exit height = 0.25 and porous block height = 1) is increased by 20–40%. As a result, the size of the heat exchanger can be lowered by 37.5 percent.

Lai et al. (2021) numerically examined the fluid flow and heat removal rate through rectangular channel partly filled with various height of porous foam layers. The porous media is placed at the centre indicate that, with increasing height of porous media the Nusselt number and dimensionless velocity increases firstly and then reduces. Also, at high value of porosity, the dimensionless velocity and Nusselt number grows sharply as specific surface area (SSA) increases.

Maerefat et al. (2011) numerically investigated the effects of partially filled porous layer inserts. In the first arrangement, increment in porous thickness augment Nusselt number, and porous thickness value that maximizes the Nusselt number range from 0.8 to 0.95 where the Da number value drops from 10^{-3} to 10^{-6} . In the second arrangement, with increment in porous thickness reduces the Nusselt number significantly for lesser values of heat conductivity, and minimal values of Nusselt number exits with optimum porous layer thickness range from 0.6 to 0.85 where the Da number falls from 10^{-3} to 10^{-6} .

Shokouhmand et al. (2011) examined the effect of insertion of porous layer thickness in partially filled conduit on augment of forced convective heat transfer. For both scenarios, the effects of several parameters such as porous media thickness, Da number,

and the ratio of porous media effective conductivity to fluid conductivity were examined and compared. Pressure loss was found to be larger in the case of a porous layer positioned in the channel core than in the case of a porous medium near to the walls. On the other hand, inserting a porous layer in the channel core results in larger Nusselt number for lower values of Da numbers.

Shokouhmand et al. (2009) reported that the channeling effect is more significant on Da and Nusselt numbers. However, in account of channeling effect the Da number increases up to optimum value that leads to increase Nusselt number. In the case of a fully filled channel, this impact was lost. As a result, channels partially filled with porous medium provide the best thermal performance.

Mahmoudi and Karimi (2014) performed the numerical investigation of partially filled porous material in a pipe for the augment of heat transfer in account of LTNE thermal model. The two thermal boundary conditions (model A and model B) were included into the interface fluid of porous material. It should be noticed that the model A and model B indicate different temperatures at solid and fluid phases for different Da numbers with variable radius of foam materials.

Golbaghi Masouleh et al.(2022) carried out analytical investigation on core flow through the cascade heat exchanger augment with open-celled porous foam filled partially in an annulus. The PEC curves showed that with increasing Darcy number or lowering the heat conductivity ratio improves heat exchanger performance significantly. The ideal porosity for the highest heat exchanger performance is 0.91 in the ratio $\lambda_f/\lambda_s = 10^{-4}$.

Peng et al. (2015) examined heat transfer enhancement on partially filled tube of diameter 0.02 m out of which 0.018 m is filled with porous medium at the core of tubes. The air flowing through a tube inserted with a λ_s (solid thermal conductivity) porous medium, has a complex effect on the ETfHE's (enhanced tube for heat exchangers) performance. The Nusselt and PEC values grow greatly when λ_s is less than 24.88 W/(m K) and marginally when λ_s is greater than 24.88 W/(m K) under moderately large Re numbers. When the $Re < 1250$, however, the Nu number and PEC attain their maximum values when the λ_s is at 24.88 W/(m K).

Saedodin et al. (2017) performed experimental and numerical investigation of conventional tubular collector and solar heat exchanger filled partially and fully with copper metal foam. From the observations, as the flow rate increases, the dimensionless temperature gradient at upper wall of the channel increases, resulting in a smaller temperature difference between the wall and the fluid, as a result higher Nu number.

Alkam and Al-Nimr (1999) examined analytical and numerical approaches through solar collector tubes which is partially filled with porous substrates at near wall of the tubes. The solar collector efficiency was increased from 15% to 130 percent, especially at higher levels of the total loss coefficient. However, the collector performance has improved up to a certain limit of porous layer substrate thicknesses, and beyond that, the thermal performance has remained static.

Li et al. (2017) explored the effect of core flow for enhancement of heat transfer with the use of thermoelectric module Bi_2Te_3 (Bismuth telluride) to improve the waste heat from the automobile exhaust gas. The study is carried out for three different filling rate of foam 0%, 50% and 75% with variation in 10 PPI, 20 PPI and 30 PPI of the foam. When the stream flow rate at the inlet is $120 \text{ m}^3/\text{h}$, the inlet temperature is $300 \text{ }^\circ\text{C}$, and the pore density is 20 PPI with a 75 percent filling rate of the foam, the wall convection coefficient increases dramatically from 70 to $300 \text{ W}/(\text{m}^2\text{K})$, or up to 4 times.

Li et al. (2018a) conducted experiments on heat removal rate enhancement of a gas tube heat exchanger partly filled with porous metallic foam. At the core region of the tube 10 mm and 15 mm thick copper foams of 10 PPI, 20 PPI and 40 PPI with constant porosity of 0.98 are filled (50% and 75% filling rate by volume) inside the tube, respectively. The wall convection coefficient found to be higher for 75% filling rate than that of 50% filling rate of the metal foam.

Yang and Hwang (2009) carried out the numerical investigation of turbulent air flow and heat dissipation through the partially filled metal foam heat exchanger. In the turbulent flow regime, the Re number is varied from 5000 – 15000, the Da number range from $10^{-1} - 10^{-6}$ and porous radius ratio altered from 0.0 – 1.0. According to the numerical results, changing the flow field and inserting porous layer thickness causes the boundary layer thickness to condense, resulting in an increased heat removal rate in

the pipe. Furthermore, when the porous radius ratio is smaller than 0.6, Da number has less impact on pressure loss.

Sener and Yataganbaba (2016) investigated the pressure drop and heat emission rate through the rectangular channel partly and fully filled with 10 PPI and 20 PPI aluminium metal foam. The experiments were carried out in a wide range of Re number ranges between 893 to 24,423. In the case of surface curvature parameter $k' > 0$, the influence of Re number on heat transmission and pressure gradient reduces for all pore densities.

Nimvari and Jouybari (2017) studied the effects of turbulence within the porous foam layer partially filled in a pipe. To examine the impact of turbulence on fluid flow and heat transfer, the findings of laminar and turbulent computations are investigated at varied Da numbers and porous layer thicknesses. For lower values of Da numbers, where the local Reynolds number based porous media (Re_p) within the porous layer is smaller than critical Re_p , TKE penetration is found to be statistically significant.

Huang et al. (2010) conducted experimental study of porous inserts at the core flow inside the tube for the enhancement of heat removal rate. The diameter of porous medium is considered which is slightly lesser than the tube diameter where the tube wall heated with a uniform heat flux. The PEC decreases progressively for porosity values of 0.951, 0.975 and 0.966 in account of laminar flow, where as in turbulent flow regime the order of porosity values of 0.951, 0.966 and 0.975.

Ahmed et al. (2019) performed numerical investigation of fluid flow and heat transfer characteristics of partially filled helical grooved metallic foam at core of tubular channels. From the results, when aspect ratio = 0.55, the influence of number of helical grooves (HG) and pitches (δ) is seen in $(4HG/2\delta)$, which displays the maximum decrease in pumping power around (25%) and a decrease in system weight of 16.74 percent, with an augment in the Nu number around 7%, and the PEC is near 1.21 when at $Re = 1000$.

Sheikhnejad et al. (2017) experimentally analysed the thermal performance of circular tube partly filled porous medium under uniform heat flux. On a ferromagnetic flow, transverse magnetic fields were assigned between two parallel fixed magnetic bar at a

certain distance from entry of the test section. On account of both magnetic field as well the porous media improve significantly the heat transfer up to 2.4 fold. But, the porous media contributes more pressure loss than that of the magnetic field.

Rabbani et al. (2019) performed the experimental study on the heat dissipation of MgO nanofluid through the tubes partially filled with copper porous metal foam. The average convective heat transfer augment to a high as 9% and 15% for tube I and II, respectively, when nanofluid was used instead of base fluid. In comparison to the empty tube, the pressure loss and Nusselt number in tubes I and II increased dramatically. The tube II, Nusselt number enhanced by 22% higher than the tube I.

Pourfarzad et al. (2021) experimentally studied the effect of silver-water nanofluid concentrations flows through a rectangular channel partially filled with copper porous foam. Results revealed that, metal foam filled channel could raise the top wall and bottom wall thermal convection coefficient by 1.6 – 3.7 times at highest Re number.

Torabi et al. (2016) reported the effect of nanofluid concentration on heat transfer through partially filled porous channel. The nanoparticles concentration has negligible effect on temperature inside the porous insert. With addition of 5% of volume concentration of nanoparticles can enhance Nusselt number up to around 15%.

Xu and Gong (2018) carried out the numerical investigation of forced convection heat dissipation through partly filled composite metal foam (CMF) in a conduit. At lower PPI, a porosity gradient has marginal influence on the friction factor, but as pore density increases, the effect grows. The friction factor reduces with progressively increment in porosity in the entire porosity zone for three-level CMF with high pore density core foam layer.

Xu et al. (2018) explored forced convection heat dissipation through the tubes partially filled with graded metal foams (GMFs) in account of local thermal non-equilibrium model (LTNE). The GMF 0.98 & 0.8 has a greater friction factor than GMF 0.8 & 0.98. The friction factor increases somewhat with fixed pore density gradients of 5 PPI & 10 PPI and 20 PPI & 5 PPI, then reduces significantly with increasing porosity.

Additionally, the porous media can be further used to increase the combustion efficiency, fuel cells, gas burners etc. (Kaushik et al. (2018)) investigated a comparative study on energy and cost savings in a self-aspirated residential LPG cook-stove with a porous radiant burner in comparison to a conventional LPG burner (CB). Recently, in order to achieve clean and effective LPG combustion, (Deb et al. (2020)) investigated the performance characterization of a cluster porous radiant burner (PRB). At an equivalence ratio of 0.7, they claimed that maximum thermal efficiency increased by 19% in comparison to the conventional burner.

Deb et al. (2021) performed the numerical investigation on combustion mode in a clustered porous radiant burner. For an equivalency ratio of 0.9, stable partially submerged combustion was obtained. When the equivalency ratio was operated at a level higher than 0.95, the burner was found to be unstable.

Devi et al. (2023) investigated the performance evaluation of a porous radiant burner to a conventional burner. They stated that, the traditional PRBs emitted greater values, 3276 ppm and 27 ppm respectively, while sideways faced PRBs emitted maximum CO and NOx, 165 ppm and 8.2 ppm respectively.

2.4 REVIEW ON OPTIMIZATION WITH/WITHOUT POROUS MEDIUM

As it was mentioned above, the enhancement of heat transfer is always accompanied with pressure drop. Although the aim of many researchers who consider both the heat transfer and pressure drop in their studies is to find a location for the best metal foam layer in a channel or tube for both maximum heat transfer and minimum pressure drop. It seems finding the best location is difficult since by increasing heat transfer the pressure drop also increases. Hence, the thermal designers should decide about a priority between two parameters of heat transfer and pressure drop. In some applications such as cooling systems of nuclear plants or cooling of supercomputers, the pressure drop can be sacrificed due to importance of heat transfer enhancement. But, in some other applications such as commercial heating systems, the pressure drop causing a considerable consuming of energy as well as a generation of noise (due to pumps or fans) plays an important role on the applicability of a heat transfer enhancer.

Hence, based on the preference of a thermal designer between pressure drop and heat transfer, the best location and thickness of a metal foam layer in the pipe must be calculated. Hence optimization study is an important to determine the trade-off between the heat transfer and pressure drop to determine the optimum porous layer thickness and optimum structural properties of porous medium etc.

Krohling and Pacheco (2015) adopted a Technique for Order Preference by Similarity to Ideal Solution (TOPSIS) method to evaluate the ranking and comparing with evolutionary algorithm. This technique can be used to identify the best algorithm, the second good and the worst. In terms of computational weight, TOPSIS has a very simple computing technique that will encourage researchers and practitioners in various fields to employ it.

Rastogi et al. (2015) TOPSIS method is incorporated in optimizing the heat comfort and energy saving air conditioning and ventilating systems applications with the use of phase change materials. This paper aims to broaden the use of the Multiple Criteria Decision Making (MCDM) method to rank and choose PCMs for household HVAC (heating, ventilation and air conditioning) applications.

Long et al. (2015) presented continuous thermally regenerative electrochemical cycle (TREC) system was optimized with varied heat source input temperatures with maximum output power and exergy efficiency as the major objective functions. From the results, the output power and thermal efficiency improve with rising heat source inlet temperature under various optimization methods.

Yang et al. (2022b) proposed optimization analysis of annular thermoelectric generator (ATEG) comprising cylindrical heat exchanger and annular thermocouples. The numerical domain of concentric ATEG is first developed using FEM (finite element method). The simulated results presents, the optimized ratio of inner and outer diameters of the heat exchanger is 0.94.

Tian et al. (2020) employed the artificial neural network (ANN) and genetic algorithm (GA) to attain the best comprehensive performance of exhaust gas heat exchanger involving porous fins and porous baffles. Results demonstrates that, with addition of porous fins and porous baffles could increase the heat transmission rate by 92.14%,

reduction in pumping power by 64.70% and decrease in weight by 11.35% with identical mass flow rate of 0.1280 kg/s.

Han et al. (2015) considered response surface method (RSM) for multi-objective optimization for designing geometric parameters of double-pipe heat exchangers. As per Pareto optimal solutions, the best design parameters of a double-pipe heat exchanger with inner corrugated conduit under the restraints $Nu_c/Nu_s \geq 1.2$ are obtained to be $H/D = 0.22$, $P/D = 0.82$, $r/D = 0.23$ with $Re = 26,263$, equivalent to highest value of overall heat transfer performance of 1.12.

Shirvan et al. (2017) the sensitivity analysis is carried out with use of response surface method to optimize the porous layer thickness for maximization of heat transfer in double pipe heat exchanger. As a result, a double-pipe heat exchanger with a high Darcy number and an ideal porous layer thickness of 1/3 or 1 is recommended, which has the best thermal efficiency.

Zheng et al. (2015a) applied genetic algorithm (GA) optimization for the optimization of porous layer inserts for the augment heat transfer in a tube. The enhanced tube region was divided into number of layers in radial flow direction. In each divided region of the tube, porosity of the foam is varied from 0.5 to 1.0. The results suggest that by employing the optimised porous layer inserts, the enhanced tube thermo-hydraulic performance may be significantly improved.

Wang et al. (2017) incorporated optimization of porous media filled in a tube banks for the augment of heat transfer in exhaust heat exchanger. The metal foams are wrapped over the tube banks with various porous layer thickness. The effect of dimensionless porous layer thicknesses (0.1, 0.15, 0.2, 0.3 and 0.4) and inlet velocity were considered and analysed in detail for pressure loss and heat transfer.

Shi et al. (2021) employed a multi-objective genetic optimization coupled Kriging surrogate model for maximizing heat transfer rate and minimizing the friction factor through the tube filled partially with gradient metal foam. The results revealed that, the performance becomes more sensitive to gradient variation as the filling ratio increases. The optimal results of flow resistance are reduced by 19.57% whereas the heat transfer rate augment by 7.088%.

Zheng et al. (2015b) studied the optimization of porous layer inserts located at central receiver tube filled partially or fully with porous medium. The receiver tube exposed to a non-uniform heat flux in the circumferential direction. When $\lambda_s/\lambda_f > 100$, the ERT with in-filling and out-filling porous inserts performs well in terms of thermo-hydraulic performance. The Nu of all types of ERTs increases as Re increases, whereas the PEC falls as Re grows.

Ge et al. (2016) examined the performance of the tube filled partially with porous inserts; the two contrary objectives of Nusselt number and friction factor are considered simultaneously. The TOPSIS method is employed to assist decision makers to examine best alternate solution from the Pareto front. In compared to the option with the highest Nu number, the results obtained by TOPSIS method drops 48.35% in Nu number while the friction factor drops by 82.21.

Siavashi et al. (2018) employed particle swarm optimization (PSO) algorithm to maximize heat transfer and minimize pumping power in account of graded porous medium (GPM) and multi-layered porous medium (MLPM). The tube of radius 0.06 m and length 5 m, filled with MLPM of six porous layer with same thickness and different properties.

Nasution et al. (2022) explored the effectiveness of an artificial intelligence (AI) technique called genetic algorithm-based fuzzy inference system (GAFIS). The result presents, the influence of GAFIS parameters such as the number of cluster, population and mutation percentage on the prediction error are studied.

2.5 SUMMARY OF LITERATURE AND RESEARCH GAPS

From the above-mentioned literature, it is understood that several experimental, analytical and numerical research have been carried out with the use of porous media like wire meshes, metal foams and perforated plates etc. under partially and fully filled inside the pipe/tubes/channels/ducts. Also, a few researchers incorporated the optimization study with and without use of the porous media. The present research mainly focuses on to capture the thermo-hydrodynamic characteristics and optimization

of optimum porous layer thickness in consideration with pore density and porosity of the porous media. Some salient points drawn from the above literature are as follows.

- Many researchers have reported that porous media can be a great passive heat transfer enhancer due to more availability of surface area.
- The open-celled porous ligaments gain more attention compared to closed-celled porous ligaments foam in terms of heat transfer and the pressure drop.
- Well-established Darcy Extended Forchheimer flow (DEF) and local thermal non-equilibrium (LTNE) models have been identified from the literature to capture the behaviour of the fluid flow and the heat transfer in the presence of porous media.
- It is also mentioned that for multi-objective optimization study, multi-attribute decision making methods are proven to be more simple, well-established and less time consuming process.

It is also pertinent to mention that based on the above literature review the authors have identified the following research gaps:

- The numerical investigation of fully and discrete filled porous media for different flow regimes (i.e., laminar, transition and turbulent) with variation of pore density and porosity of the aluminium metal foam with constant heat flux and variable heat flux have been reported less.
- The study of thermo-hydrodynamic characteristics and the effects of porous layer thickness located partially near wall and at core of the pipe for the augment of heat transfer with reasonable pressure drop is unnoticed.
- Numerical simulations are needed to investigate the best configuration of a metal foam layer in a tube by considering the change of PPI as well as Reynolds number.
- Optimization study for maximization and minimization of heat transfer and pressure drop for the best possible configurations, locations, thickness and structure of the metal foam layer in the preference of thermal designer is not addressed fully.

2.6 MOTIVE AND SCOPE FOR THE PRESENT WORK

It is understood that more experimental and numerical insights are required to understand the physics behind the flow and heat transfer in the presence of metal foam. Hence, in order to obtain more meaningful understanding of fluid flow and heat dissipation through porous medium both numerical simulations and experiments are required. But, the detailed parametric exploration with the experimental study is a time consuming and more expensive one. Henceforth, the numerical investigation is carried out for various configurations of fully and discrete metals foams filled along the length of the pipe/conduit in this thesis. It is also pertinent to mention that the numerical investigation is quite challenging in the presence of metal foams under partially filled conditions with different Reynolds number due to the physical nature of the metallic foam.

Further, the authors identified that the enhancement of heat transfer was achieved with the help of high porosity metal foams. Meanwhile, such enhancement happens at the expense of pressure drop. To achieve better enhancement and reasonable pressure drop, many researches preferred partial filling of metal foams. Partially filled channels or tubes/pipes by inserting a metal foam layer can be a solution in order to reduce pressure drop without trade-off heat transfer too much. Number of reported studies on the partially filled channel or tubes/pipes considering both heat transfer enhancement and pressure drop by using metal foam layers are limited compared to studies performed just for heat transfer enhancement. For the optimization study on this issue, the main parameter for determination of the best location, thickness and structure of metal foam layer is the preference of the thermal designer between heat transfer and pressure drop. In coordination with this, this thesis emphasizes the numerical investigation and multi-objective optimization of forced convection heat transfer and fluid flow through conduit/tube without and with open-celled porous medium.

2.7 OBJECTIVES OF THE WORK

1. To model and investigate the numerical simulation of forced convection heat transfer in the presence of fully and discrete filled aluminium metal foam in a pipe.
2. To model and determine the performance evaluation of partially filled high porosity metal foam configurations in a pipe.
3. To study and determine the performance score based multi-objective optimization for thermal design of partially filled high porosity metal foam pipes under forced convection.

2.8 CLOSURE

The detailed explanations of the literature survey on porous media partially or fully filled inside a pipe/tube/channel is given and the optimization study with and without porous media are also discussed in this chapter.

CHAPTER 3

NUMERICAL SIMULATION OF FORCED CONVECTION HEAT TRANSFER IN THE PRESENCE OF FULLY AND DISCRETE FILLED ALUMINIUM METAL FOAM IN A PIPE

3.1 INTRODUCTION

This chapter investigates and describes numerically the forced convection heat transfer through the pipe with the effects of completely and discrete (discontinuous) foam filled lengths, pore density and porosity under forced convection for various flow regimes to improve the performance of the heat exchangers. The results in terms of velocity distribution, solid-fluid temperature distribution, wall temperature, heat transfer convection coefficient, Nusselt number (Nu), pressure drop, friction coefficient (f), Colburn j factor (j), heat transfer enhancement ratio and thermal hydrodynamic performance factor for all the aluminium metal foams involved in the present analysis are plotted and discussed.

3.2 PROBLEM GEOMETRY

The present investigation considers a horizontal cylindrical pipe of diameter 0.1 m and a thickness of 7 mm made up of aluminium material (Baragh et al. (2018)). The wall of the pipe is attached with heater around the circumference of the pipe and the heater is assigned with constant heat input. Aluminium metal foam of various pore densities with different porosities is fully filled in the pipe to improve the thermal performance. The metal foam having a length of 0.6 m which is completely filled exactly at the centre of the pipe of diameter 0.1 m. In the present analysis, the pore densities of 5, 10, 20 and 30 metallic foam whose porosities varying from 0.85 to 0.95 is considered as per (Lu et al. (2016)) for increasing the heat dissipation rate from the pipe wall to the fluid inside the pipe. The schematic of the pipe along with the metal foam is shown in Figure

3.1. The hydrodynamic and thermal performances through the pipe are determined for laminar ($Re = 1125$), transition ($Re = 3500$) and turbulent ($Re = 6437$) flow regimes.

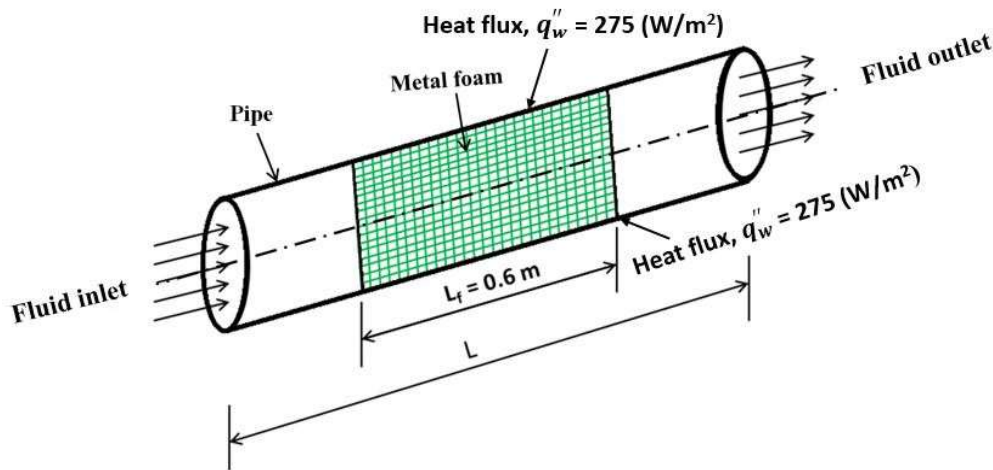


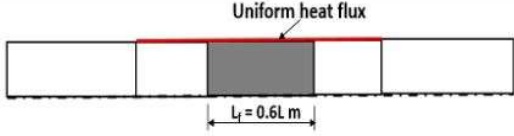
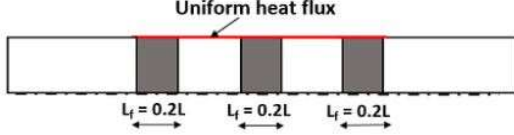
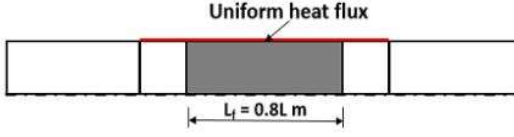
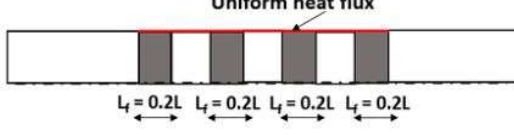
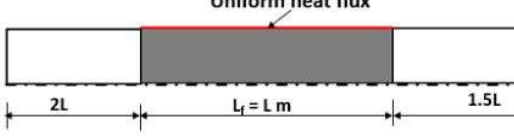


Figure 3.1 Illustration of the circular pipe.

3.3 PROBLEM STATEMENT

The present analysis involves a cylindrical pipe of diameter 0.1 m and a thickness of 7 mm made up of aluminium (Baragh et al. (2018)). The problem domain is analogous to the experimental setup considered by (Baragh et al. (2018)). The pipe wall is attached with heater around the circumference and the heater is assigned with constant heat input. Various computational domains (five numerical domains) are considered in the present study to investigate the fluid flow characteristics and thermal performance and the schematic is shown in Table 3.1. Initially a detailed analysis is performed for 0.6L m fully filled foam placed exactly at centre of the pipe with the appropriate boundary conditions. Subsequently, a novel parametric study is performed by keeping in mind that the pressure drop and the heat transfer performance must be decreased and increased, respectively. To accomplish this, four more numerical models have been created apart from the one mentioned above. The details of the four models are: $L_f = 0.6L$ m discrete filled foam, $L_f = 0.8L$ m fully filled foam, $L_f = 0.8L$ m discrete filled foam and $L_f = L$ m fully filled foam, refer Table 3.1. In the current study, four different pore densities of 5, 10, 20 and 30 PPI aluminium metallic foam and their porosities

changes from 0.85 to 0.95 is considered as per Lu et al. (2016). The hydrodynamic and thermal performances through the pipe are determined for laminar ($Re = 1125$), transition ($Re = 3500$) and turbulent ($Re = 6437$) flow regimes.

Table 3.1 Various computational domains considered for present study.

Computational domain	Metallic foam filled
	$L_f = 0.6L$ m filled foam
	$L_f = 0.6L$ m discrete filled foam
	$L_f = 0.8L$ m filled foam
	$L_f = 0.8L$ m discrete filled foam
	$L_f = L$ m filled foam
	

The pipe is axis symmetry at the centreline along the z-direction of flow (Pavel and Mohamad (2004)); hence, a 2-D computational domain is considered for further numerical computations and is shown in Figure 3.2. The upstream domain is extended by $2L$ in order to accomplish a developed flow (Sunden (2012)). Likewise, the downstream of the domain is extended by $1.5L$ to avoid the exit effects (Mohammed et al. (2013) and Lin et al. (2016)). A uniform velocity profile is applied at the inlet while zero pressure is defined at the outlet. The upstream and downstream walls of the pipe

are assigned with adiabatic wall conditions. The heater is coupled to pipe wall and is defined with uniform heat flux while the axis of the pipe is defined with axis symmetry boundary condition. At the interior surface amongst the foam and foam free region, the continuous in shear stress and energy is incorporated. Here, L_f denotes the length of metal foam filled in a pipe and L denotes the length of the pipe which is considered as $L = 1$ m.

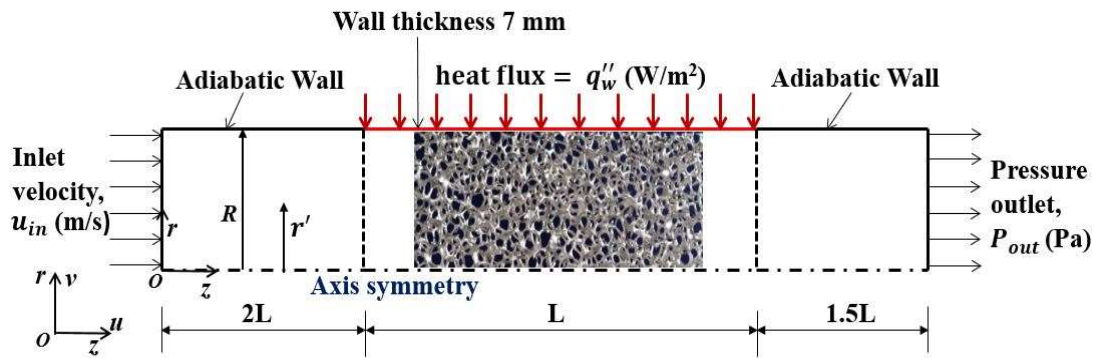


Figure 3.2 Illustration of numerical domain for 0.6L m fully filled foam.

3.4 BOUNDARY CONDITIONS

Due to axis symmetry, only upper half of the pipe is considered for computational domain (Mahmoudi and Karimi (2014)). At $r = 0$, symmetry at centerline causes the velocity gradients and temperature gradients to be zero in r direction. At the entry of the fluid, $Z = 0$, $v = 0$, $T = T_{in}$, $u = u_{in}$ and at the exit of the pipe $Z = 4.5L$, the gradients of u , v and T along Z – direction are zero. Details of boundary conditions used for the computational domain are presented in Table 3.2 as per (Mahmoudi and Karimi (2014)).

Table 3.2 Boundary conditions used for the computational domain.

Boundaries	Boundary conditions
Inlet	$Z = 0, u = u_{in}, v = 0, T = T_{in}$
Outlet	$Z = 4.5 L, P = P_{atm}, \frac{\partial T}{\partial Z} = 0$
Entry wall and exit wall	$r = R, v = 0, u = 0, \frac{\partial T}{\partial r} = 0$
Heated wall	$r = R, u = 0, v = 0, q_w'' = q''$
Horizontal axis	$r = 0, v = 0, \frac{\partial u}{\partial r} = 0, \frac{\partial T}{\partial r} = 0$
Interface between wall and metal foam	$r = R, u = 0, v = 0, q_w'' = -\left\{k_{fe} \frac{\partial T_f}{\partial r} + k_{se} \frac{\partial T_s}{\partial r}\right\}_{Interface}$

3.5 DETAILS OF NUMERICAL SIMULATION

The numerical calculations are performed using commercially existing software ANSYS FLUENT 19.2 (ANSYS FLUENT (2019)). An investigation on conjugate heat transfer is explored for the computational domain as it involves both conduction heat transfer in the thickness of the pipe (solid region) as well as convection in the non-foam porous section of the channel. The fluid considered is air and the properties are calculated based on inlet temperature. The entry velocity of the fluid varies from 0.17 m/s to 0.95 m/s; hence, the Reynolds numbers evaluated based on the hydraulic diameter of pipe ranges from 1125 to 6437 as per (Baragh et al. (2018)). Based on the values of Reynolds number, the flow is assumed as laminar, transition and turbulent. The use of a well-known $k-\varepsilon$ turbulence model to capture the turbulent aspects of the flow in the open section of the channel/pipe was initially examined, and it was discovered that the convergence of the variables took more CPU time. The convergence of the identical solution using $k-\omega$ turbulence model was faster than the $k-\varepsilon$ turbulence model, and it was discovered that the hydrodynamic and thermal performance with both turbulence models were observed to be the same. Hence, for further numerical simulations in the turbulent aspects $k-\omega$ turbulence model were adopted. The $k-kl-\omega$

model (ANSYS FLUENT (2019) and Walters (2019)) and $k-\omega$ model (ANSYS FLUENT (2019); Kotresha and Gnanasekaran (2020); Lin et al. (2016)) are adopted in the non-porous foam region to capture the characteristics of transition and turbulent flows in the channel. The critical Reynolds number for the fluid flow is assumed to be laminar flow regime when $Re < 2200$, transition flow regime when $2200 < Re < 4000$ and turbulent flow regime is assumed to be when $Re > 4000$. The thermo-physical properties of air are presented as follows: $T = T_{in} = 300$ K, $C_p = 1005$ J/(kg.K), $\mu_f = 1.8 \times 10^{-5}$ N-s/m², $\lambda_f = 0.0279$ W/(m.K), $\rho_f = 1.22$ kg/m³ and $Pr = 0.71$.

The governing equations are employed to compute non-foam region of fluid flow through the pipe are as follows (Huang et al. (2010) and Mahmoudi and Karimi (2014)).

Continuity equation:

$$\frac{\partial}{\partial z}(\rho u) + \frac{1}{r} \frac{\partial}{\partial r}(r \rho v) = 0 \quad (3.1)$$

Z- momentum equation in clear region:

$$\begin{aligned} \frac{\partial}{\partial z}(\rho u u) + \frac{1}{r} \frac{\partial}{\partial r}(r \rho v u) \\ = -\frac{\partial p}{\partial z} + \frac{1}{r} \frac{\partial}{\partial r} \left(r(\mu + \mu_t) \frac{\partial u}{\partial r} \right) + \frac{\partial}{\partial z} \left((\mu + \mu_t) \frac{\partial u}{\partial z} \right) \end{aligned} \quad (3.2)$$

r-momentum equation in clear region:

$$\begin{aligned} \frac{\partial}{\partial z}(\rho u v) + \frac{1}{r} \frac{\partial}{\partial r}(r \rho v v) \\ = -\frac{\partial p}{\partial r} + \frac{1}{r} \frac{\partial}{\partial r} \left(r(\mu + \mu_t) \frac{\partial v}{\partial r} \right) - \frac{(\mu + \mu_t)v}{r^2} \\ + \frac{\partial}{\partial z} \left((\mu + \mu_t) \frac{\partial v}{\partial z} \right) \end{aligned} \quad (3.3)$$

Turbulent kinetic energy equation:

$$\begin{aligned} \frac{1}{r} \frac{\partial}{\partial z}(r \rho v k) + \frac{1}{r} \frac{\partial}{\partial r}(r \rho u k) \\ - \frac{1}{r} \left[\frac{\partial}{\partial r} \left(r \left(\mu + \frac{\mu_t}{\sigma_k} \right) \frac{\partial k}{\partial r} \right) + \frac{\partial}{\partial z} \left(r \left(\mu + \frac{\mu_t}{\sigma_k} \right) \frac{\partial k}{\partial z} \right) \right] \\ = G_k - \rho k \omega \end{aligned} \quad (3.4)$$

Turbulent specific dissipation rate:

$$\begin{aligned} & \frac{1}{r} \frac{\partial}{\partial z} (r \rho v \omega) + \frac{1}{r} \frac{\partial}{\partial r} (r \rho u \omega) \\ & - \frac{1}{r} \left[\frac{\partial}{\partial r} \left(r \left(\mu + \frac{\mu_t}{\sigma_\omega} \right) \frac{\partial \omega}{\partial r} \right) + \frac{\partial}{\partial z} \left(r \left(\mu + \frac{\mu_t}{\sigma_\omega} \right) \frac{\partial \omega}{\partial z} \right) \right] \\ & = \frac{\omega}{k} (C_1 G_\omega - C_2 k \omega) \end{aligned} \quad (3.5)$$

Energy equation in clear region:

$$\begin{aligned} & \frac{\partial}{\partial z} (\rho C_p u T) + \frac{1}{r} \frac{\partial}{\partial r} (\rho C_p r v T) \\ & = \frac{\partial}{\partial z} \left(\left\{ \frac{\mu}{Pr} + \frac{\mu_t}{\sigma} \right\} \frac{\partial T}{\partial z} \right) + \frac{1}{r} \frac{\partial}{\partial r} \left(r \left\{ \frac{\mu}{Pr} + \frac{\mu_t}{\sigma} \right\} \frac{\partial T}{\partial r} \right) \end{aligned} \quad (3.6)$$

where μ and μ_t are air and turbulent dynamic viscosity, respectively. The value of μ_t can be calculated from following equation

$$\mu_t = \frac{C_\mu \rho k^2}{\omega} \quad (3.7)$$

σ_t , σ_ω , σ_k , C_1 and C_2 are turbulent constants ref. ANSYS FLUENT 19.2 (ANSYS FLUENT (2019)). G_k and G_ω in Eqs. (3.4) and (3.5) are detailed in ANSYS Fluent (ANSYS FLUENT (2019)).

The details regarding the governing equations of k - kl - ω transition and k - ω turbulent models are listed in (ANSYS FLUENT (2019) and Walters (2019)) and (ANSYS FLUENT (2019); Kotresha and Gnanasekaran (2020); Lin et al. (2016)) respectively. The porous metallic foam is taken as isotropic homogeneous medium and modelled using DEF flow model in the present computations. The DEF model is added to the momentum equation as a source term and the inertial and viscous loss terms which are considered because of permeability and form drag coefficient of the porous medium. The governing equations adopted for computing the highly porous state are as follows (Huang et al. (2010) and Mahmoudi and Karimi (2014)).

Continuity equation:

$$\frac{\partial}{\partial z} (\rho \langle u \rangle) + \frac{1}{r} \frac{\partial}{\partial r} (r \rho \langle v \rangle) = 0 \quad (3.8)$$

Z-momentum equation in porous region:

$$\begin{aligned}
& \frac{1}{\varepsilon^2} \frac{\partial}{\partial z} (\rho \langle u \rangle \langle u \rangle) + \frac{1}{r \varepsilon^2} \frac{\partial}{\partial r} (r \rho \langle v \rangle \langle u \rangle) \\
&= -\frac{\partial \langle p \rangle}{\partial z} + \frac{1}{\varepsilon} \frac{\partial}{\partial z} \left(\mu_{eff} \frac{\partial \langle u \rangle}{\partial z} \right) + \frac{1}{r \varepsilon} \frac{\partial}{\partial r} \left(r \mu_{eff} \frac{\partial \langle u \rangle}{\partial r} \right) \\
& - \frac{\rho F \varepsilon}{\sqrt{K}} \left| \sqrt{\langle u \rangle^2 + \langle v \rangle^2} \right| \langle u \rangle
\end{aligned} \tag{3.9}$$

r-momentum equation in porous region:

$$\begin{aligned}
& \frac{1}{\varepsilon^2} \frac{\partial}{\partial z} (\rho \langle u \rangle \langle v \rangle) + \frac{1}{r \varepsilon^2} \frac{\partial}{\partial r} (r \rho \langle v \rangle \langle v \rangle) \\
&= -\frac{\partial \langle p \rangle}{\partial r} + \frac{1}{\varepsilon} \frac{\partial}{\partial z} \left(\mu_{eff} \frac{\partial \langle v \rangle}{\partial z} \right) + \frac{1}{r \varepsilon} \frac{\partial}{\partial r} \left(r \mu_{eff} \frac{\partial \langle v \rangle}{\partial r} \right) \\
& - \frac{\mu_{eff} \langle v \rangle}{K} - \frac{\rho F \varepsilon}{\sqrt{K}} \left| \sqrt{\langle u \rangle^2 + \langle v \rangle^2} \right| \langle v \rangle - \frac{\mu_{eff} \langle v \rangle}{\varepsilon r^2}
\end{aligned} \tag{3.10}$$

Since a local thermal non-equilibrium approach is used in the study, two energy equations are required,

for fluid phase of the porous region:

$$\begin{aligned}
& \frac{\partial}{\partial z} (\rho C_p \langle u \rangle \langle T \rangle_f) + \frac{1}{r} \frac{\partial}{\partial r} (\rho C_p r \langle v \rangle \langle T \rangle_f) \\
&= \frac{\partial}{\partial z} \left(\lambda_{fe} \frac{\partial \langle T \rangle_f}{\partial z} \right) + \frac{1}{r} \frac{\partial}{\partial r} \left(r \lambda_{fe} \frac{\partial \langle T \rangle_f}{\partial r} \right) \\
& + h_{sf} a_{sf} (\langle T \rangle_s - \langle T \rangle_f)
\end{aligned} \tag{3.11}$$

for solid phase of the porous region:

$$0 = \frac{\partial}{\partial z} \left(\lambda_{se} \frac{\partial \langle T \rangle_s}{\partial z} \right) + \frac{1}{r} \frac{\partial}{\partial r} \left(r \lambda_{se} \frac{\partial \langle T \rangle_s}{\partial r} \right) - h_{sf} a_{sf} (\langle T \rangle_s - \langle T \rangle_f) \tag{3.12}$$

where, the bracket of $\langle \ \rangle$ in Eqs. (3.8-3.12) shows the volume average of the considered dependent variable since flow in a porous medium exists. λ_{se} and λ_{fe} are effective thermal conductivity for the fluid and solid phases,

where,

$$\lambda_{se} = (1 - \varepsilon) \lambda_s \quad \text{and} \quad \lambda_{fe} = \varepsilon \lambda_f \tag{3.13}$$

where, λ_{se} and λ_{fe} represents the effective thermal conductivity of solids and fluid respectively, λ_f represents the thermal conductivity of fluid, μ_{eff} represents effective viscosity which is equivalent to the viscosity of operating fluid, K denotes the permeability, ε is the porosity of the metal foam and F represents form drag coefficient or inertia parameter.

The solution method includes pressure-velocity linked through pseudo transient explicit relaxation factors scheme. The spatial discretization of second order is considered for momentum, pressure, turbulent dissipation rate, turbulent kinetic energy and energy equation. The convergence criteria for the continuity equation is fixed as 10^{-5} and momentum equation is fixed as 10^{-5} , for k - kl - ω and k - ω is fixed as 10^{-3} and for energy equation is fixed as 10^{-10} . In the present work, the metal foam properties such as superficial area density (a_{sf}) and interfacial heat transfer coefficient (h_{sf}) are evaluated based on Eq.(3.14) and Eq.(3.16), respectively as suggested by (Calmidi and Mahajan (2002) and Zukauskas (1987)).

Superficial area density,

$$a_{sf} = \frac{3\pi d_f \left(1 - \exp^{-\left(\frac{1-\varepsilon}{0.04}\right)}\right)}{(0.59d_p)^2} \quad (3.14)$$

Interfacial heat transfer coefficient,

$$h_{sf} d_f \frac{\left(1 - \exp^{-\left(\frac{1-\varepsilon}{0.04}\right)}\right)}{\lambda_f} = \begin{cases} 0.76 Re_{d_f}^{0.4} Pr^{0.37}, & (1 \leq Re_{d_f} \leq 40) \\ 0.52 Re_{d_f}^{0.5} Pr^{0.37}, & (40 \leq Re_{d_f} \leq 10^3) \\ 0.26 Re_{d_f}^{0.6} Pr^{0.37}, & (10^3 \leq Re_{d_f} \leq 2 \times 10^5) \end{cases} \quad (3.15)$$

where, λ_f is the thermal conductivity of operating fluid, Pr represents Prandtl number, Re_{d_f} represents Reynolds number which is evaluated based on the fiber diameter of the porous, refer Eq. (3.16).

$$Re_{d_f} = \left\{ u d_f \left(\frac{1 - \exp^{-\left(\frac{1-\varepsilon}{0.04}\right)}}{\varepsilon \nu} \right) \right\} \quad (3.16)$$

where, d_f represents the fiber diameter in m and d_p represents the pore diameter. The properties of metallic foam such as pore size, fiber diameter, permeability and inertial coefficient are calculated using Table 3.3 according to Lu et al. (2016).

Table 3.3 Correlation used to compute the properties of metallic foam.

S. No.	Properties	Correlations
1	Pore size (d_p)	$d_p = \frac{0.0254}{PPI}$
2	Fiber diameter (d_f)	$\frac{d_f}{d_p} = 1.18 \sqrt{\frac{(1-\varepsilon)}{3\pi}} \left(\frac{1}{1 - e^{-\left(\frac{1-\varepsilon}{0.04}\right)}} \right)$
3	Permeability (K)	$K = 0.00073 (1 - \varepsilon)^{-0.224} \left(\frac{d_f}{d_p} \right)^{-1.11} d_p^2$
4	Inertial/Form coefficient (CI)	$CI = 0.00212(1 - \varepsilon)^{-0.132} \left(\frac{d_f}{d_p} \right)^{-1.63}$

3.6 GRID INDEPENDENCE STUDY

Optimal size of grids for the numerical investigation is obtained by carrying out grid independence study. 10 PPI metallic foam with porosity of 0.9 for the heat flux of 275 W/m² is considered. Computations are performed for three different grid sizes of 67281, 86811, and 106341 to obtain the optimal grid size. The temperature variation on the wall of the pipe and pressure drop for all the three grid sizes is shown in the Table 3.4. Based on the highest number of grid size, the deviation of average wall temperature and pressure drop for other three grid sizes is calculated and found that the grid size of 67281 and 86811 shows a deviation of 1.12%, 0.079% and 0.37%, 0.02% respectively

with respect to 106341 grid size. The grid size of 86811 is preferred for further numerical investigation because it shows less deviation compared to other grid sizes.

Table 3.4 Grid independence analysis for 0.6L fully filled foam.

Grid sizes	$\overline{T_w}$ (°C)	ΔP (Pa)	Deviation (%)	
			$\overline{T_w}$	ΔP
67281	46.24	50.53	1.12	0.079
86811	45.89	50.56	0.37	0.02
106341	45.72	50.57	Base line	

3.7 VALIDATION OF THE NUMERICAL RESULTS

3.7.1 Temperature on Top Surface Validation

The variation of temperature at the top surface ($x = 0.5 h$) is measured with the flow Reynolds number. In order to validate the present approach, the results obtained using numerical simulations is compared with the experimental results of (Garrity and Klausner (2015)). Three pore densities of fully filled aluminium metal foam have been considered i.e., 10 PPI, 20 PPI and 40 PPI and a large deviation is observed from Figure 3.3 at low mean velocity of the fluid for all the PPI considered. Later, the deviation reduces as the velocity of the fluid flow increases. Similar results have been reported in (Lin et al. (2016)).

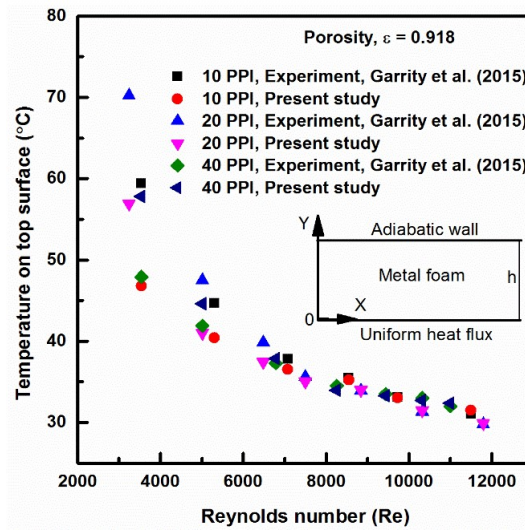


Figure 3.3 Variation of temperature on the top surface ($x = 0.5 h$) of aluminium metallic foam.

3.7.2 Pressure Drop Study

Likewise, a comparison is made between the pressure drop of present simulations for fully filled aluminium metallic foam and experimental data of (Garrity and Klausner (2015)), refer Figure 3.4. Pressure drop results are matching with experimental results with an average deviation of 5.3%.

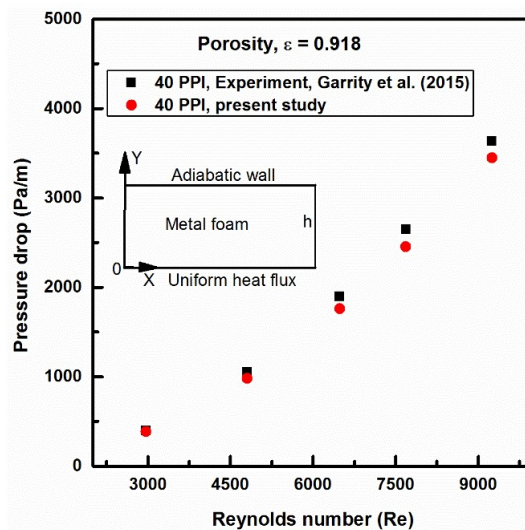


Figure 3.4 Variation of pressure drop through aluminium metal foam ($l = 0.1524$ m) with mean velocity of fluid.

3.7.3 Velocity Distribution for Fully and Partially Filled Foams

To further buttress the solution methodology, the results are compared with the analytical results of (Lu et al. (2016)) which is flow through parallel plates fully and partly filled with metal foam. The dimensionless velocity of the present study agrees well with the analytical results, refer Figure 3.5(a). The numerical results for fully filled metallic foam are also compared with the analytical results of (Xu et al. (2011)) which is depicted in Figure 3.5(b).

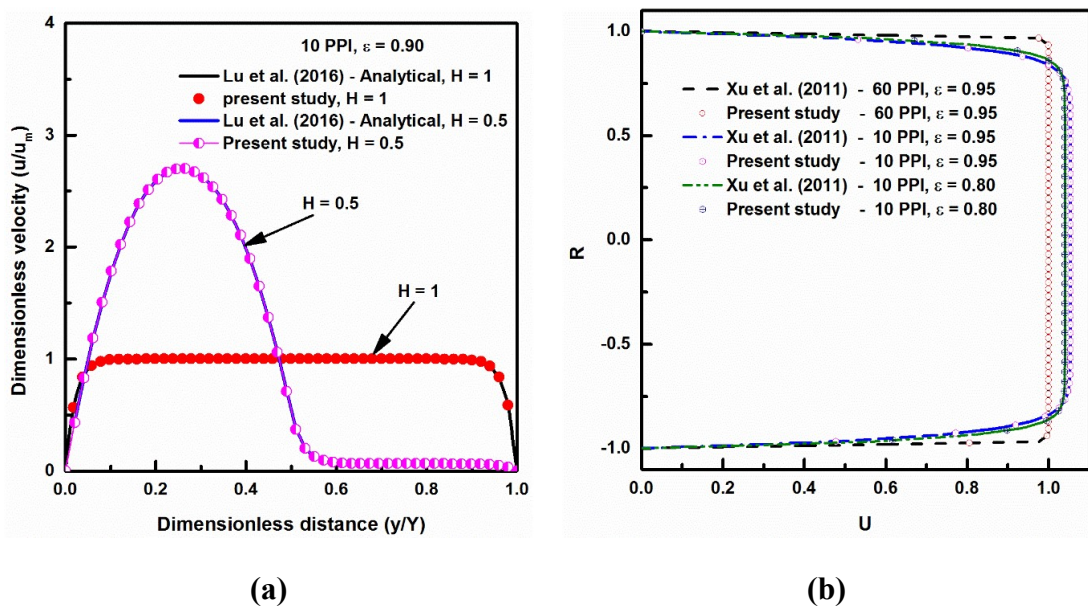


Figure 3.5 (a) Variation of velocity profile for fully/partially filled aluminium metal foam with (Lu et al. (2016)) and (b) validation of velocity profile for fully filled metal foam with (Xu et al. (2011)).

Further, numerical simulations are performed for the turbulent forced convection heat transfer and the results of the average Nusselt number is compared with experimental results obtained by (Hamadouche et al. (2015) and Zhao et al. (2001)) which is shown in Figure 3.6. The average Nusselt number results is compared with experimental results obtained by (Hamadouche et al. (2015)) for the pore density of 40 PPI with a height (h_p) of metal foam block is 20 mm, refer Figure 3.6. In the similar way, numerical simulation are performed for pore density of 10 PPI with the porosity of 0.933 and is compared with experimental results of (Zhao et al. (2001)) which is depicted in Figure 3.6. From the Figure 3.6, it confirms that the results of average

Nusselt number is very close to the experimental results of (Hamadouche et al. (2015) and Zhao et al. (2001)).

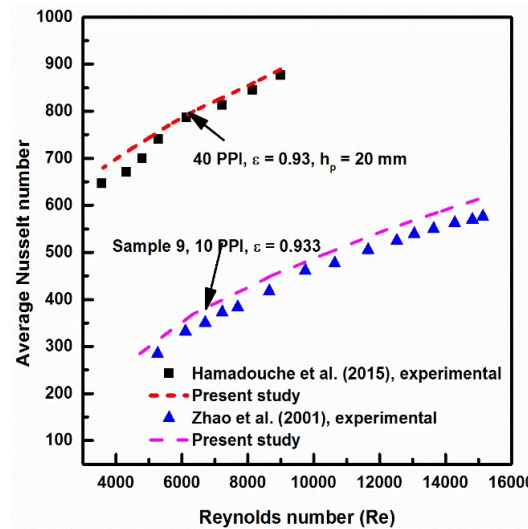


Figure 3.6 Comparison average Nusselt number for the present study with (Hamadouche et al. 2015) and (Zhao et al. 2001).

3.7.4 Comparison of Wall Temperature

Further, to adopt the computational methodology for the pipe filled with aluminium metallic foam, the wall temperature obtained along the length of the pipe is compared with experimental data of (Baragh et al. (2018)) depicted in Figure 3.7. In the numerical computation, the aluminium metal foam of 30 PPI and 20 PPI laminar and transition regimes of flow, respectively, with different porosities is compared with the experimental data reported by (Baragh et al. (2018)). The uniform heat flux is assigned over entire 1 m length of the pipe and the metallic foam is attached exactly at the centre of the pipe along the flow direction i.e., 0.2L to 0.8L. As the fluid enters the test section (i.e., non-foam region of the pipe 0 to 0.2L) the heat is transferred instantly to the fluid due to the temperature difference between the flowing fluid and heated wall by means of convection heat transfer. Also, the wall temperature at the entry region of pipe (i.e., 0 to 0.2L) is lower compared to the exit region (i.e., 0.8 to 1L), since the heat transfer rate at the entry region is higher between flowing fluid and the pipe wall. However, a high conducting metallic foam is attached exactly at the centre of the pipe which is also trying to absorb more amount of heat from the wall and then it instantly transfers the

heat to the fluid which tends to decrease the wall temperature at the foam attached region (i.e., 0.2L to 0.8L) compared to non-foam region of the pipe (i.e., 0 to 0.2L and 0.8 to 1L), clearly seen in Figure 3.7. It is observed from the comparison that the temperature profile obtained in the current study follows the similar tendency of the experimental data of (Baragh et al. (2018)). In case of the experimental result obtained by (Baragh et al. (2018)), wire mesh of 17 wires per inch was placed at different locations along the pipe length while in the current investigation metallic foam of 30 PPI and 20 PPI having a length of 0.6 m along the pipe length is considered. The foremost reason to adopt metal foams instead of wire mesh in the current study is because of well-established fluid flow and heat dissipation models of metal foam reported in the literature. Due to insufficient literature and no firm establishment of heat dissipation models in the case of wire mesh, the present work uses metal foams for the heat enhancement study. As a result, the variation in the temperature profile has been noticed between the numerical and experimental results; but, the deviation of wall temperature amongst different porosities of 30 PPI and 20 PPI metal foam for different locations is found to be less.

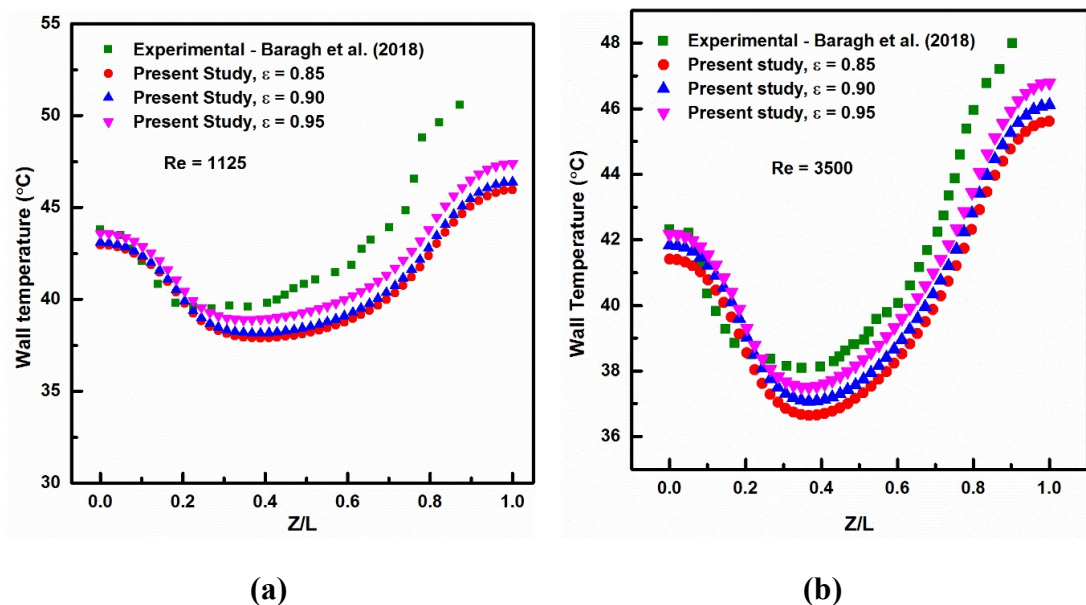


Figure 3.7 Wall temperature of the present study is compared with experimental results of (Baragh et al. (2018)) (a) $Re = 1125$, (b) $Re = 3500$.

3.8 RESULTS AND DISCUSSION

3.8.1 Solid-Fluid Temperature and Velocity Profile

The variation of solid and fluid temperatures for different locations of the pipe are presented in Figure 3.8(a-b). Figure 3.8(a) explored the solid temperature and fluid temperature variation for fully filled (i.e., $L_f = L$ m) metallic foam along the radius of the pipe. From the figure, it is observed that at entry length of the metal foam (i.e., $Z = 2$ m) the fluid temperature is constant and significantly lesser than that of solid temperature except near the wall. This is because, due to low thermal conductivity of the fluid, the fluid absorbs lesser amount of heat. As length of the metallic foam increases, the solid and fluid temperatures increase and become equal except near the wall.

Figure 3.8(b) examined the variation of solid and fluid temperatures for discrete metallic foam (i.e., $L_f = 0.6L$ m) along the radius of the pipe. From the figure, it is observed that the fluid temperature is constant at the entry of the metal foam region while solid temperature is also constant but higher than the fluid temperature except near the wall. As the length of pipe increases (i.e., at non-foam region $Z = 2.3$ m and 2.7 m), the fluid temperature shows almost constant at core of the pipe and it approaches the wall fluid temperature. However, in the foam region (i.e., $Z = 2.5$ m) the solid and fluid temperatures are found similar except near the wall. Figure 3.8(c) presents the velocity distribution for fully filled metallic foam (i.e., $L_f = L$ m) for pore density of 10 and porosity of 0.90. From the figure, we can observe that the velocity distribution in the metallic foam increases with increasing flow Reynolds number. It is also seen that the velocity distribution is constant from the core of the pipe to the adjacent wall and it reduces to zero as the fluid approaches the wall of the pipe.

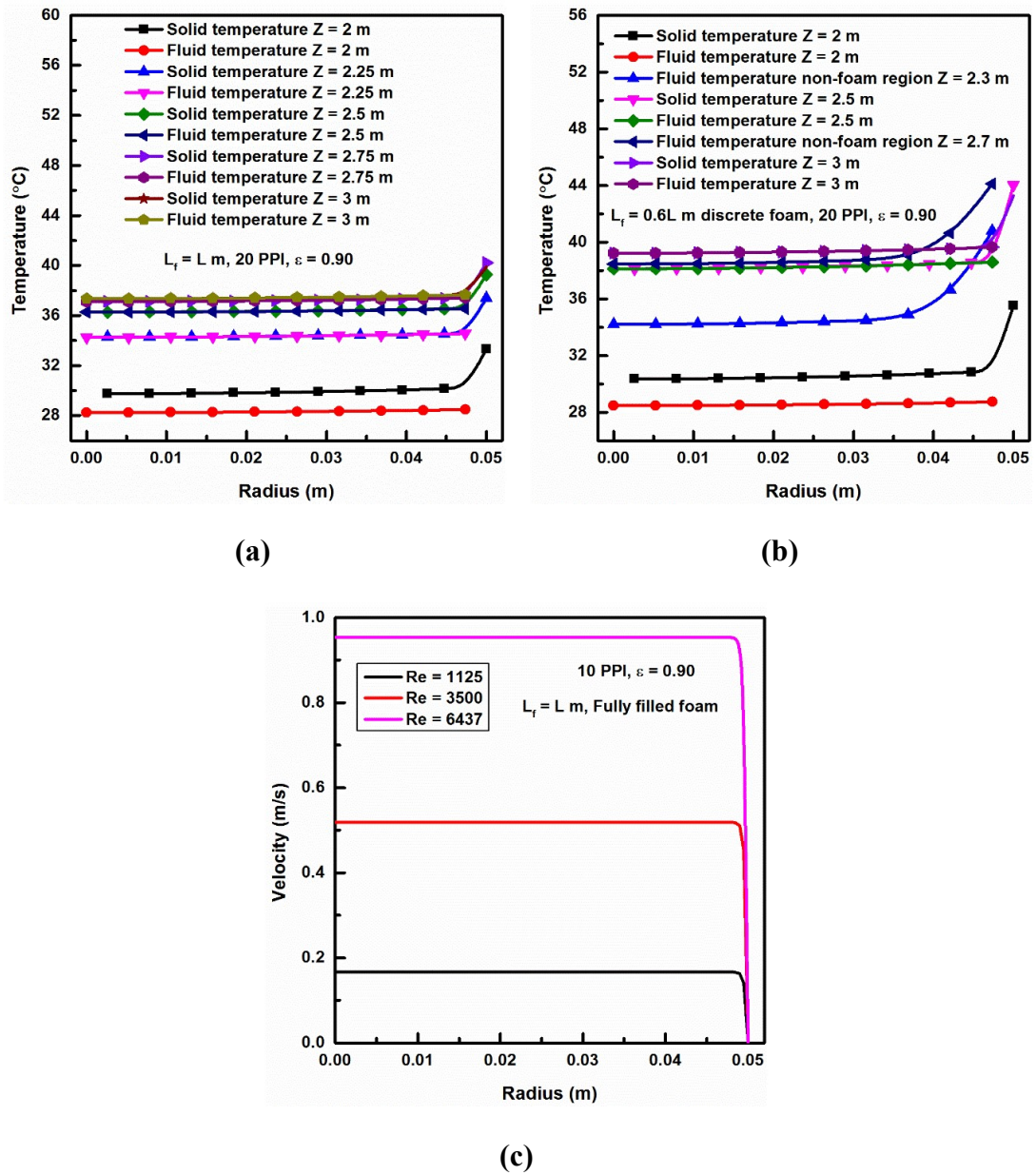


Figure 3.8 Solid-fluid temperature variation along the length of pipe in radial direction (a) $L_f = L$ m and (b) $L_f = 0.6L$ m. (c) Velocity distribution for $L_f = L$ m at different Re .

3.8.2 Wall Temperature of Pipe

The changes in wall temperature obtained for four different PPIs with same porosity for distinct Reynolds number is shown in Figure 3.9. The variation of wall temperature for laminar ($Re = 1125$), transition ($Re = 3500$) and turbulent ($Re = 6437$) flow regimes is shown in Figure 3.9(a) - (c), respectively. From the results, it is understood that the

wall temperature declines with the increase in the PPI of the aluminium metallic foam for all the flow features considered in the study. For example, the 30 PPI metal foam shows average decrease of 29.78% in wall temperature than 5 PPI metal foam in the laminar flow regime and similar results are observed in the other two flow regimes. It is also noticed that the temperature on the wall of the pipe reduces at the metal foam attached region compared to non-porous region of the pipe for each PPI of the metallic foam. This is because the metal foam absorbs more heat from the pipe wall since it is directly attached to the wall; hence, conduction plays significant contribution for dissipation of heat.

The wall temperature at the entry region of pipe is lower compared to the exit region since the heat transfer rate at the entry region is higher between flowing fluid and the pipe wall. It is also clear from the results that, for particular metallic foam pore density, the wall temperature decreases as flow Reynolds number increases. For example, the pore density of 10 metal foam shows a mean decrease of 21.89% and 31.44% in wall temperature for transition and turbulent flows compared to laminar flow. This is due to effective momentum transfer among the fluid in both the transition and turbulence region compared to laminar region. Due to high PPI, less difference in the wall temperature is observed between 20 and 30 PPI for all the flow regimes considered. This is due to increase in interfacial surface area.

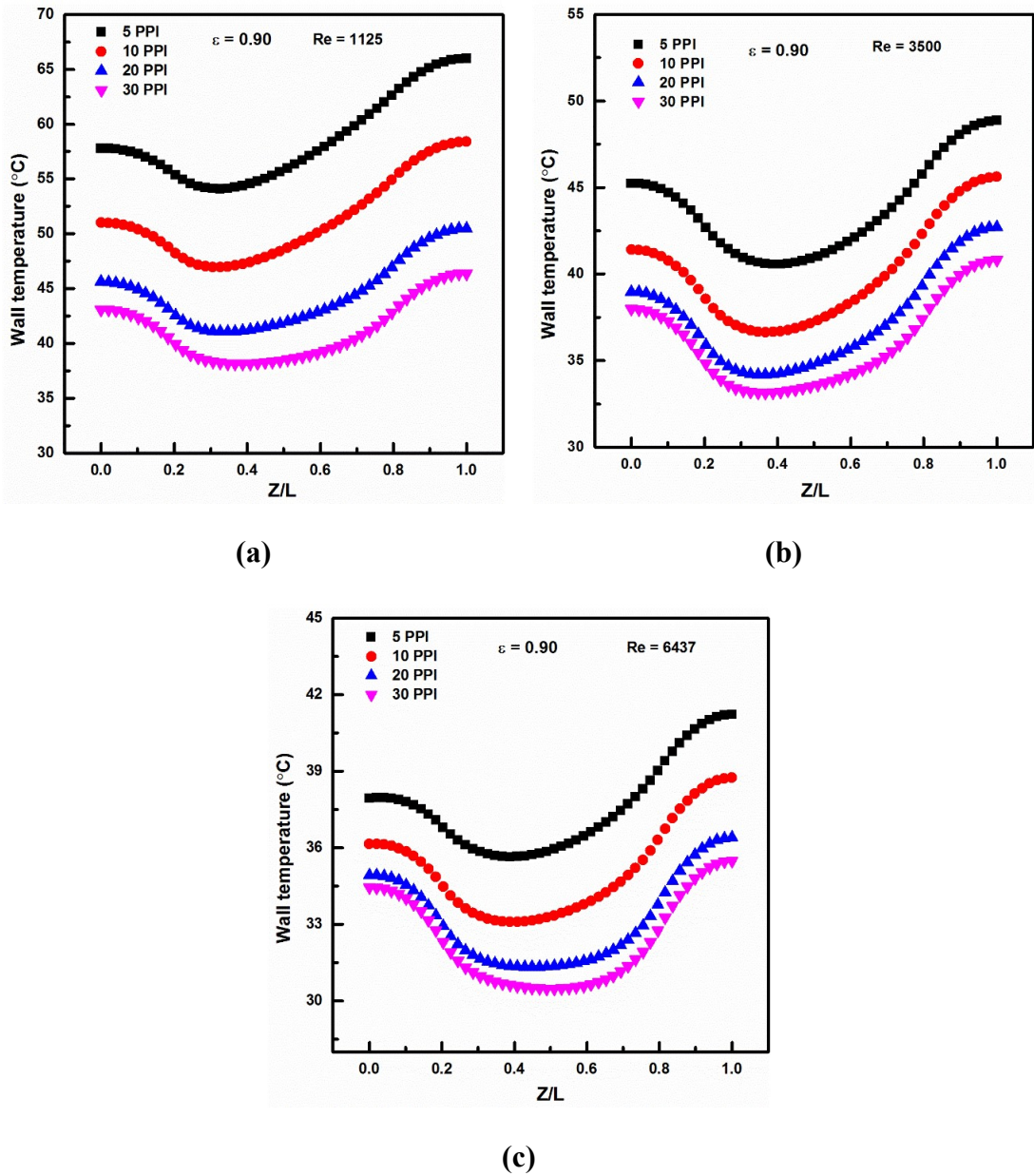


Figure 3.9 Changes in wall temperature along the pipe length of 0.6L m filled foam for (a) laminar $Re = 1125$ (b) transition $Re = 3500$ and (c) turbulent flow $Re = 6437$.

3.8.3 Convective Heat Transfer Coefficient

The local convection heat transfer coefficient is evaluated by Eq. (3.17).

$$h = \frac{q_w''}{T_w - T_{mf}} \quad (3.17)$$

Where, h_i represents local convection coefficient in $W/(m^2 \cdot K)$ for each locations of data points, q_w'' represents continuous heat flux boundary condition assigned on the wall in W/m^2 , T_w and T_{mf} represents wall temperature and mean fluid temperatures in $^{\circ}K$.

The mean heat transfer coefficient is evaluated by Eq. (3.18).

$$\bar{h} = \frac{\sum_1^N h_i}{N} \quad (3.18)$$

where, \bar{h} represents average heat transfer coefficient in $W/(m^2 \cdot K)$, N represents total number of samples or each data points of calculated local heat transfer coefficient.

Figure 3.10(a-c) demonstrates the changes in convection heat dissipation coefficient for different PPI of the metallic foam of porosity 0.95 for laminar ($Re = 1125$), transition ($Re = 3500$) and turbulent ($Re = 6437$) flow regimes. From the results, it is realized that the convection coefficient increases with increase in the PPI of the metallic foam for laminar, transition and turbulent flows. For turbulent flow, the 30 PPI metal foam shows average increase of 51.9% convection coefficient compared to 5 PPI aluminium metallic foam. This is because the metal foam enhances the thermal performance owing to high conductivity of metallic foam and due to combined modes of heat dissipation such as conduction and convection. For a particular PPI of the metallic foam, the convection coefficient increases with respect to increase in Re . The transition and turbulent flows of the 30 PPI metallic foam shows an average increase of 17.22% and 39.54% in convection heat transfer coefficient respectively, compared to laminar flow.

Figure 3.10(d) demonstrates the various filling rate of metallic foam for 30 PPI with porosity of 0.85 along the length of pipe with respect to Re . The 1L m fully filled metal foam shows an increase in convection coefficient of 103.13%, 96.52% and 78.62% compared to 0.6L m fully filling rate of metallic foam for laminar, transition and turbulent flow regimes, respectively. It is also seen from the figure that the insertion of 0.6L m discrete and 0.8L m discrete metallic foam throughout the length of pipe shows a decrease in convection coefficient with respect to the flow Reynolds number compared to 0.6L m continuous and 0.8L m continuous filling rate of metallic foams. It is also noticed that the results of 0.6L m filled foam and 0.8L m discrete filled metallic foam shows similar results at $Re = 6437$. It can be inferred from the obtained results

that placing discrete metallic foam in a pipe is not so effective in enhancing the heat dissipation. Similar kind of tendency is observed in the porous medium literature (Bamorovat Abadi and Kim (2017)).

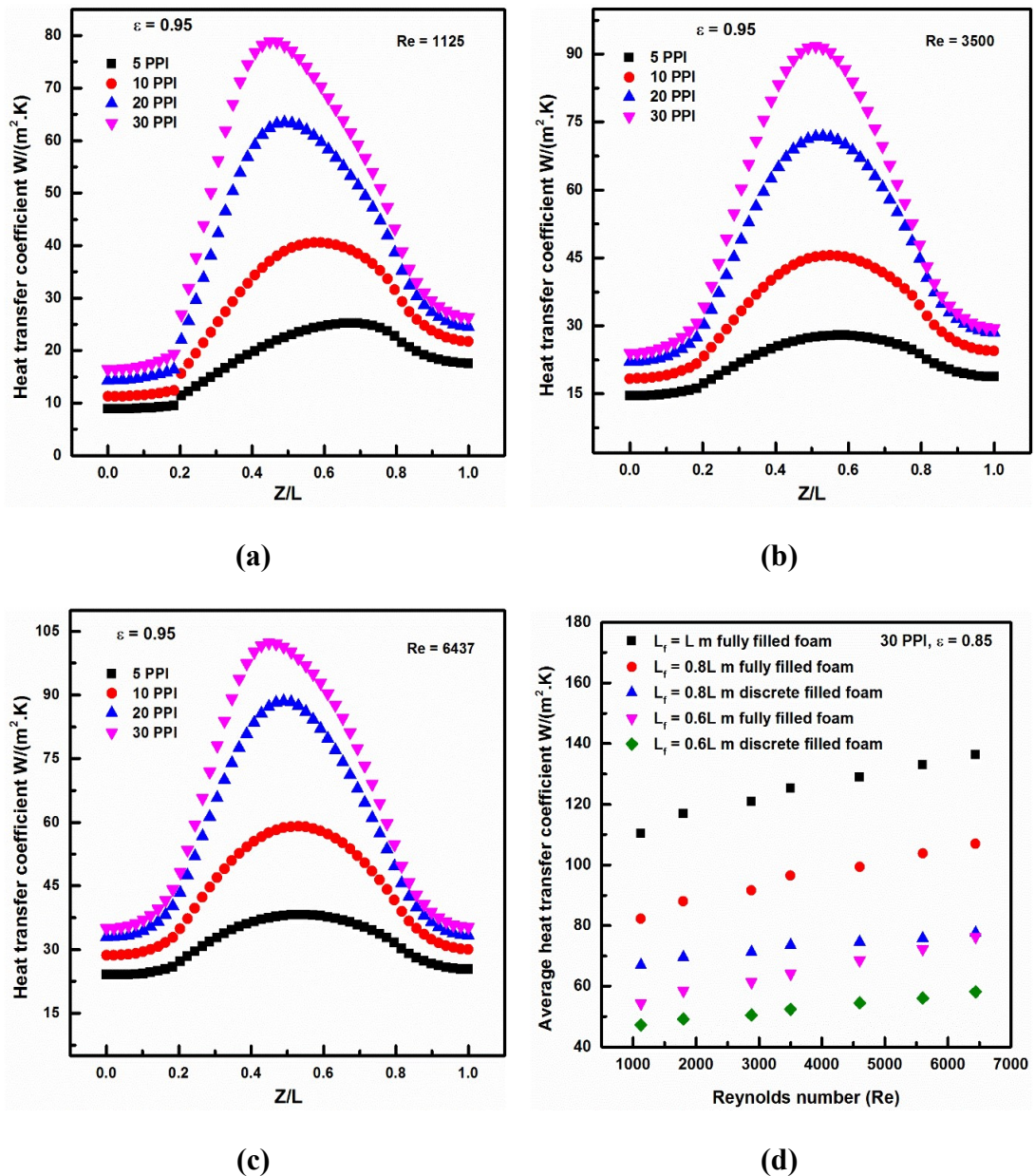


Figure 3.10 Illustration of convection coefficient for 0.6L m filled foam with various PPI of metallic foam for (a-c), (a) laminar, (b) transition, (c) turbulent flows and (d) Average convection coefficient for different filling rate of metallic foam.

3.8.4 Average Nusselt Number

The local Nusselt number is computed based on D_h of the pipe and it is defined in Eq. (3.19).

$$Nu_i = \frac{h_i D_h}{\lambda_{air}} \quad (3.19)$$

Where, Nu_i represents local Nusselt number of each set of data points, h_i represents local convection heat transfer coefficient of each data set of points in $W/(m^2.K)$, D_h represents hydraulic diameter of the pipe in m and λ_f represents fluid thermal conductivity in $W/(m.K)$.

The hydraulic diameter of the pipe is calculated using Eq. (3.20).

$$D_h = \frac{4A_c}{P} \quad (3.20)$$

Where, A_c represents cross sectional area of the pipe in m^2 and P is the perimeter of the pipe in m.

The average Nusselt number is evaluated by Eq. (3.21).

$$\overline{Nu} = \frac{\bar{h} D_h}{\lambda_f} \quad (3.21)$$

Where, \overline{Nu} is the average Nusselt number, \bar{h} represents the average heat transfer coefficient $W/(m^2.K)$ and D_h is hydraulic diameter (m) and λ_f is thermal conductivity of fluid $W/(m.K)$.

The Reynolds number is computed based on the hydraulic diameter and is defined as

$$Re = \frac{\rho_f u D_h}{\mu_f} \quad (3.22)$$

The variation of mean Nusselt number for the pipe for different flow characteristics is depicted in Figure 3.11. Figure 3.11(a) demonstrates the changes in mean Nusselt number of different porosities for all the flow features of 30 PPI metal foam. From the results, it is noticed that the average Nusselt number decreases with increment in the porosity of the metal foam for all the flow characteristics. This is due to the fact that with increasing porosity of the metallic foam, the surface area density reduces that tends

to decrease the heat transfer coefficient which is directly proportional to the surface Nusselt number. At a particular porosity of the metallic foam, the heat dissipation rate decreases with increase in Re . For the porosity of 0.90 the decrease of 4.47% in average Nusselt number is obtained compared to porosity of 0.85 for $Re = 6437$. Similar results are obtained for other PPI's of the metal foam for different flow regimes.

Figure 3.11(b) demonstrates the variation of mean Nusselt number for four distinct PPI's (i.e. 5, 10, 20 and 30 PPI) for laminar, transition and turbulent flow for porosity of 0.85 metal foam. The result reveal that with increase in the PPI of the metallic foam the average Nusselt number increases for all flow regimes. The heat dissipation increases as Reynolds number increases for a particular PPI of the metallic foam. For example, 20 PPI metal foam shows 20.44% and 49.99% increase in heat transfer for transition and turbulent flows compared to laminar flow regime. Similar kind of results is observed for other PPI of the metallic foam.

Figure 3.11(c) demonstrate the changes in mean Nusselt number with flow Reynolds number for distinct PPI of metallic foam with a porosity of 0.95. For the purpose of comparison, the Nusselt number obtained for clear pipe (empty pipe) is also shown in the figure. As expected, an increase in the thermal performance is seen with increase in Re for all the pore density metal foams as well as for the clear pipe. The improvement in rate of heat transfer by adding metallic foam porous structures is seen clearly from the plot and it is also noticed that at particular Re , the thermal performance augments with increase in the PPI of the metallic foam. For example, at $Re = 1125$, the 20 PPI and 30 PPI metallic foams give 42.92% and 71.22% increase in heat dissipation compared to 10 PPI metallic foam.

Figure 3.11(d) explored the difference in average Nusselt number for various filling rate metallic foam for 30 PPI with respect to flow Re . From the results it is observed that the 1L m fully filled metal foam shows the highest average surface Nusselt number compared to other filling rate of metallic foam with respect to flow Reynolds number. 1L m fully filled metallic foam shows the average Nusselt number increase of 98.67%, 91.06% and 75.04% compared to 0.6L filled metallic for laminar, transition and turbulent flow regimes, respectively. However, with insertion of 0.6L m discrete and 0.8L m discrete metallic foams, it is found that the highest decrease in the average

Nusselt number occurs at higher flow rates compared to 0.6L m filled and 0.8L m fully filled foams. The average Nusselt number decrease of 15.03% and 20.93% is observed compared to 0.6L m filled and 0.8L m continuous filled foam in the range of Re 1125 to 6437.

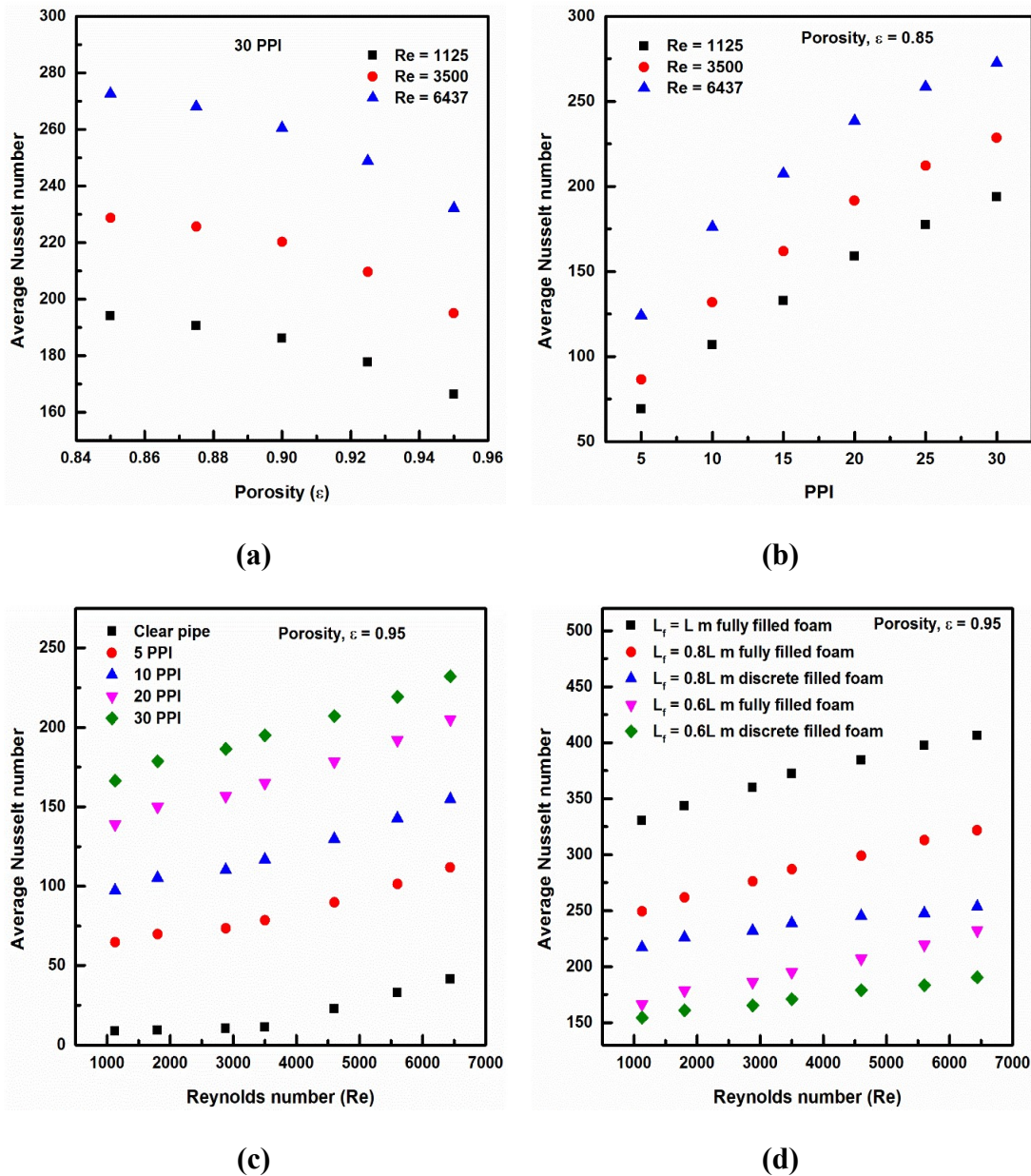


Figure 3.11 Average Nusselt number of 0.6L m fully filled foam for (a-c), (a) varying porosities (b) varying PPI (c) varying Re for 0.6L m fully filled foam and clear pipe and (d) Average Nusselt number of various filling rate of metallic foams with Re .

From the Figure 3.11(d), it is also noticed that, 0.6L m discrete metal foam gives marginally similar heat transfer rate compared to 0.6L m filled foam while 0.8L m discrete metallic foam gives significant changes in mean Nusselt number compared to 0.8L m continuous filling metal foam in the laminar flow regime. Hence, for better augmentation of heat dissipation the discrete insertion of metallic foam is not preferable.

The changes in mean Nusselt number for a range of Re number is shown in Figure 3.12. Figure 3.12(a) demonstrates the changes in mean Nusselt number with Re for distinct pore densities of metallic foam for a porosity of 0.90. The result obtained for average Nusselt number is compared with (Baragh et al. 2018). The average Nusselt number increases by 86.22%, 119.55% and 141.86% for 20 PPI, 30 PPI and 40 PPI respectively in the range of $Re = 1125$ to 6437 compared to (Baragh et al. 2018). Similar kind of results is observed in the literatures (Baragh et al. 2018; Pavel and Mohamad 2004).

Figure 3.12(b) demonstrate the changes in mean Nusselt number with inflow Re for distinct PPI metallic foam for a porosity of 0.95. The result of average Nusselt number is compared with the results reported in (Baragh et al. 2018). As estimated, the heat transport rate increases for 20 PPI, 30 PPI and 40 PPI of the metallic foam compared to (Baragh et al. 2018) for laminar ($Re = 1125$), transition ($Re = 3500$) and turbulent ($Re = 6437$) flow regimes. By extending the present analysis for 40 PPI metallic foam with the porosity of 0.9, the increase of 146.3% and 162.5% in average Nusselt number is obtained compared to (Baragh et al. 2018) for transition and turbulent flow regimes. Furthermore, for 40PPI with porosity of 0.95, the increase of 88.8%, 151.1% and 130.11% in average Nusselt number corresponding to laminar, transition and turbulent flows is observed compared to (Baragh et al. 2018) with penalty of pressure drop.

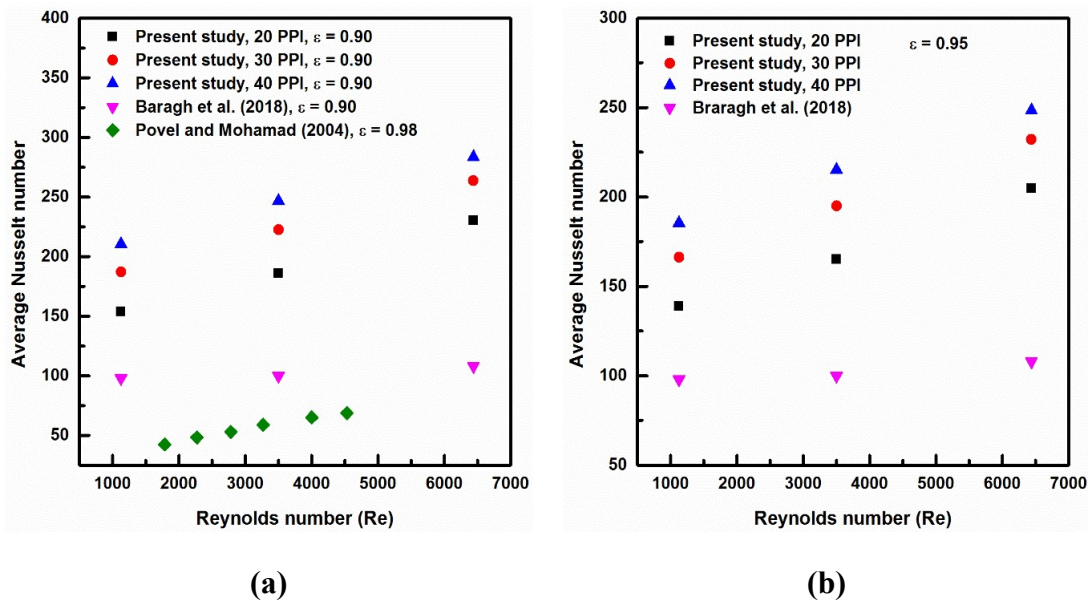
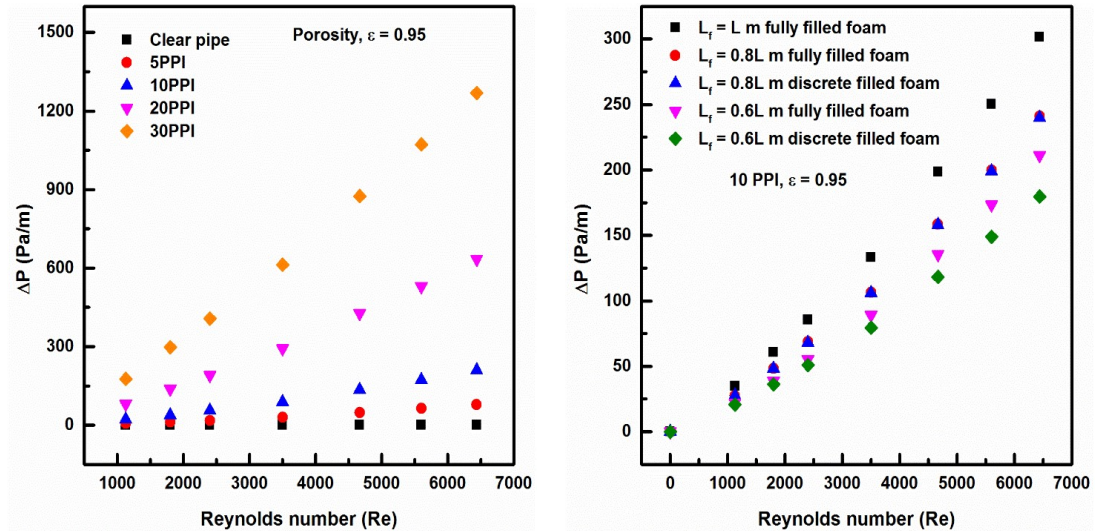


Figure 3.12 Comparison of mean Nusselt number for different PPI, (a) comparative results (b) porosity 0.95, with (Baragh et al. 2018).

3.8.5 Pressure Drop Study

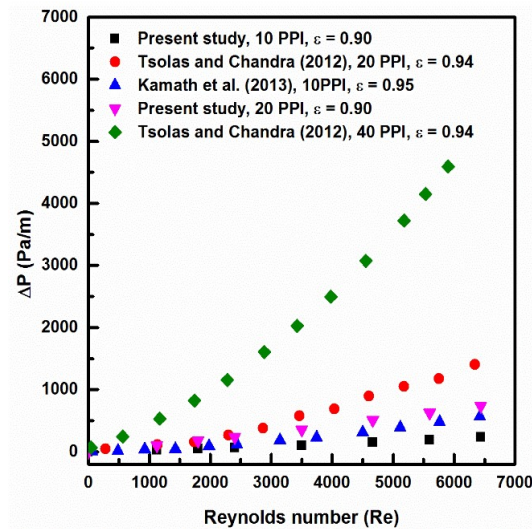
Figure 3.13(a) shows the variations in pressure loss across the length of pipe with inlet velocity for metal foam of 0.95 porosity with varying pore densities. The pressure loss increases as inflow velocities of fluid increases for all the PPI of the metallic foam. It is noticed that at specific velocity the pressure loss increases as PPI of the metallic foam increases. Figure 3.13(b) explored the pressure loss across the length of pipe for various filling rate of 10 PPI metallic foam with different fluid velocity. From the figure, it is observed that the pressure drop increases with increasing filling rate of metallic foam. Among various filling rate of metallic foam, 1L m fully filled metal gives the highest pressure drop across the length of pipe than the other filling rate of the metallic foam. From the figure, it is noticed that the pressure drop for 0.8L m discrete metal foam and 0.8L m continuous filled foam is the same for all velocity of fluid. Nevertheless, for fluid velocity less than 0.6m/s, the deviation of the pressure drop among all the cases considered in this work is marginally comparable. Though there is no change in the pressure drop for 0.8L m discrete metal foam and 0.8L m continuous filled foam cases, there is a slight deviation in pressure drop for 0.6L m discrete metal foam compared to 0.6L m fully filled foam for the fluid velocity more than 0.6m/s. Similar pressure drop

study is seen in literature (Kamath et al. 2013; Tsolas and Chandra 2012) which is also illustrated in Figure 3.13(c).



(a)

(b)



(c)

Figure 3.13 (a) Pressure drop for varying PPI and clear pipe, (b) changes in pressure drop for various filling rate of metallic foams and (c) comparisons of pressure drop results.

3.8.6 Friction Coefficient (f) Study

The friction coefficient across the pipe is evaluated using the pressure drop among the entry and outlet of the pipe and is given by Eq. (3.23).

$$f = \frac{2\rho_f \Delta P D_h}{u_{in}^2 L} \quad (3.23)$$

where, ΔP is the difference in pressure among the entry and outlet of the pipe (Pa), D_h is the hydraulic diameter (m), u_{in} is the inlet velocity (m/s) and L is the length of the pipe (m).

Figure 3.14(a) shows the changes in average friction coefficient with inlet flow velocities for distinct pore densities of 0.95 porosity metallic foam. The friction coefficient shows a decline with respect to fluid entry velocity for all pore densities of metallic foams considered in the current study. It is clear from the results that the friction coefficient increases as PPI of the metallic foam increases for range of Reynolds number studied. This is due to more obstruction of the flow as PPI increases, hence the friction is expected to be more compared to clear pipe case. When the fluid velocity increases the fluid is forced to enter the pores of the metal foam that results in less friction at higher velocities. The changes in friction coefficient across the length of pipe for various filling rate of metallic foam with fluid velocity is depicted in Figure 3.14(b). The figure explored that the friction coefficient reduces with increasing fluid velocity for all filling rate of the metallic foams. From the figure, it is noticed that the 0.8L m fully filled foam and 0.8L m discrete metal foam provide very similar results for all flow rates while 0.6L m discrete metallic foam reduced the friction coefficient compared to 0.6L m fully filled foam with respect to inlet fluid velocity.

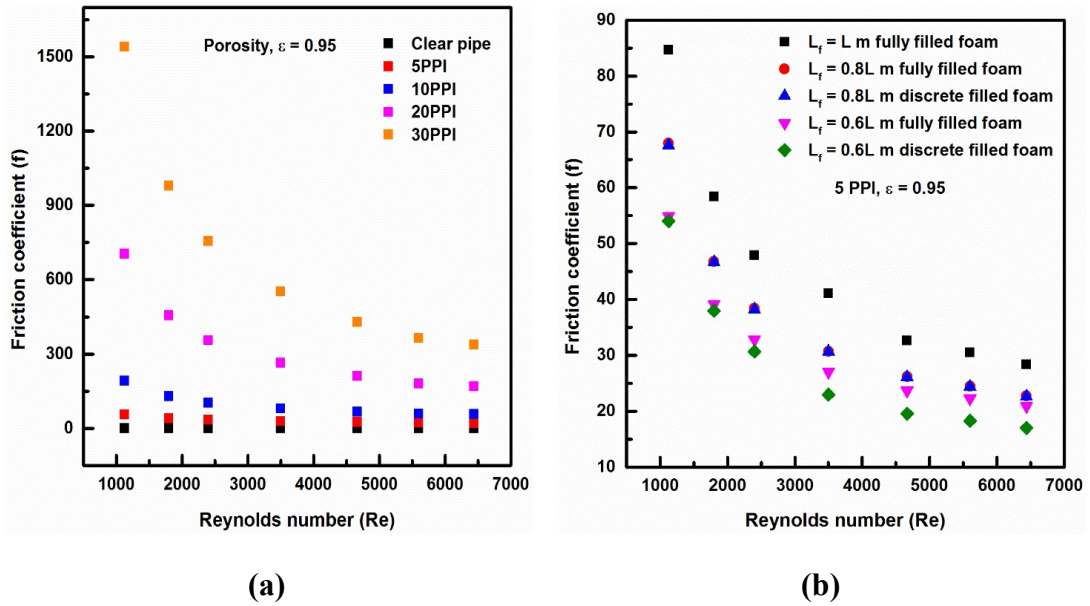


Figure 3.14 (a) Friction coefficient for varying PPI and clear pipe and (b) Friction coefficient for various filling rate of metallic foams.

3.8.7 Heat Transfer Enhancement Ratio (Nu_{ER})

The effectiveness of heat exchanger is examined from heat transfer enhancement ratio and is defined as the ratio of mean Nusselt number for fully filled foam to the mean Nusselt number for the clear pipe.

$$Nu_{ER} = \frac{\overline{Nu}}{\overline{Nu}_{\phi}} \quad (3.24)$$

where, Nu_{ER} is referred as heat transfer enhancement ratio, \overline{Nu} represents mean Nusselt number for metallic foam filled in the pipe and \overline{Nu}_{ϕ} represents mean Nusselt number of empty pipe.

The Nu_{ER} for different PPI with corresponding Re is presented in Figure 3.15(a). It is recorded that the heat transfer enhancement ratio declines with increasing velocity of the flowing fluid for all the metallic foams considered in the current study. It is also seen that the Nu_{ER} is greater at lower flow rate related to higher flow rates, this is because of less residence time of the fluid in conjunction with the metal foam during higher Reynolds number. The metal foam of 30 PPI shows higher rate of heat transfer enhancement ratio than the other PPI's of the porous metallic foam considered in the

current research for various Reynolds numbers studied. Hence, from the results it is concluded that the increase in PPI of the porous metallic foam increases the Nu_{ER} for all the flow regimes. Similar kind of results are obtained for other porosities and pore density of the porous metallic foam in a fully filled pipe.

The Nu_{ER} for various filling rate of metallic foam with corresponding Re is depicted in Figure 3.15(b). The 1L m fully filled metal foam shows the highest Nu_{ER} than the other filling rate of metallic foam in laminar, transition and turbulent flow regimes respectively. The 1L m fully filled foam shows the increase in Nu_{ER} of 102.05%, 94.03% and 77.93% than the 0.6L m filled foam when Re equal to 1125, 3500 and 6437, respectively. From the figure it is observed that the 0.8L m discrete and 0.6L m fully filled foam shows same Nu_{ER} in turbulent flow regime. Beyond $Re = 6437$, one can choose 0.6L m fully filled foam rather than 0.8L m discrete filled metal foam for the same heat dissipation with less pressure drop.

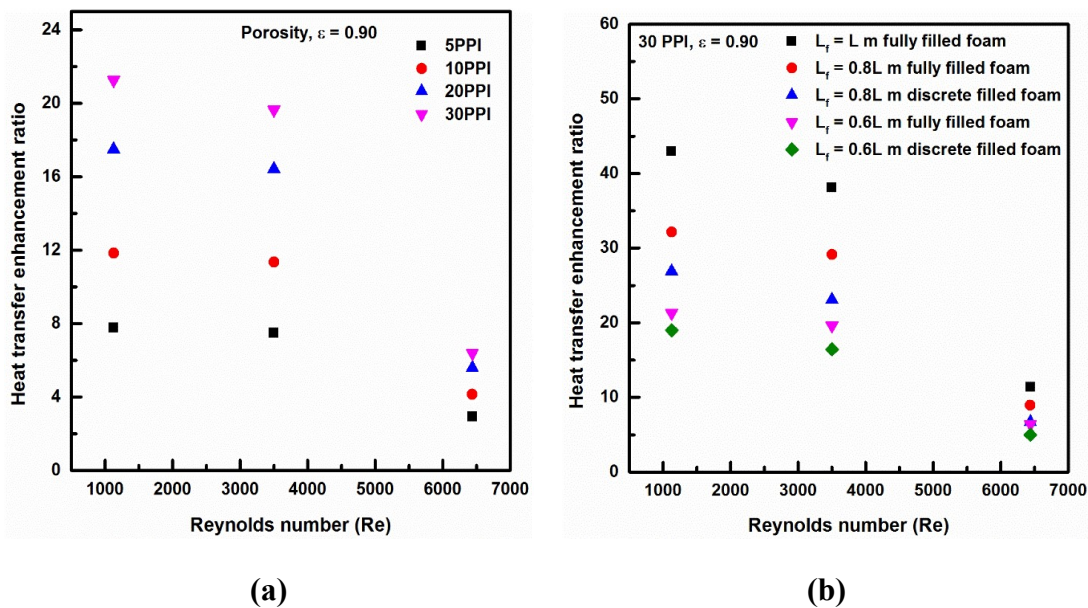


Figure 3.15 Nu_{ER} with varying Re (a) For 0.6L m fully filled foam varying PPI of metal foam and (b) various filling rate of metal foam.

3.8.8 Performance Factor (η_p)

The thermal performance factor is computed using the dimensionless parameter called performance factor which is defined as ratio of Colburn j factor to pumping power of the fluid which is given by (Manglik (2003)).

$$\eta_p = \frac{j}{f^{\frac{1}{3}}} \quad (3.25)$$

The performance factor increases with increasing filling rate of metallic foams and reduces with increasing flow rates of the fluid. Figure 3.16(a) explored that the performance factor is found to be highest for 1L m and 0.8L m fully filled metallic foams in laminar flow regime and it reduces in transition and turbulent flow regimes respectively. From the figure, it is noticed that there is a significant change in performance factor in transition flow regime and similar results are found in turbulent flow regime for 0.8L m discrete and 0.6L m fully filled foam.

The present study is also extended to 40 PPI with various filling rate of metallic foams. The variation of performance factor for various filling rate of metallic foam with flow Reynolds number is presented in Figure 3.16(b). From the figure, it is observed that the performance factor is found to be above 1 for 1L m fully filled and 0.8L m filled metallic foams and is closer to 1 for 0.8L m discrete metallic foam in laminar flow regime. The increase in performance factor of 105.56%, 52.5% and 17.5% for 1L m fully filled, 0.8L m continuous filled and 0.8L m discrete filled metallic foam, respectively compared to 0.6L m filled foam at Re equal 1125. From the figure, it is also noticed that the performance factor found to be the same beyond $Re = 3500$ for 0.8L m discrete and 0.6L m filled foam. By comparing Figure 3.16(a & b) for 40 PPI metallic foam, the performance factor increases 13.82%, 20.2% and 7.2% compared to 30 PPI metallic foam for 1L m fully filled, 0.8L m fully filled and 0.8L m discrete filled foam in laminar flow regime, respectively. Moreover, the 30 PPI metallic foam shows significant changes in the performance factor in the transition flow regime while 40 PPI metallic foam shows marginally similar results in transition flow regime for 0.6L m fully filled foam rather than 0.8L m discrete metallic foam. Additionally, the performance factor shows similar results in turbulent flow regime. Nonetheless, beyond

Re equal to 3500 one can select 0.6L m filled foam rather than 0.8L m discrete metallic foam for the same performance factor with minimum pressure drop.

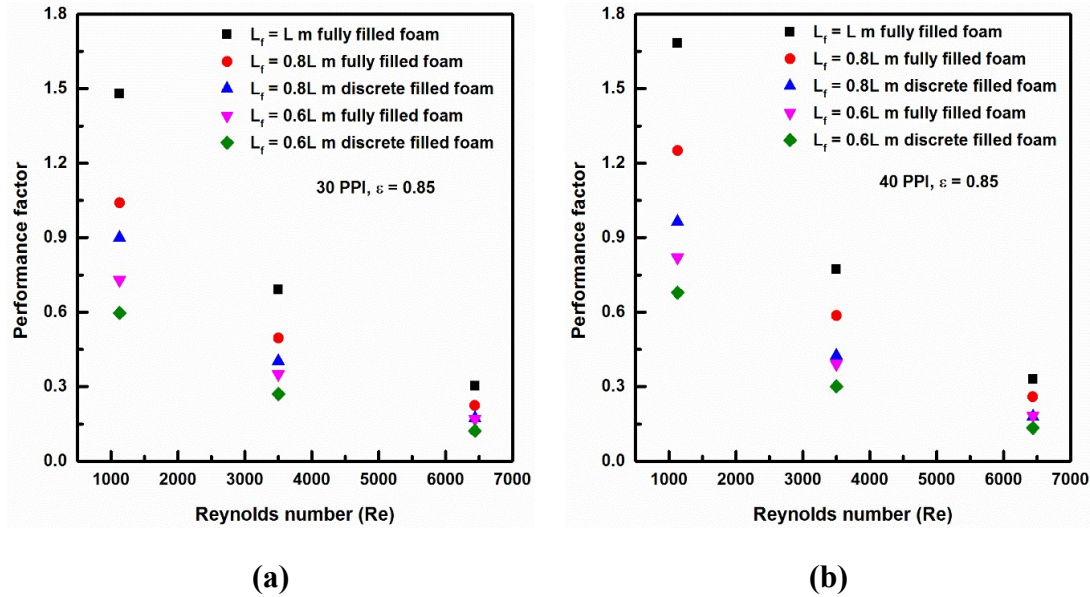


Figure 3.16 Variation of η_p for various filling rate of metallic foams with Re for (a) 30 PPI metallic foam (b) 40 PPI metallic foam.

3.9 SUMMARY

The horizontal pipe of length 1 m, diameter 0.1 m and 7 mm thick filled with aluminium metal foam of different pore density and porosities was considered for the numerical exploration. The features of fluid flow and heat transfer are computed for various flow regimes like laminar ($Re = 1125$), transition ($Re = 3500$) and turbulent ($Re = 6437$). Based on the present study, the salient features made are as follows.

- The wall temperature of 0.6L m fully filled foam reduces with increasing PPI of the metallic foam for all the flow characteristics considered in the investigation.
- The convection coefficient increases with increasing PPI of the metallic foam for a constant Re . 1L m fully filled foam shows highest heat transfer coefficient compared to other filling rate of the metallic foam in laminar ($Re = 1125$), transition ($Re = 3500$) and turbulent ($Re = 6437$).

- The 1L m fully filled and 0.8L m fully filled metallic foam shows the average Nusselt number increase of 86.95% and 44.64% compared to 0.6L m fully filled foam for the range of Re number from 1125 to 6437 with the penalty in pressure drop.
- For the insertion of 0.8L m discrete metallic foam, the average heat dissipation rate decreases by 17.3% compared to 0.8L m fully filled foam for the Reynolds number 1125 to 6347. In general, one can choose 0.8L m fully filled foam rather than 0.8L m discrete metallic foam for augment in heat transfer with the same pressure drop and friction coefficient.
- The Nu_{ER} is higher at low flow rate and improves with increasing PPI and length of the metallic foam and reduces with increasing flow Re . Beyond or $Re = 6437$ one can select 20 PPI and 0.6L m fully filled foam instead of 30PPI and 0.8L discrete metallic foam with the minimum pressure drop.
- The performance factor increases with increasing the length of the foam (i.e., $L_f = 0.6L$ m fully filled foam, $L_f = 0.8L$ m fully filled foam and $L_f = 0.6L$ m fully filled) and PPI of the metallic foam for laminar ($Re = 1125$), transition ($Re = 3500$) and turbulent ($Re = 6437$) flow regimes respectively. Beyond $Re = 3500$, one can choose 0.6L m fully filled foam rather than 0.8L m discrete metallic foam with minimum pumping power.

3.10 CLOSURE

The detail explanation of the forced convection heat transfer through the pipe filled with high porosity aluminium metal foam was discussed in this chapter. The five different numerical domains were considered with the effect of metal foam length (i.e., fully and discrete filled metal foam), pore density and porosity of the foam with mass flow rate for the investigation. The next chapter considers the variation of foam layer thickness (partial filling foam) from the wall side and from core side of the pipe in order to reduce the pressure drop and improve the thermo-hydrodynamic performance of the heat exchanger.

CHAPTER 4

PERFORMANCE EVALUATION OF PARTIALLY FILLED HIGH POROSITY METAL FOAM CONFIGURATIONS IN A PIPE

4.1 INTRODUCTION

This chapter explores the numerical investigation of performance evaluation of partially filled high porosity metal foam configurations in a pipe. The investigation includes six different models partially filled with metallic foams by varying inner diameter of foams from the wall side and external diameter of foam from the core of the pipe. The pore density of the aluminium foam ranges from 10 to 45 PPI and their porosity varies from 0.90 - 0.95 and copper foam having a pore density of 10 PPI with porosity of 0.88. The methodology considered to compute the complex porous structure of the metal foam is described and the results of velocity distribution, solid-fluid temperature distribution, Nusselt number, heat transfer enhancement ratio and thermo-hydrodynamic performance of partially filled foam pipe are plotted and discussed.

4.2 PROBLEM STATEMENT

In this study, a straight horizontal pipe of length 1 m, diameter 0.10 m, and a wall thickness of 7 mm is considered according to (Baragh et al. (2018)). The heater is embedded circumferentially over the pipe wall along its length and the heater is defined with uniform heat flux of 275 W/m^2 (Baragh et al. (2018)). In the existing research, the aluminium foam is filled partially inside the pipe with four different pore densities of 10 PPI, 20 PPI, 30 PPI and 45 PPI with their porosities ranging from 0.90 to 0.95 and a comparison is made with the copper foam having a pore density of 10 with porosity of 0.88 (Kamath et al. (2011 & 2013) and Kotresha and Gnanasekaran (2018)). The flow inside the pipe is assumed to be turbulent whose Reynolds number is varying from 4500 to 20500 and is evaluated based on hydraulic diameter of the pipe. However, flow

inside the porous layer thickness is considered to be laminar where the Reynolds number based on permeability is less than 150 as per (Neild and Bejan 2006). Subsequently, a novel parametric exploration is performed in order to improve the thermal performance and minimize the pressure drop of the metal foam filled pipe. For a detailed analysis, totally six different models (domains) are considered for the computational domain and the turbulent flow characteristics and the thermal performance of partially filled foams inside the pipe are examined, shown in Table 4.1. In model 1 to model 3 (i.e., M1, M2 and M3), the external diameter of the foam is fixed and is equal to the diameter of the pipe while the internal diameter of foam is varied from the wall to the core of pipe. In the model 4 to model 6 (i.e., M4, M5 and M6), the external diameter of the foam is increased from the core to towards the wall of the pipe while internal diameter of the foam is made equal to zero which is clearly shown in the Table 4.1. The dimensions of all the six models are presented in the Table 4.2.

Table 4.1 Schematic of the various models considered for the present study.

Models	M1	M2	M3	M4	M5	M6
Partially foams filled in a pipe						
	Grey colour indicates metal foam filled region.					
	White colour indicates clear region.					

Table 4.2 Dimensions of the partially filling metallic foams.

Models	d_{if} (m)	D_{of} (m)
M1	0.06	0.10
M2	0.04	0.10
M3	0.02	0.10
M4	0.00	0.04
M5	0.00	0.06
M6	0.00	0.08

4.3 NUMERICAL DOMAIN AND BOUNDARY CONDITIONS

The pipe is axis symmetry about the centerline along the stream (i.e., z -direction) flow (Pavel and Mohamad (2004)); henceforth, a two-dimensional computation domain is considered which is shown in Figure 4.1. At the entrance, the length of pipe is extended by $2L$ in order to achieve a developed flow (Sunden (2012)); while at the exit, length of the pipe is extended by $1.5L$ to eliminate the exit effect (Mohammed et al. (2013) and Lin et al. (2016)). A constant velocity profile is defined at the inlet of the pipe. The adiabatic wall boundary conditions are defined at entry and exit length of the pipe walls. The heater is fixed to the pipe wall and is assigned with constant heat input of 275 W/m^2 as per (Baragh et al. (2018)).

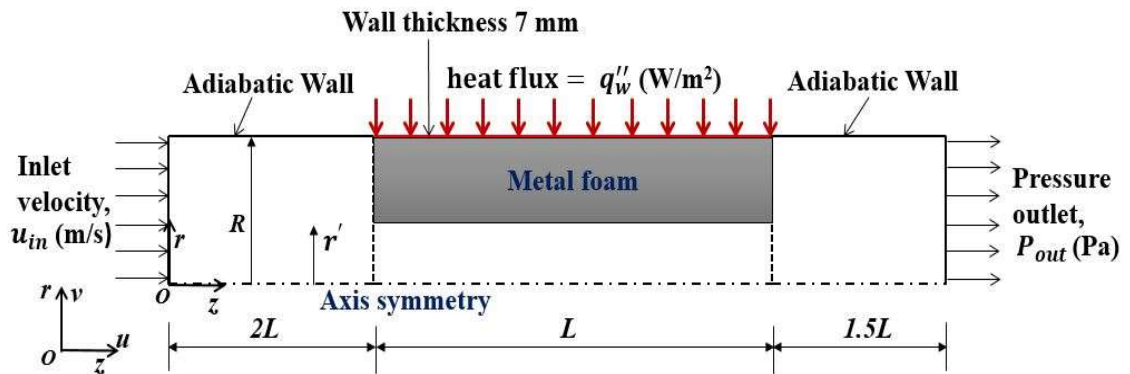


Figure 4.1 Representation of computational domain.

Because of the axis symmetry, only above half part of the pipe is considered for the computational domain (Mahmoudi and Karimi (2014)). For the computational domain, the details of the boundary conditions are incorporated based on the literature (Mahmoudi and Karimi (2014)), which are depicted in Table 4.3.

Table 4.3 Boundary conditions imposed for the numerical investigation.

Boundaries	Boundary conditions
Inlet	$Z = 0: u = u_{in}, v = 0, T = T_{in}$
Outlet	$Z = 4.5 L: P = P_{atm}, \frac{\partial T}{\partial Z} = 0$
Entry wall and exit wall	$r = R: v = 0: u = 0, \frac{\partial T}{\partial r} = 0$
Heated wall	$r = R: u = 0: v = 0, q = q''_w$
Horizontal axis	$r = 0: v = 0: \frac{\partial u}{\partial r} = 0, \frac{\partial T}{\partial r} = 0$
Interface between wall and metal foam	$r = R: u = 0, v = 0, q''_w = - \left\{ \lambda_{fe} \frac{\partial \langle T \rangle^f}{\partial r} + \lambda_{se} \frac{\partial \langle T \rangle^s}{\partial r} \right\} \Big _{Interface}$

Apart from the boundary conditions, interfacial coupling conditions between porous medium and clear fluid are required to close the governing Eqs. (3.1) – (3.12) presented in Chapter 3. For the heat and fluid flow, the continuity in velocity, shear stress and heat flux at porous medium and clear fluid interface must be assured to have physical significance as depicted in Table 4.4 as per literature (Alazmi and Vafai (2001); Mahmoudi and Karimi (2014); Qu et al. (2012); Xu and Gong (2018)). The porous foam zone and the clear fluid zone are modelled by creating two different cell zones in the ANSYS FLUENT 19.2. The interfaces at the two cell zones assist as coupling conditions at the porous zone and clear fluid zone. In ANSYS FLUENT 19.2, on account of LTNE model the solid and fluid phases bifurcate separately. In the porous zone, the computed values of input properties of the metallic foam are given as per LTNE model to determine the characteristics of heat transfer between the fluid and solid phases.

Table 4.4 The interface coupling conditions at porous medium and the clear fluid.

Velocity of fluid	$u _{Interface^+} = u _{Interface^-}$
Temperature of fluid	$T_s _{Interface^+} = T_f _{Interface^-}$
	$\left(\lambda_{fe} \frac{\partial \langle T \rangle^f}{\partial r} + \lambda_{se} \frac{\partial \langle T \rangle^s}{\partial r} \right) \Big _{Interface^+} = \lambda_f \frac{\partial T_f}{\partial r} \Big _{Interface^-}$
Shear stress	$\frac{\mu_f}{\varepsilon} \frac{\partial \langle u \rangle}{\partial r} \Big _{Interface^+} = \mu_f \frac{\partial u}{\partial r} \Big _{Interface^-}$
Heat flux	$\lambda_{se} \frac{\partial T_s}{\partial r} \Big _{Interface^+} = h_{sf} (T_s _{Interface^+} - T_f _{Interface^-})$

4.4 DETAILS OF NUMERICAL COMPUTATION

The numerical computations are examined using software ANSYS FLUENT 19.2. The properties of air are computed based on the inlet temperature of the fluid. The velocity of air is varying from 0.6639 m/s to 3.0246 m/s; henceforth, the Re is calculated based on hydraulic diameter (i.e., $D_h = 4A_c/P$) of pipe that ranges from 4500 to 20500 (Kamath et al. (2013); Lin et al. (2016); Yang and Hwang (2009)). The flow inside the pipe is assumed to be turbulent. The two equation $k-\omega$ turbulence model is employed to predict the features of turbulent flow in the non-foam region of the pipe. The governing equations involved in non-porous region of the pipe are reported in Chapter 3 of Eqs. (3.1) – (3.7).

The governing equations of the $k-\omega$ turbulence model is given in detail in (ANSYS FLUENT (2019)). The porous region of the pipe is assumed to be an isotropic homogeneous medium. The Darcy extended Forchheimer (DEF) flow model is employed to envisage the features of air flow in the porous foam region inside the pipe. In the momentum equation, the DEF model is added as a source term. In the porous medium; the viscous and inertial loss terms are taken into account in the momentum equation due to permeability and form drag coefficient, respectively. The flow within the aluminium foam layer is assumed to be laminar whose permeability based Reynolds is less than 150 (Neild and Bejan (2006)). The governing equations are considered for calculating in foam filled region of the pipe are reported in Chapter 3 of Eqs. (3.8) –

(3.13) (ANSYS FLUENT (2019); Huang et al. (2010); Mahmoudi and Karimi (2014); Yang and Hwang (2009)).

The heat dispersion in the porous region is considered to be insignificant in the present numerical analysis due to high conductivity of foams and working fluid air (Calmidi and Mahajan (2002)). The pressure-velocity coupling with pseudo transient scheme is employed for the numerical computation. The second order discretization is considered for the pressure, momentum and energy equations. The convergence criteria for continuity and momentum and for $k-\omega$ turbulence model and for energy equations are 10^{-5} , 10^{-3} and 10^{-10} respectively. For the present numerical study, the properties of the metallic foams are considered as per (Kamath et al. (2011 & 2013); Kotresha and Gnanasekaran (2018)) which is shown in the Table 4.5.

Table 4.5 Properties of aluminium and copper metallic foams (Kamath et al. (2011 & 2013); Kotresha and Gnanasekaran (2018)).

Foam Material	PPI	Porosity	Permeability (K) 10^7 , m^2	Uncertainty in (K) (%)	Form drag coefficient (C)	Uncertainty in (C) (%)
Al	10	0.95	2.480	± 7.95	94.98	± 2.45
	20	0.90	2.177	± 9.67	208.82	± 2.21
	30	0.92	1.644	± 9.83	148.97	± 3.68
	45	0.90	0.420	± 5.87	397.01	± 5.80
Cu	10	0.88	1.742	± 19.20	176.75	± 4.60

In the present study, the properties of metallic foam such as interfacial area density (a_{sf}) and interfacial heat transfer coefficient (h_{sf}) are evaluated based on suggested by (Calmidi and Mahajan (2002)) and (Zukauskas (1987)) reported in Chapter 3 of Eqs. (3.14) – (3.16). The superficial surface area properties of the metallic foams are evaluated and presented in the Table 4.6.

Table 4.6 Superficial surface area of aluminium and copper metallic foams.

Material	PPI	Pore size, d_p (mm)	Fiber size, d_f (mm)	Porosity, ε	Interfacial surface area, a_{sf} (m ⁻¹)
Aluminium foam	10	4.952	0.445	0.95	360.60
	20	3.416	0.451	0.90	960.65
	30	2.324	0.216	0.92	936.38
	45	1.654	0.184	0.90	1671.76
Copper foam	10	4.644	0.687	0.88	822.83

4.5 GRID INDEPENDENCE STUDY

The grid independence study is accomplished for the proposed numerical model to obtain optimum number of grids. 10 PPI aluminium foam with $\varepsilon = 0.95$ at $Re = 5000$ is selected for the study. A constant heat flux of 275 W/m^2 is assigned at wall of the pipe. In the present study rectangular element is considered for numerical simulations. The numerical study is accomplished for five different grid sizes of 31461, 38481, 45501, 52521 and 59541. The deviation of average wall temperature and pressure loss along the length of the pipe are computed based on higher grid size (base line data) and presented in the Table 4.7. Among the five distinct grid sizes, the grid size of 52521 is found to be significant in terms of percentage deviation of $\overline{T_w}$ and ΔP . Henceforth, the subsequent numerical computations are performed for the grid size of 52521.

Table 4.7 Grid independence study for 10 PPI, $\varepsilon = 0.95$ at $Re = 5000$ for model 3.

Number of grids	$\overline{T_w}$ (°C)	ΔP (Pa)	Deviation (%)	
			$\overline{T_w}$	ΔP
31461	37.59	44.77	1.51	5.23
38481	37.32	45.67	0.77	3.32
45501	37.19	46.78	0.43	0.97
52521	37.11	47.18	0.22	0.13
59541	37.03	47.24	Base line data	

4.6 VALIDATION OF NUMERICAL MODEL

In order to adopt the present approach, the results of top surface temperature and the pressure drop are compared with experimental results reported by (Garrity and Klausner (2015)) for 10 PPI and 40 PPI with a constant porosity of 0.918 aluminum foam which is shown in Figure 4.2. From the Figure 4.2(a), when the mean fluid velocity is less, the deviation between the present numerical and experimental results is found to be more for 10 PPI and 40 PPI aluminum foams. However, the deviation becomes less at higher mean velocity of air flow. Similar results have been reported in (Kotresha and Gnanasekaran (2019) and Lin et al. (2016)). The results of pressure drop is compared with experimental results of (Kamath et al. (2013)) for 10 PPI aluminum foam which is shown in Figure 4.2(b). The results of pressure drop are matching with (Kamath et al. (2013)). On the other hand, the deviation of pressure drop increases gradually at higher flow rate. The mean deviation of the pressure drop results is found to be 5.9%.

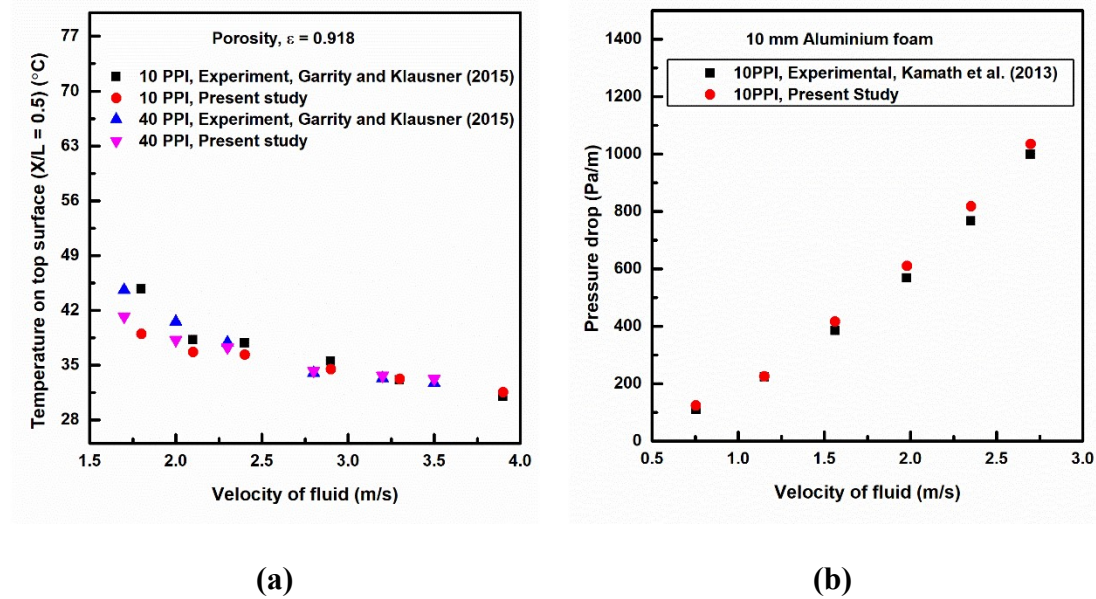


Figure 4.2 The variation of (a) temperature on the top surface with (Garrity and Klausner (2015)) and (b) pressure drop with (Kamath et al. (2013)).

In Figure 4.3, validation is done for dimensionless velocity. Validation of the numerical approach is important before analyzing the various model proposed in the present work. The validation study consists of parallel plates for three different heights (i.e., $H = 1$,

0.8 and 0.5 i.e., fully and partially filled foam) of 10 PPI aluminium metallic foam with porosity of 0.90 as per (Lu et al. (2016)) and the results are shown in Figure 4.3. The results of dimensionless velocity distribution along the dimensionless height of the channel obtained for the present study is agreeing well with the analytical results of (Lu et al. (2016)).

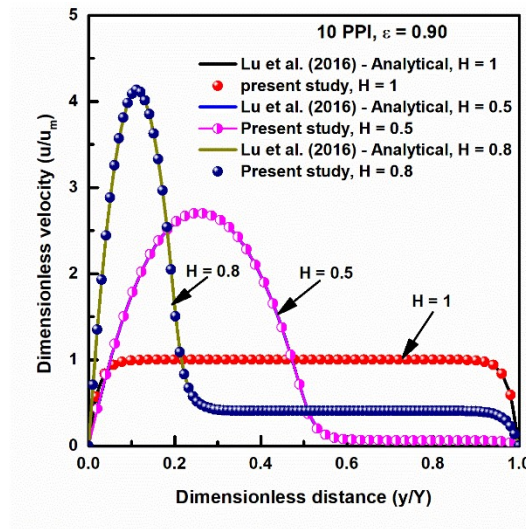


Figure 4.3 Variation in dimensionless velocity versus dimensionless height.

4.7 RESULTS AND DISCUSSION

4.7.1 Velocity and Temperature Distributions

Though we are interested in investigating the heat performance, the characteristics of the fluid in partially filled metal foam is very important. Therefore, the velocity variation is reported for different flow rates in the porous as well as non-porous foam filled region at exit ($Z = 3$ m) of the conduit. With these corresponding velocity profiles the temperatures are being measured at the exit ($Z = 3$ m) for Model 2 and Model 5. The velocity and temperature distribution results are plotted at the exit ($Z = 3$ m) of the pipe. Figure 4.4(a-b) presents the results of velocity of the fluid with respect to radius. Increasing inlet velocity of the air more flow happens in open-space region of the pipe; but, the velocity of the air decreases in the foam filled region. But, the trend of the velocity profile differs for the model 2 and model 5. The tendency of the velocity profile

is similar to the study of (Lu et al. (2016)).

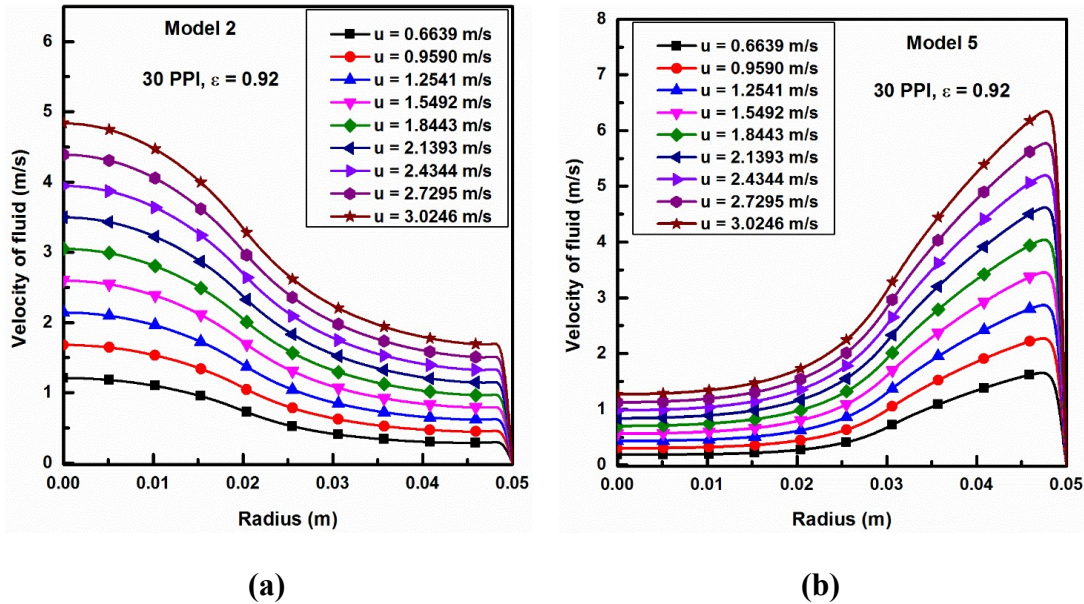


Figure 4.4 Velocity distribution at exit of the conduit along the radius for model 2 and model 5.

The variation in the temperature profile at the exit of the pipe with different flow rates of the fluid for the models 2 and 5 is shown in Figure 4.5(a) and (b), respectively. For any given velocity, say $u = 0.6639$ m/s, the temperature showed almost constant except near the wall of the pipe. However, the temperature at the exit of the pipe decreases with increasing inlet velocities of the fluid. It is also observed that for higher velocity of the fluid there is a significant reduction in exit temperature; however, as the velocity of the fluid approaches maximum the changes in the exit temperature are minimum which is clearly observed from Figure 4.5. The gradient of temperature at the surface of the pipe also takes attention. For the model 2 the gradient is higher than model 5 since inner surface of pipe is covered by metal foam. Hence more heat transfer from the surface to the fluid for the model 2 is expected.

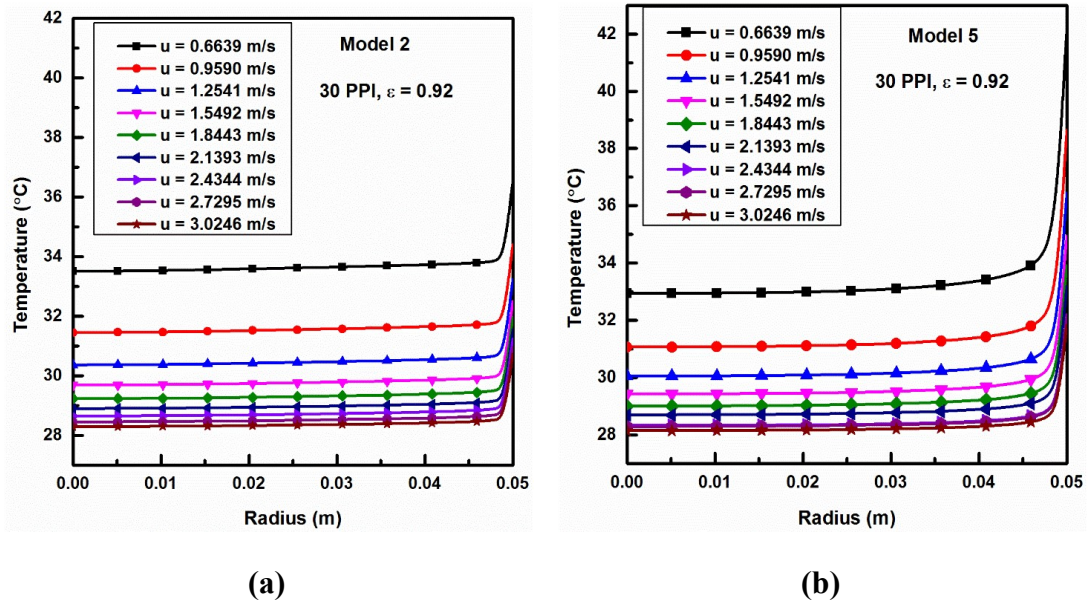
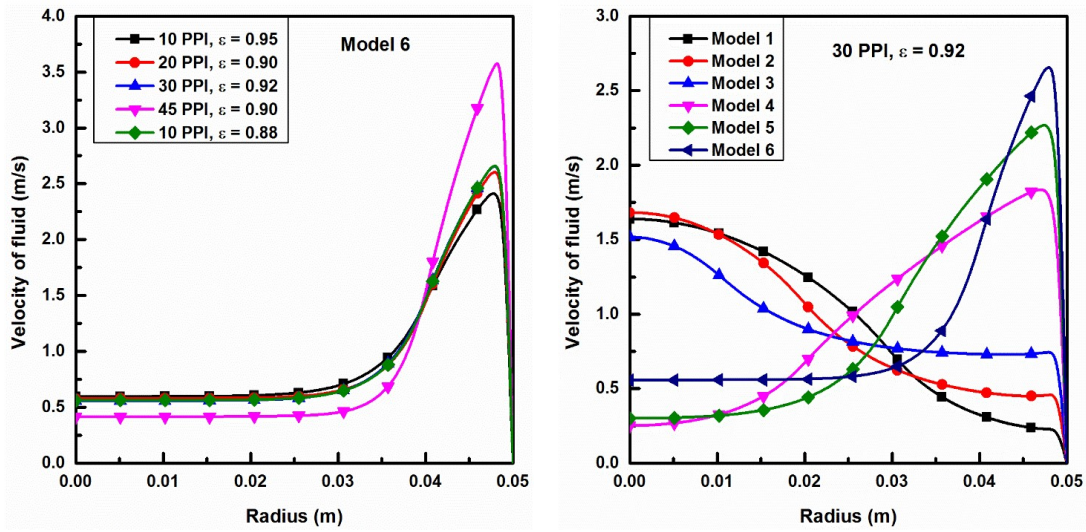


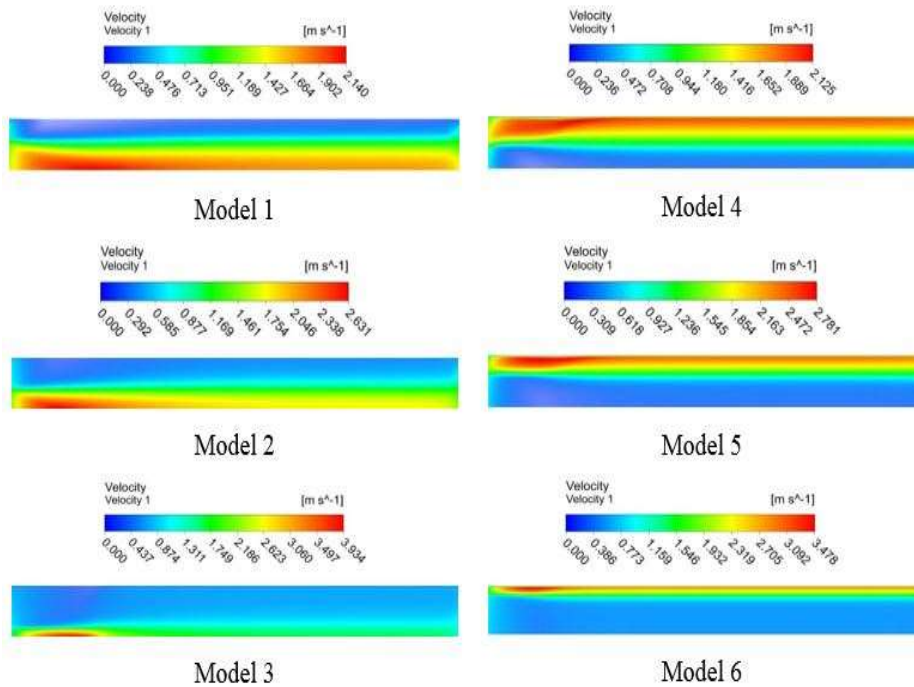
Figure 4.5 Temperature distribution at exit of pipe along the radius for model 2 and model 5.

In this context, the results of 45 PPI metallic foam show the highest decrease in velocity for the foam filled region and maximum velocity in the open passage of the pipe compared to the lower PPI's of the metallic foam as shown in Figure 4.6(a). With increasing PPI of the metallic foam, the size of the pore decreases which in turn increases the inertial resistance to the air motion; hence, the fluid rushes towards the open passage of the pipe. Reducing the internal diameter of the foam from wall towards core of the pipe (i.e., model 1, model 2 and model 3) the velocity distribution in the porous region decreases due to the resistance offered by the metal foam. Also, the model 3 shows lesser velocity in the non-foam region than the model 1 and model 2. This may be due to more amount of fluid concentrated at the porous region than the core of the pipe and narrow gap between foam and non-foam region. However, as the diameter of the foam increases from core to towards the wall of the pipe (i.e., model 4, model 5 and model 6), the velocity distribution increases in the foam as well as non-foam region of the pipe which is shown in Figure 4.6(b) and (c). This is because of the decrease in the open passage between the foam filled and the wall of the pipe that leads to more flow in the foam filled region. The tendency of velocity distribution is similar to (Kotresha and Gnanasekaran (2018) and Lu et al. (2016)). Similar kind of results is observed for the model 1, model 2 and model 3.



(a)

(b)



(c)

Figure 4.6 Velocity distribution for (a) Model 6 with varying PPI, (b) Model 1 – Model 6 for 30 PPI and (c) velocity contours for Model 1 – Model 6 for 30 PPI.

From the results, it is seen that the temperature variation at the exit of the pipe along the radius is found to be marginally higher for 45 PPI compared to other PPI's of the metallic foam in porous region while it reduces in the non-foam filled region of the pipe

which is shown in Figure 4.7(a). This is because the velocity in the foam filled region decreases due to smaller pore size which creates more turbulence that results in absorption of more heat from the wall. As the air flows through the open passage, the velocity of the flow increases which in turn reduces the capacity of heat absorption rate that leads to decrease in variation in exit temperature at higher PPI of the metallic foam. Similarly, for a 30 PPI of the metallic foam the temperature variation at exit of the pipe shows marginally higher for the model 1, model 2 and model 3 than that of model 4, model 5 and model 6 which is shown in Figure 4.7(b). This may be due to direct contact of the foams with the heated wall of the pipe for the first three models while metal foams are placed at core of the pipe for the last three models.

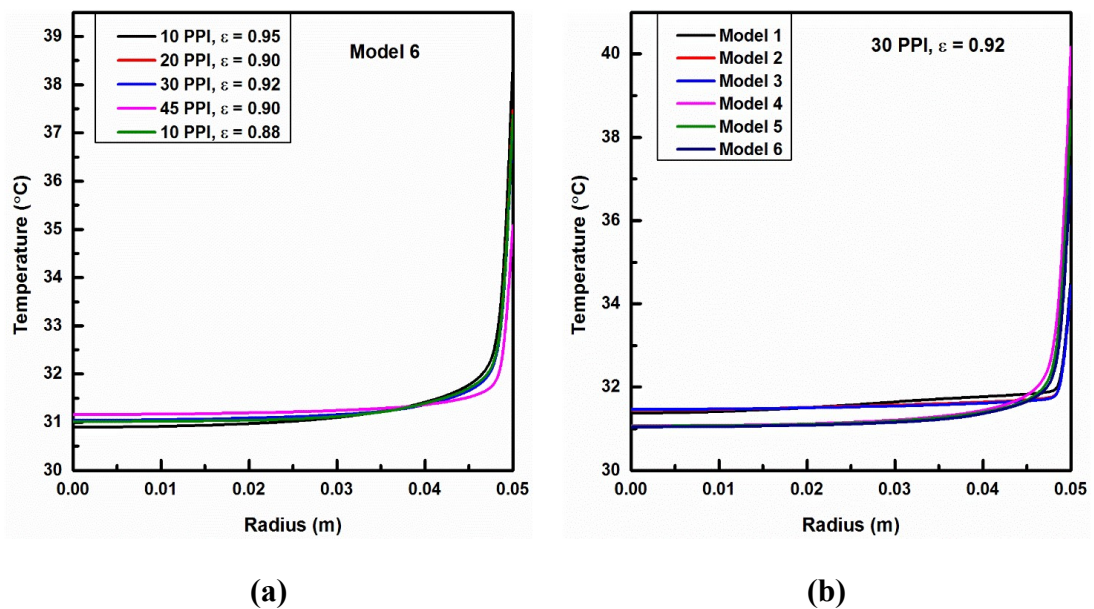


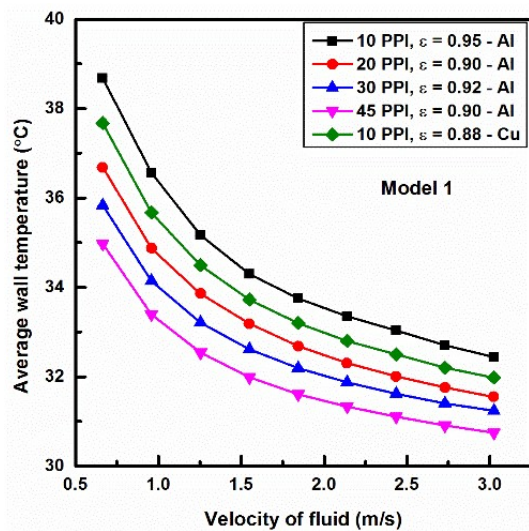
Figure 4.7 Temperature distribution along radius of the pipe (a) model 6 and (b) comparative results of all models.

4.7.2 Average Wall Temperature ($\overline{T_w}$)

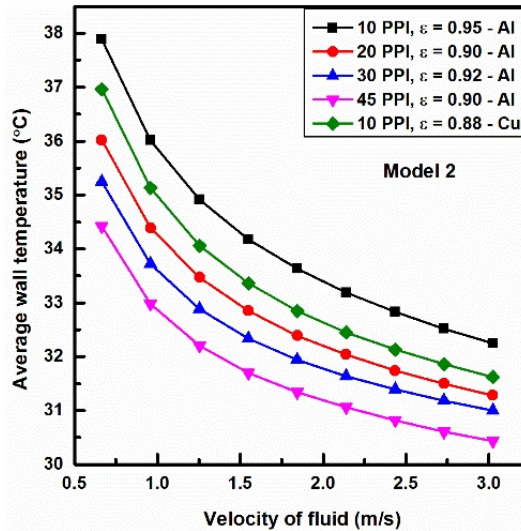
The $\overline{T_w}$ decreases with increasing the velocity of the flow for all the six models which is shown in Figure 4.8(a-f). Figure 4.8(a-c) explored that by fixing the external diameter of foam equal to the diameter of the pipe and reducing the internal diameter of the foam below 0.06 m, there is no substantial decrease in the $\overline{T_w}$ of the pipe wall. It has been found that the $\overline{T_w}$ for model 2 and model 3 is the same when the velocity is varied from

0.6639 to 3.0246 m/s. Henceforth, it is suggested that highly conductive foams should be fixed to the wall side of the pipe. Favorable heat transfer occurs in model 2 where maximum reduction in the \overline{T}_w of the conduit is achieved, revealed in Figure 4.8(a-c). It is also observed that the 45 PPI aluminium foam affirms maximum reduction in the \overline{T}_w than the other PPI's of the foams. This is due to decreased fiber diameter and proper mixing of the fluid that flows through the small opening.

It has also been observed that the 20 PPI and 30 PPI aluminium foams and 10 PPI copper foam are found to be similar in terms of \overline{T}_w for the model 4, model 5 and model 6 as shown in Figure 4.8(d-e). This is due to the specific surface area density which is marginally the same for the 20 PPI and 30 PPI of the aluminium foam; contrarily, 10 PPI copper foam possess higher thermal conductivity at the same time the specific surface area nearer to the 20 PPI and 30 PPI of the aluminium foam. Figure 4.8(f) explored the comparative study for all the six models for the pore density of 30 and porosity of 0.92 of the aluminium foam. Model 1, model 2 and model 3 show least \overline{T}_w compared to the model 4, model 5 and model 6. This is because highly conductive foams are embedded with hot surface which absorbs more amount of heat by means of conduction heat transfer and then instantly transfers to the fluid by means of convection heat transfer.



(a)



(b)

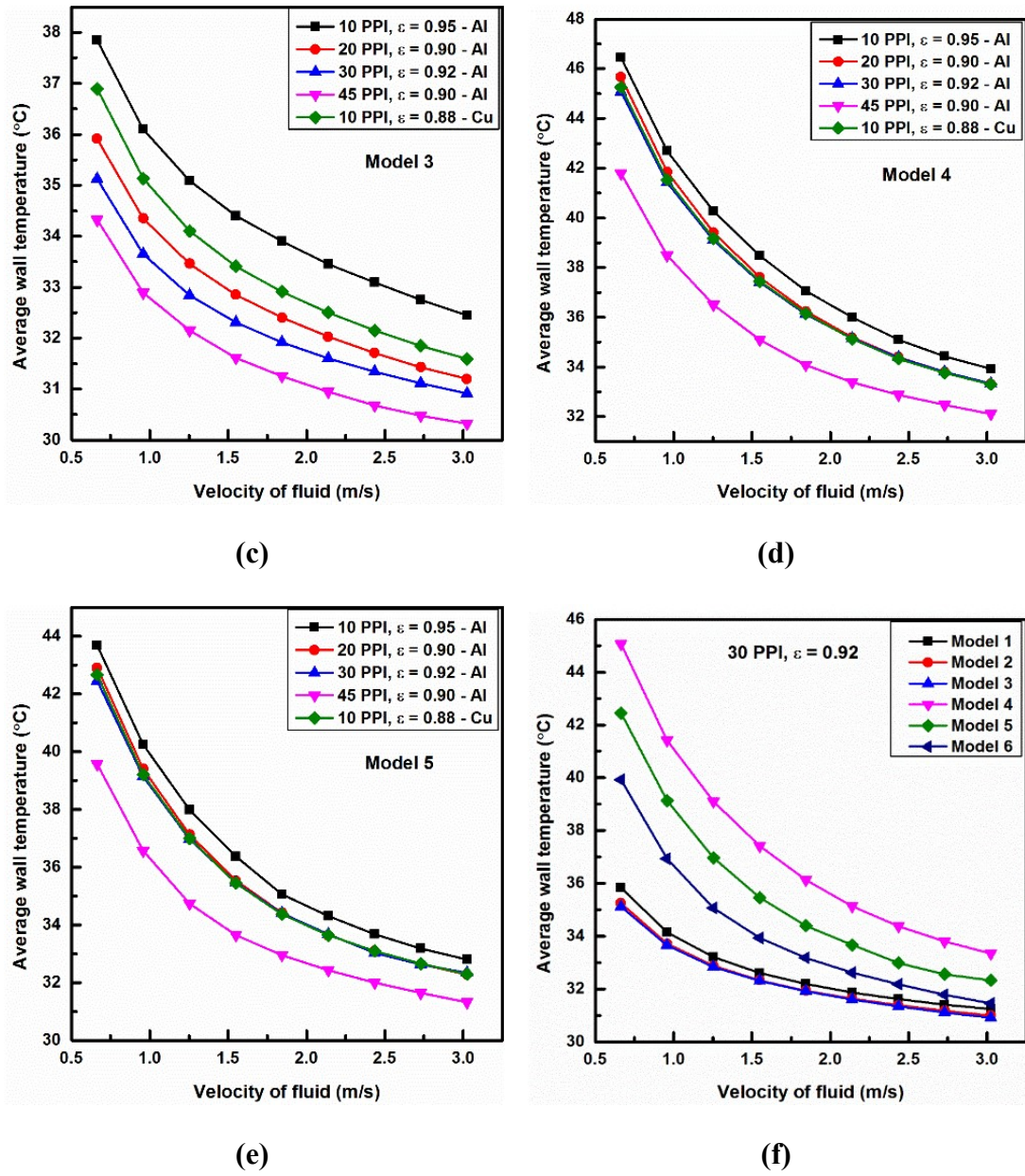


Figure 4.8 Variation in (a-e) the $\overline{T_w}$ with respect to velocity of air for model 1-model 5 and (f) comparative study of $\overline{T_w}$ for all the six models.

4.7.3 Forced Convection Coefficient

The average heat transfer coefficient (\bar{h}) is computed using the Eq. (4.1).

$$\bar{h} = \frac{\sum_1^N h_i}{N} \quad (4.1)$$

The local forced convection coefficient (h) is evaluated using Eq. (4.2).

$$h = \frac{q_w}{T_w - T_{mf}} \quad (4.2)$$

where, T_w and T_{mf} are the wall and mean fluid temperatures, respectively.

The results of \bar{h} versus Re for model 1, model 2 and model 3 for the aluminium and copper metallic foams are shown in Figure 4.9(a-c). From the results, it is explored that with increasing Re , the \bar{h} increases for all the PPI of the metallic foam considered for the study. This is because the highly conductive aluminium and copper foams are attached to the circumferential direction along its length of the pipe which tends to absorb more amount of heat from the wall and transfer immediately to the incoming air. The temperature difference between the wall and fluid decreases with increasing Re and is inversely proportional to the convection coefficient. The 45 PPI aluminium foam has an increase of 63.90%, 70.11% and 83.12% in \bar{h} compared to 10 PPI of the aluminium foam for the model 1, model 2 and model 3, respectively in the range of Re from 4500 to 20500. Moreover, the \bar{h} for 20 PPI and 30 PPI lies between 10 PPI and 45 PPI of the aluminium metallic foam. Furthermore, 10 PPI copper metallic foam has an augment of 13.68%, 15.55% and 19.45% in \bar{h} compared to 10 PPI aluminium metallic foam for the model 1, model 2 and model 3, respectively in the range of Re from 4500 to 20500.

Figure 4.9(d) explored the comparative study performed for 30 PPI with porosity 0.92 of the aluminium metallic foam with all the six models. The results showed that the model 2 and model 3 has augment of 7.14% and 8.66% in \bar{h} compared to model 1 while model 3 has an increase of only 1.41% in \bar{h} compared to the model 2 for the range of Re considered. From the study, model 2 seems to be better in terms of heat dissipation compared to model 3. It is also pertinent to mention that with increasing external diameter of foam from the core of the pipe to the wall, the \bar{h} increases progressively for model 4, model 5 and model 6. The increasing \bar{h} is due to the narrow gap between the foam and wall of the pipe that tends to increase velocity of the air in the non-foam (near the wall) region of the pipe. However, the model 4, model 5 and model 6 show lesser \bar{h} than that of model 1, model 2 and model 3. The model 2 has an enhancement of 108.38%, 68.19% and 36.44% in \bar{h} compared to model 4, model 5 and model 6, respectively. Also, model 5 and model 6 have augment of 23.87% and 52.66% in \bar{h} than

that of model 4 in the range of Re varied from 4500 to 20500.

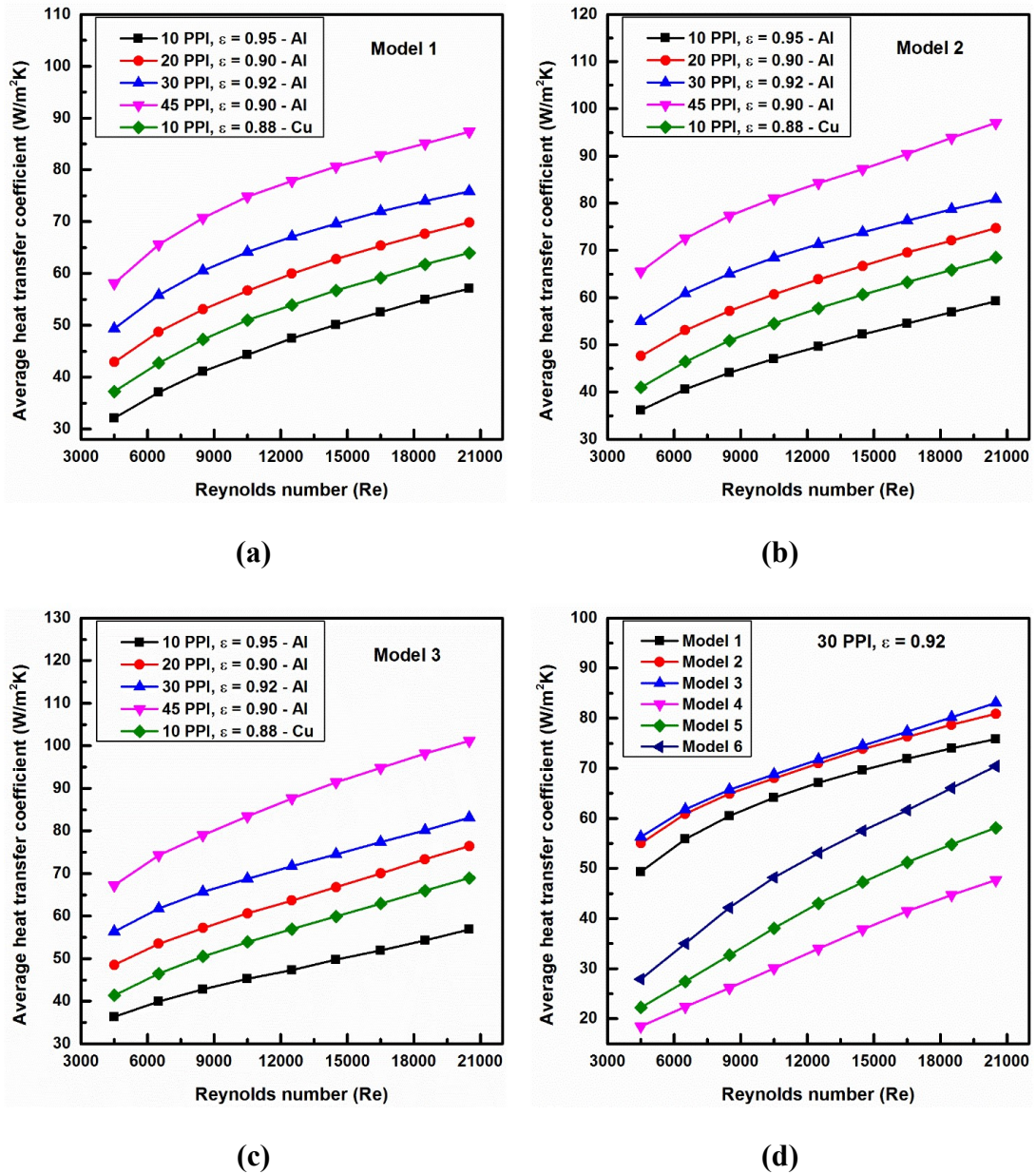


Figure 4.9 Variation of (a-c) \bar{h} vs. Re for model 1-model 3 and (d) comparative study of \bar{h} for all six models.

4.7.4 Average Nusselt Number (\overline{Nu})

The mean Nusselt number is evaluated by the Eq. (4.3).

$$\overline{Nu} = \frac{\bar{h}D_h}{\lambda_{air}} \quad (4.3)$$

The hydraulic diameter of pipe is computed using the Eq. (4.4).

$$D_h = \frac{4A_c}{P} \quad (4.4)$$

The Re is computed based on the hydraulic diameter of the conduit which is defined as in Eq. (4.5).

$$Re = \frac{\rho_f u_{in} D_h}{\mu_f} \quad (4.5)$$

The results of average Nusselt number versus Re for the model 2 and model 6 for aluminium and copper metallic foams and clear pipe are depicted in Figure 4.10(a-b). From the Figure 4.10(a) it is clearly observed that with increasing Re , the average Nusselt number increases for all PPI's of aluminium and copper metallic foams as well as clear pipe. The model 2 has shown a significant increase in the heat dissipation rate compared to clear pipe with flow Re number. Since, highly conductive metallic foams are attached to the periphery of the pipe wall the flow of air accelerates in the foam filled region which in turn increases the velocity gradient in the vicinity of the wall and creates thinner boundary layer compared to the clear pipe. This leads to a proper mixing of the flow in porous region which tends to increase the heat dissipation rate. Consequently, the 45 PPI aluminium metal foam has an augment of 654.95% in average Nusselt number compared to the clear pipe and 70.11% of average Nusselt number compared to 10 PPI of the aluminium metallic foam; furthermore, 10 PPI copper foam has an augment of 15.55% in average Nusselt number compared to 10 PPI of the aluminium metallic foam for the model 2. In addition to that, the heat dissipation rate is more or less similar for 20 PPI, 30 PPI of aluminium foam and 10 PPI of copper metallic foam for the model 6 which is depicted in Figure 4.10(b). This is because the superficial surface area density of the 20 and 30 PPI of the aluminium foam is similar and 10 PPI copper foam gains higher thermal conductivity and the specific surface area is found to be nearer to the 20 PPI and 30 PPI of the aluminium metallic foam.

From the results it is observed that the model 3 has a marginal increase in the average Nusselt number compared to the model 2 and significant increase in average Nusselt number compared to model 1 as shown in Figure 4.10(c). Consequently, model 3 has an augment of 13.61% in average Nusselt number compared to model 1 and only 3.54% in average Nusselt number compared to model 2. In addition, the model 2 has an augment of 9.72% in average Nusselt number than that of model 1. It is also observed

that, the heat dissipation rate increases beyond $Re = 16500$ for the model 6 compared to model 1 with the penalty of pressure drop. However, the model 2 and model 3 gives more or less similar results of average Nusselt number for the 10 PPI copper metallic foam with respect to Re which is presented in Figure 4.10(d).

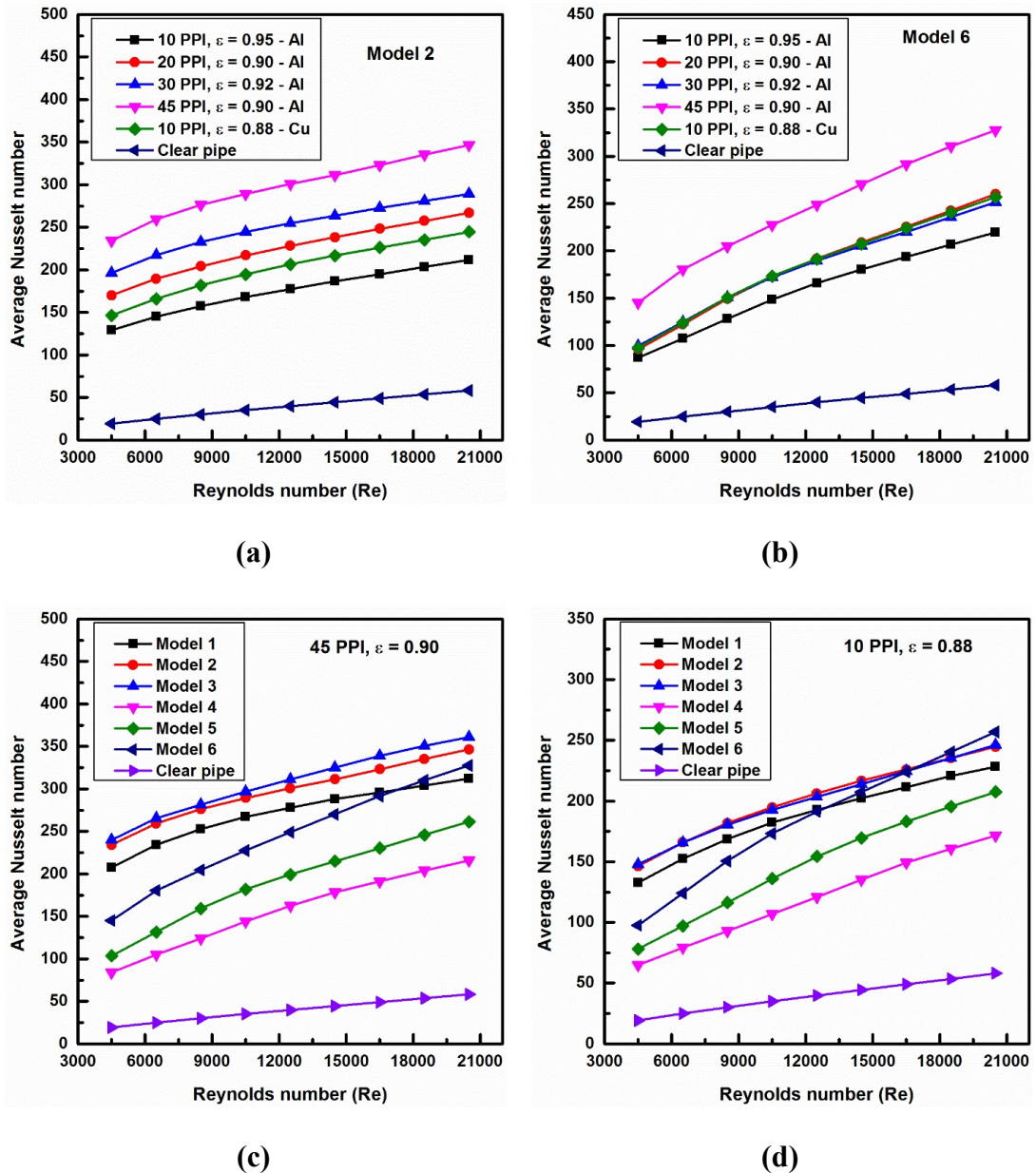


Figure 4.10 Changes in (a-b) average Nusselt number vs. Re for model 2 and model 6 and (c-d) comparative results of average Nusselt number for all six models filled with 45 PPI aluminium and 10 PPI copper foams respectively.

From the results of Figure 4.10(d), it is seen that the average Nusselt number increases

progressively for the model 6 beyond $Re = 12500$ compared to model 1 and above $Re = 16500$ for the model 2 and model 3. In addition, the model 1 shows better heat dissipation rate with minimum pressure drop than that of model 4 and model 5 with respect to flow Re .

The comparison of present study with (Baragh et al. (2018)) for 20PPI and 0.9 porosity is reported in the following Table 4.8. In addition, 45PPI with 0.9 porosity has also been considered to find out percentage increase in heat transfer compared to (Baragh et al. (2018)). For the same metal foam configurations, with insertion of aluminium metal foam the percentage enhancement is 16.79%, 15.55%, 57.94% and 58.45%, 59.59% and 132.92% of average Nusselt number compared to (Baragh et al. (2018)) respectively, for the turbulent flow regime as shown in Table 4.8. This enhancement is due to high thermal conductivity of metal foam which is having more specific surface area density and smaller structure of pores that leads to enhancement in the heat dissipation rate.

Table 4.8 Percentage increase in average Nu for 20 PPI and 45 PPI with porosity of 0.90 compared to Baragh et al. (2018).

Baragh et al. (2018)	Present study	Baragh et al. (2018) ($Re = 6437$) \overline{Nu}	Present study ($Re = 6500$) \overline{Nu}	(%) increase \overline{Nu}	Present study ($Re = 6500$) \overline{Nu}	(%) increase in \overline{Nu}
Model 1	Model 4	66.12	77.22	16.79	104.77	58.45
Model 2	Model 5	82.5	95.26	15.55	131.66	59.59
Model 3	Model 6	77.5	122.4	57.94	180.51	132.92

Note: (Baragh et al. (2018)) of model 1, model 2 and model 3 is equal to the present study of model 4, model 5 and model 6.

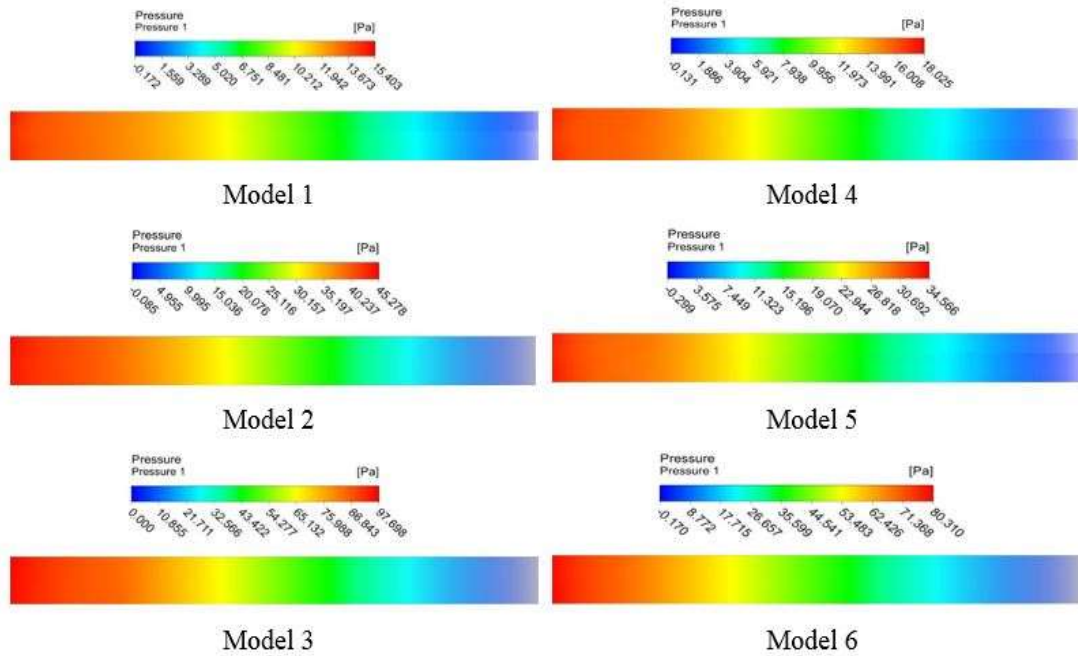
4.7.5 Pressure Drop

Figure 4.11(a) presents the contour plots for the variation of pressure drop along the length of the pipe for the pore density of 30 for the Model 1 – Model 6 at constant velocity of 0.9590 m/s respectively, shown in Figure 4.11(a). Model 1 – Model 3 shows pressure drop marching higher values while the diameter of the foam increasing from the wall to the core of the pipe. However, the diameter of foam placed at core of the pipe found to have lesser pressure drop except the model 4.

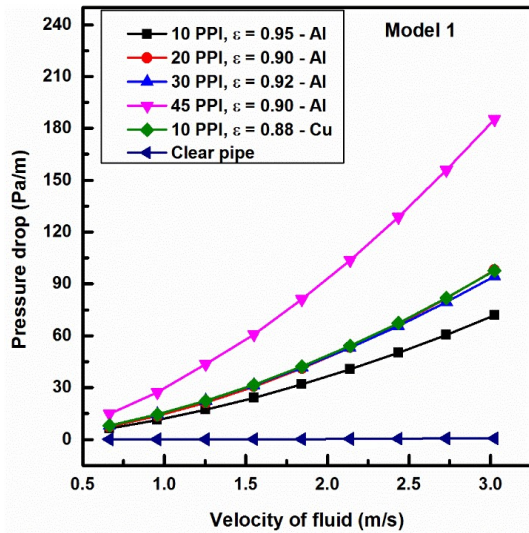
The pressure drop was measured between the inlet and outlet of the test section (i.e., $Z = 2$ m is at inlet of the test section and $Z = 3$ m is at outlet of the test section) of the pipe. The results of pressure drop versus velocity of fluid for the model 1 and model 2 which are partly filled with various PPI's of the foams and the clear pipe are shown in the Figure 4.11(b-c). With insertion of foams inside the pipe the pressure drop per unit length of the pipe increases in comparison with the clear pipe and it increases with increasing the velocity of flow. This may be due to the increase of the resistance caused by the metal foam. Also, in this context, the pore density of 45 with porosity of 0.90 has shown the highest pressure drop compared to the other PPI's of the porous foams. Here, due to higher PPI of the metallic foams the fiber diameter reduces which tends to increase the inertial resistance of the foam thereby leading to increase in the pressure drop. In addition, 20 PPI and 30 PPI of aluminium foam and 10 PPI of copper foam show the similar results of pressure drop. This may be due to the difference in PPI and porosities of the foam considered in the study.

Figure 4.11(d-e) presents the comparative results of pressure drop per unit length of the pipe for all the six models which are filled partly for the pore density of 30 and 45 and the clear pipe considered in the study. From the results, the pressure drop is found to be higher for all the models compared to the clear pipe. However, the pressure drop for model 1 and model 4 are found to be the same while it decreases significantly for the model 5 and model 6 compared to the model 2 and model 3 in the range of air velocity of 0.6639 to 3.0246 m/s. The reason is that as the metallic foam is placed at the core of the pipe there is a decrease in the velocity gradient in the vicinity of the wall which tends to reduce the pressure drop. It is also observed that with decrease in the internal diameter of the foam (i.e., model 1, model 2 and model 3) and increase in the external diameter of the foam (i.e., model 4, model 5 and model 6) the pressure drop along the

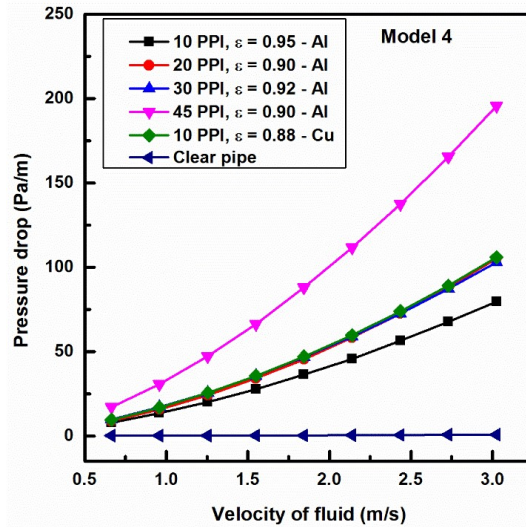
length of the pipe increases significantly. The tendency of the pressure drop is similar to (Kamath et al. (2013) and Lu et al. (2016)).



(a)



(b)



(c)

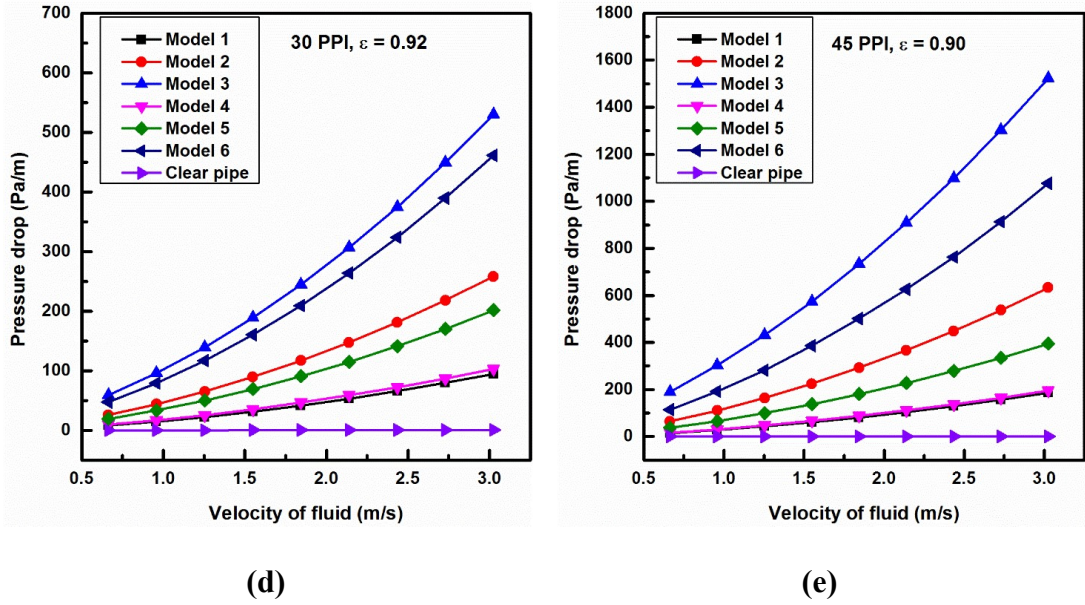


Figure 4.11 Changes in pressure drop for (a) contour plots for model 1 – model 6, (b-c) comparative study for model 1 and model 4 (d-e) comparative study of model 1 – model 6 for 30 PPI and 45 PPI partly filled foam and clear pipe.

4.7.6 Friction Coefficient (f)

The friction coefficient in the presence of partially filled foam inside the pipe and the clear pipe across its length is calculated using Eq. (4.6).

$$f = \frac{2\rho_f \Delta P D_h}{u_{in}^2 L} \quad (4.6)$$

In Eq. (4.6) the velocity is measured at the inlet ($Z = 0$) of the pipe. Figure 4.12(a-b) presents the friction coefficient for the model 1 and model 4 filled partly with various PPI's of the foams and the clear pipe. The friction coefficient decreases with increasing flow rates of the air for partly filled foam and the clear pipe. However, all PPI's of the partly filled foam inside the pipe encounter more friction compared to the clear pipe. The insertion of higher PPI of the metallic foam leads to increase the friction coefficient compared to other PPI's of the metallic foams. It is also observed that the pore density of 20 PPI and 30 PPI of aluminium foam and 10 PPI of copper foam show more or less similar coefficient of friction for the model 1 and model 4 respectively and this is due to the difference in the porosities of foams considered.

Figure 4.12(c-d) explored the comparative study of friction coefficient for all the six

models filled partially with the pore densities of 30 and 45 and their porosities of 0.92 and 0.90. The friction coefficient is found to be higher for all the models than that of the clear pipe.

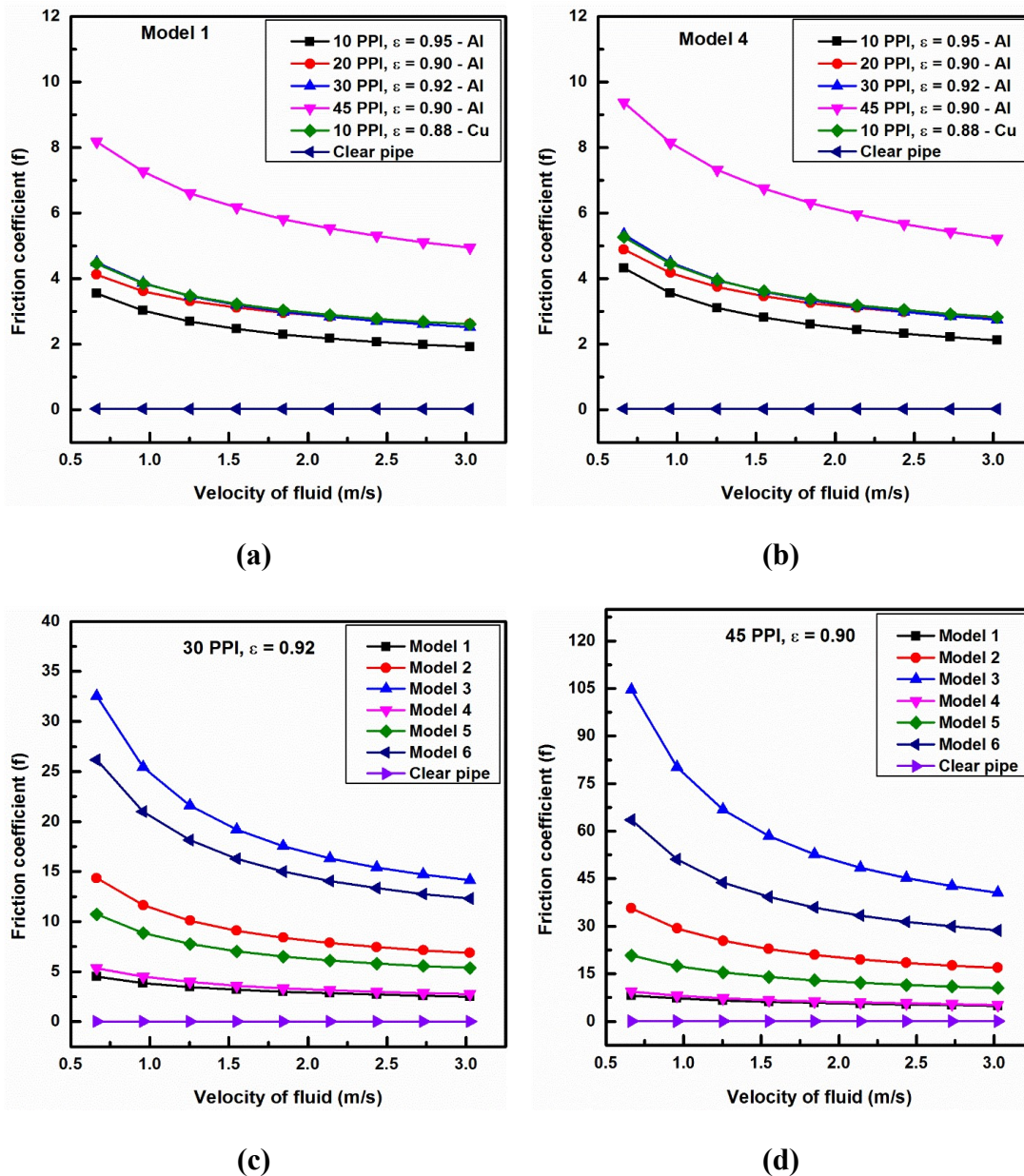


Figure 4.12 Changes in (a-b) friction coefficient vs. velocity of air for model 1 and model 4 and (c-d) comparative study of pressure drop for 30 PPI and 45 PPI partly filled foam and clear pipe.

However, the model 1 and model 4 show similar fashions of friction coefficient and decrease in friction factor significantly for the model 5 and model 6 in comparison with the model 2 and model 3 in account of the pore densities of 30 and 45 with respect to the flow rates. The reason is that as the metallic foam is placed at the core of the pipe a decrease in the velocity gradient in the vicinity of the wall occurs which tends to reduce the pressure drop.

4.7.7 Heat transfer Enhancement Ratio (Nu_{ER})

The enhancement ratio is an important parameter to determine the effectiveness of the heat exchanger by means of increasing the surface area within the fluid flow with insertion of various configurations of the metallic foams. Nu_{ER} is defined as heat transfer with insertion of metallic foams to heat transfer without insertion of metallic foam inside the pipe which is evaluated using Eq. (4.7). At the same time, it is possible to find out the best optimal model on account of foam samples to achieve higher Nu_{ER} .

$$Nu_{ER} = \frac{\overline{Nu}}{\overline{Nu}_{\phi}} \quad (4.7)$$

From the results, model 1, model 2 and model 3 with 45 PPI aluminium metallic foam shows highest Nu_{ER} while the 10 PPI aluminium foam shows the least Nu_{ER} . 10 PPI copper foam shows significantly Nu_{ER} than the 10 PPI of aluminium foam with Re number which is shown in Figure 4.13(a-c). In addition, the Nu_{ER} is higher at lower flow rates and decreasing with increasing flow rates of the air for all the PPI and porosity of foams considered for the model 1, model 2 and model 3. However, the 45 PPI aluminium foam shows the enhancement of 65.40% in Nu_{ER} compared to 10 PPI of the aluminium metallic foam while 10 PPI copper foam has an increase of 12.95% in Nu_{ER} than that of 10 PPI aluminium metallic foam for the model 1 in the range of $Re = 4500$ to 20500.

The Nu_{ER} is compared for the all the six models for the 30 PPI aluminium metallic foam filled partly in a pipe which is shown in Figure 4.13(d). From the results, it is revealed that the model 2 and model 3 show the highest Nu_{ER} compared to the other models for all flow rates of the air. Model 2 will be a better choice rather than the model 3 because of lesser pumping power. Successively, the model 2 has an average

enhancement of 7.69%, 122%, 79.58% and 44.73% compared to model 1, model 4, model 5 and model 6, respectively in the range of Re varied from 4500 to 20500. Furthermore, the model 1 has secured better Nu_{ER} than that of model 4, model 5 and model 6. Subsequently, the model 1 has an average increase of 105.82%, 66.49% and 34.18% in Nu_{ER} than that of model 4, model 5 and model 6 respectively in range of Re consider for the study.

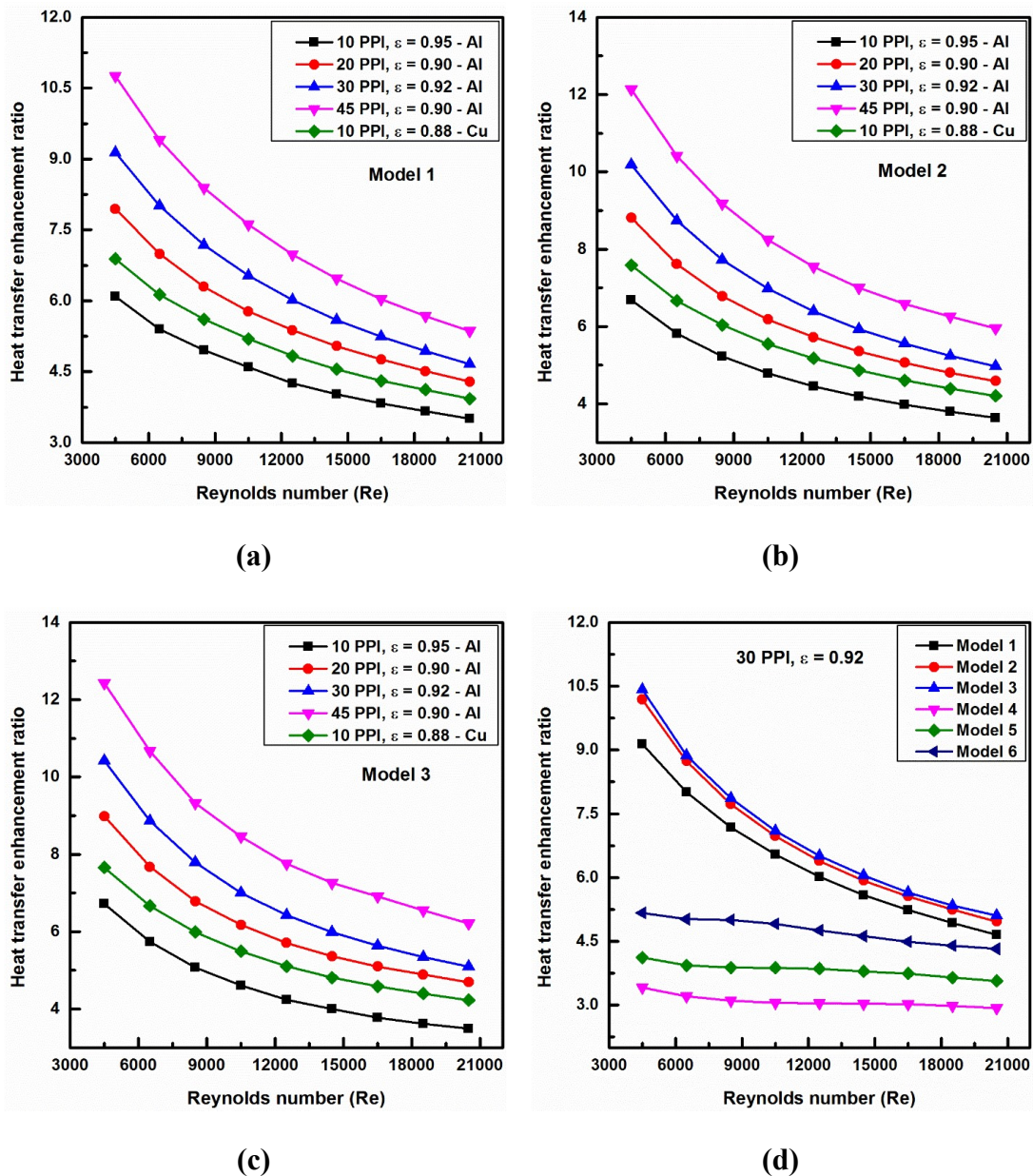


Figure 4.13 Nu_{ER} vs. flow Re for (a-c) model 1- model 3 and (d) comparative results for 30 PPI aluminium foam.

4.7.8 Colburn j Factor (j) and Performance Factor (η_p)

The performance factor and the Colburn j factor are the important findings parameters to design and measures the overall performance of any of the heat exchanger. The Colburn j factor is computed from Eq. (4.8).

$$j = St. (Pr)^{\frac{2}{3}} \quad (4.8)$$

The results revealed that j decreases with increasing flow rates of the fluid for the clear pipe as well as partially foam filled pipe as depicted in Figure 4.14(a). However, the j is higher for the lower Re and decreases progressively with increasing Re for all PPI's of the metallic foams. In addition, the j is found to be higher for all PPI's of the metallic foam compared to the clear pipe with flow rates of air. In the presence of metal foam, the air is forced to flow through the open pores that leads to accelerating the flow resulting into increased turbulence and increased Stanton number (St) at lower flow rates. It is also seen that at higher PPI of the metallic foam the j increases significantly and decreases with decreasing PPI of the metallic foam. Also, 10 PPI copper foam attains higher j than that of 10 PPI aluminium foam due to its higher thermal conductivity and higher superficial surface area.

From the results, the j for all the models increases significantly compared to the clear pipe which is revealed in Figure 4.14(b). However, the j for the model 2 and model 3 remain the same and model 1 performs slightly nearer to the model 2 and model 3 in the range of Re considered. Furthermore, for the model 1 there is a significant increase in the j compared to the model 4, model 5 and model 6 at lower flow rates while the significance is less at high flow rate ($Re = 20500$) for the model 1 and model 6. Therefore, in terms of performance the heat exchanging device should be the model 1.

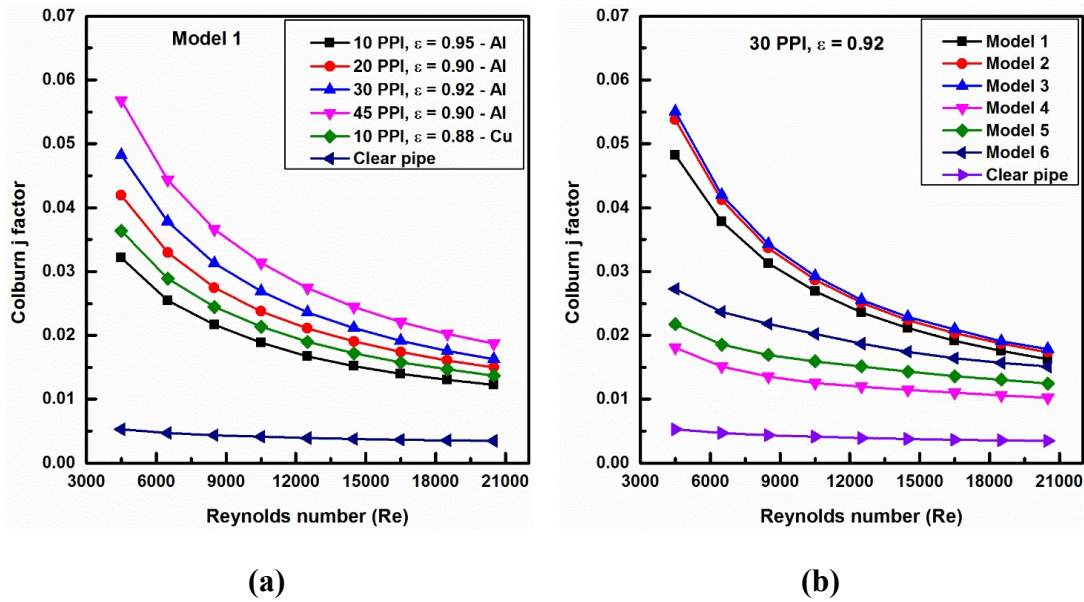


Figure 4.14 Colburn j factor vs. Re for (a) model 1 and (b) comparative results of 30 PPI aluminium foam for all six models.

To compute the overall thermal performance of the any heat exchanging devices a dimensionless parameter called performance factor which is the ratio of Colburn j factor to the power required to pump the fluid given by (Manglik (2003)) in Eq. (4.9).

$$\eta_p = \frac{j}{f^{\frac{1}{3}}} \quad (4.9)$$

Figure 4.15(a) presented the performance factor that decreases with increasing the flow rates of the fluid for all the PPI's of the foams. At higher flow rates the air is forced to flow through the small pores; as a result, more pumping power is required to overcome the obstruction of the fluid. This results in a significant reduction of the performance factor. The 30 PPI with porosity of 0.92 aluminium foam shows the highest performance factor compared to other PPI's of the metallic foams. This is because the porosity of the foam increases that allows more amount of air to flow through the opening resulting to decrease in the pressure drop. However, beyond $Re = 10500$ the 20 PPI and 45 PPI aluminum foam gives more or less similar performance factor. In addition, the 10 PPI with porosity of 0.95 aluminium foam perform very closer to 10 PPI with porosity of 0.88 copper foam with lesser pumping power.

From the Figure 4.15(b), the model 1 performs the highest performance factor

compared to the other models. The model 1 has average increase of 32.35%, 68.22%, 116.86%, 125% and 136.84% in the performance factor compared to the model 2, model 3, model 4, model 5 and model 6, respectively. This is because the model 1 requires minimum pumping power to lift the fluid from inlet to the exit section of the pipe compared to the other models except the model 4. Hence, by comparing Figure 4.15(a & b) it is concluded that for better performance factor of the heat exchanging devices one can choose model 1 filled with 30 PPI with porosity of 0.92 aluminium foam compared to the other models.

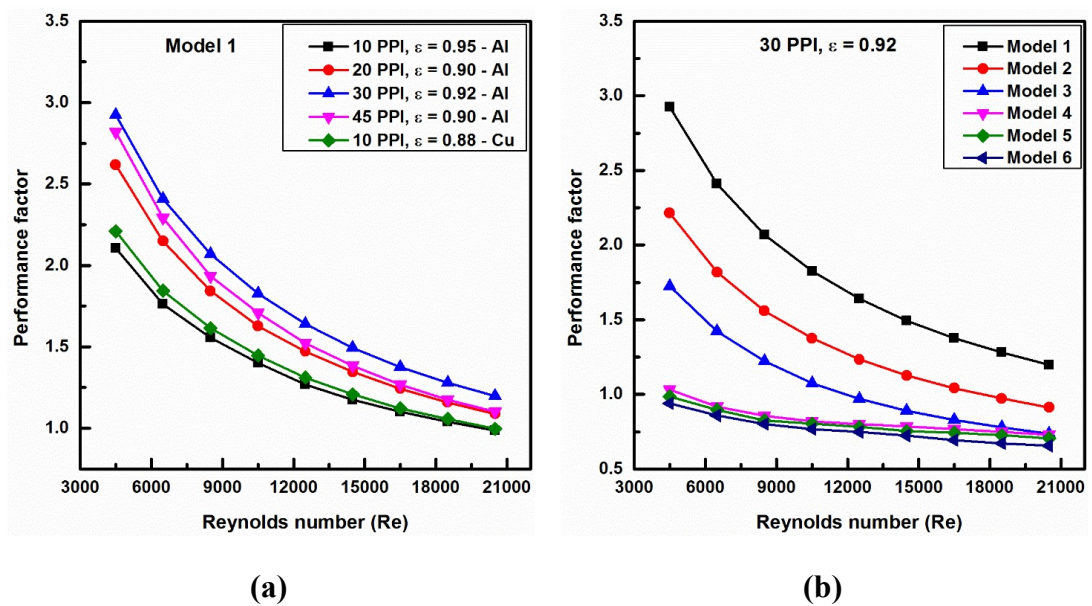


Figure 4.15 Performance factor versus Re for (a) model 1 and (b) comparative results for 30 PPI aluminium foam for all six models.

4.8 SUMMARY

Two dimensional simulations were carried out to study the effect of partial filling of high porosity metal foams in a horizontal pipe of diameter 0.1 m and length 1 m. The numerical exploration considered six different models with variation in PPI's and Porosity of the aluminium and copper metallic foams. The analysis was carried out for turbulent forced convection heat dissipation with wide range of Reynolds number from 4500 to 20500. Based on the present investigation, the salient points are drawn below:

- With increasing velocity of the air, the velocity distribution at the exit of the tube increases in the porous as well as non-porous region. While, the

temperature at the exit of the conduit is not significant at higher velocity of the air.

- The convection heat transfer coefficient and the Nu_{ER} showed more or less similar results for the model 2 and model 3 compared to the other models for 30 PPI aluminium foam sample. Hence, for better convective heat transfer coefficient and Nu_{ER} with minimal pressure drop it is better to choose model 2 rather than model 3.
- On account of 45 PPI aluminium foam, the model 3 has marginal and significant augment in average Nusselt number compared to model 2 and model 3 respectively, in the range of Re number. However, model 6 was observed to have more enhancement beyond Reynolds number of 16500 compared to model 1 at the expense of pressure drop.
- For 10 PPI copper foam, the model 6 showed the highest average Nusselt number beyond Reynolds number 16500 compared to model 2 and model 3. However, the model 1 has an augment of 55.87% and 26.47% in average Nusselt number compared to model 4 and model 5, respectively in the range of Reynolds number from 4500 to 20500.
- 30 PPI aluminium metal foam showed the highest thermal performance factor for the model 1 compared to other PPI of the metal foams in the range of Reynolds number considered. However, the thermal performance factor of 10 PPI aluminium foam is very close to the expensive 10 PPI copper foam. Hence, one can choose 10 PPI aluminium foam with reasonable performance factor with minimal pressure loss and lesser cost of the foam.

4.9 CLOSURE

In this chapter, the numerical investigation of partially filled high porosity metal foam configurations in a pipe were carried out with wide range of Reynolds number. In the current chapter, six different porous layer thicknesses were varied from the wall side as well as from core of the pipe. The next chapter presents the continuation of the present chapter. Since the pressure drop and heat transfer are major concerns of the present study, a more detailed parametric study is required for the optimum configuration

proposed in the current chapter. Therefore, the next chapter considers the optimization study employed for multi-objective function for minimization and maximization of friction resistance and heat transfer rate, respectively in order to determine best configuration, porous layer thickness and pore density of the aluminium metal foam.

CHAPTER 5

PERFORMANCE SCORE BASED MULTI- OBJECTIVE OPTIMIZATION FOR THERMAL DESIGN OF PARTIALLY FILLED HIGH POROSITY METAL FOAM PIPES UNDER FROCED CONVECTION

5.1 INTRODUCTION

This chapter explores the continuation of the previous chapter 5. Aluminium foam layer with four different values of pore density are 10 PPI, 20 PPI, 30 PPI and 45 PPI and thickness (but almost the same porosity, i.e., 0.90 – 0.95) are located at two different positions as center and lateral surface of the pipe, and totally 6 models are emerged. Since the pressure drop and heat transfer are major concerns of the present study, a more detailed parametric study is required for the optimum configuration proposed in the chapter 4. Hence, Chapter 5 explores the performance score multi-objective optimization to minimize and maximize the friction resistance and heat transfer rate, respectively. The TOPSIS method is applied to solve multi-objective functions. This chapter presents that how TOPSIS method can provide the best model for finding location, thickness and PPI of a porous layer based on the priority of the thermal designer for the weight of heat transfer and friction effects.

5.2 PROBLEM STATEMENT

In the present chapter, a straight circular pipe of diameter 0.10 m, length 1 m and thickness of wall 7 mm is considered. The heater is coupled with the pipe wall along its length. Four different aluminum foam samples are taken into account for the numerical investigations. The pore densities and porosities of aluminum foam samples vary from 10 PPI to 45 PPI and 0.90 to 0.95 (Kamath et al. (2011 & 2013); Kotresha and Gnanasekaran (2018)), respectively and they are partially inserted inside the circular

pipe. The flow in the open passage of the pipe is turbulent whose Reynolds number ranges from 4500 to 16500 as per (Yang and Hwang (2009)), evaluated based on the hydraulic diameter (i.e., $D_h = 4A_c/P$) of circular pipe. Totally six different models are emerged. In model 1 to model 3 (i.e., M1, M2 and M3), the external diameter of the foam is fixed and is equal to the diameter of the pipe while the internal diameter of foam is varied from the wall to the core of pipe. In the model 4 to model 6 (i.e., M4, M5 and M6), the external diameter of the foam is increased from the core to towards the wall of the pipe while internal diameter of the foam is made equal to zero. The schematic views of the studied 6 different models (M1, M2, M3, M4, M5 and M6) are shown in Table 5.1 and the details of the dimensions are depicted in the Table 5.2.

Table 5.1 Numerical domains considered for all six models.




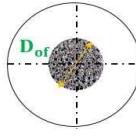
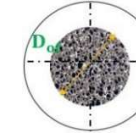
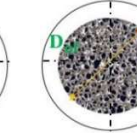
Models	M1	M2	M3	M4	M5	M6
Partially filled foam						

Table 5.2 Details of the dimensions of all six models.

Models	d_{if} (m)	D_{of} (m)
M1	0.06	0.10
M2	0.04	0.10
M3	0.02	0.10
M4	0.00	0.04
M5	0.00	0.06
M6	0.00	0.08

For numerical computation, two-dimensional axis symmetry about its centerline along the flow direction is taken into account which is depicted in Figure 5.1. The pipe is extended $2L$ at the entrance to attain a developed flow (Sunden (2012)) while $1.5L$ is extended at the outlet of the pipe to avoid the exit effect (Mohammed et al. (2013) and

Lin et al. (2016)). A uniform velocity profile and zero pressure are assigned at the inlet of the circular pipe. It should be mentioned that there are two definitions of Reynolds number in this study. One of them is Re number based on hydraulic diameter used for the flow in the free passage and the second one Re number based on the permeability of aluminum foam employed for flow in the aluminum foam.

$$Re = \frac{\rho_f u_{in} D_h}{\mu_f} \quad (5.1)$$

$$Re_K = \frac{\rho_f u_{in} \sqrt{K}}{\mu_f} \quad (5.2)$$

where K is permeability depends on aluminum foam and D_h is hydraulic diameter of pipe evaluated by the following Eq. (5.3).

$$D_h = \frac{4A_c}{P} \quad (5.3)$$

where A_c and P are the cross-section area and perimeter of the pipe, respectively. The average value of velocity in metal foam is less than u_{in} but in order to have a fix reference velocity for all obtained results including results of free region and metal foam, it is used in Eq. (5.2). As it was mentioned before, the flow is turbulent in the clear region of the pipe. For the aluminum foam layer, Re number based on the permeability changes from 9.22 to 82.17 and flow is laminar since it is less than 150 (Neild and Bejan (2006)). The thermal dispersion is not considered in this work due to high thermal conductivity of metal foam and low thermal conductivity working fluid (Calmidi and Mahajan (2002)). The structural and hydrodynamic properties of the studied aluminium foam are presented in Table 5.3 and Table 5.4 (Kamath et al. (2011 & 2013); Kotresha and Gnanasekaran (2018)).

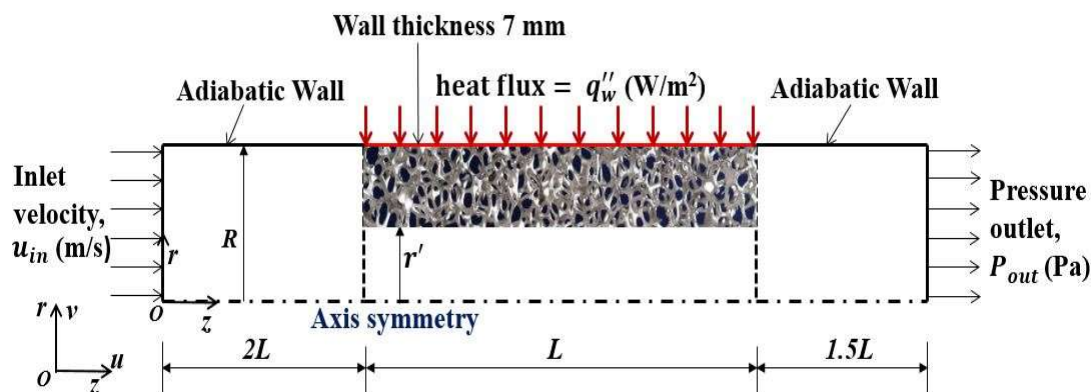


Figure 5.1 Schematic of computing domain.

Table 5.3 Properties of aluminium metallic foams Aluminium (Kamath et al. (2011 & 2013); Kotresha and Gnanasekaran (2018)).

PPI (Pores per inch)	Porosity (ϵ)	Permeability (K) 10^7 , m^2	Uncertainty in (K) (%)	Form drag coefficient (C)	Uncertainty in (C) (%)
10	0.95	2.480	± 7.95	94.98	± 2.45
20	0.90	2.177	± 9.67	208.82	± 2.21
30	0.92	1.644	± 9.83	148.97	± 3.68
45	0.90	0.420	± 5.87	397.01	± 5.80

Table 5.4 Superficial surface area of aluminium metallic foam.

PPI	Pore size, d_p (mm)	Fiber size, d_f (mm)	Porosity, ϵ	Interfacial surface area, a_{sf} (m^{-1})
10	4.952	0.445	0.95	360.60
20	3.416	0.451	0.90	960.65
30	2.324	0.216	0.92	936.38
45	1.654	0.184	0.90	1671.76

Briefly, in the chapter 4, heat transfer can be considerably enhanced by using metal foams; however, it considerably increases pressure drop in a pipe. Partially filled pipes by inserting a metal foam layer can be a solution in order to reduce pressure drop without trade-off heat transfer too much. Hence, the partially filled pipes considering

both heat transfer enhancement and pressure drop by using metal foam layers are limited compared to studies performed just for heat transfer enhancement. The chapter 6 explore the optimization study on this issue, the main parameter for determination of the best location, thickness and structure of metal foam layer is the preference of the thermal designer between heat transfer and pressure drop. According to the priority assigned by a thermal designer, TOPSIS can accurately evaluate the best position and thickness as well as PPI (Pore Per Inch) and porosity of a metal foam layer. TOPSIS is a multi-objective optimization method. This study focuses on the design criteria of friction factor to average Nusselt number and we assumed that the wall temperature is not the primary interest. However, any parameters such as maximum wall temperature, minimum entropy generation, weight and heat exchanger size can be objective and the optimization can be done based on the required design parameters can be achieved.

The aforementioned advantages of TOPSIS motivated authors to perform the present study. A numerical study is performed by considering aluminum metal foam layers inside a pipe with different porous layer arrangement and various aluminum foam as well. Instead of doing a parametric research by changing the values of governing parameters, six real cases with real structural parameters of aluminium foam are considered. Aluminum foam layer with different values PPI and thickness (but almost the same porosity) are located at two different positions as center and lateral surface, and 6 models are emerged. The best model and PPI for 5 different weights of heat transfer and friction factor for the wide range of Reynolds number are calculated by using TOPSIS method. TOPSIS is applied at lower and higher flow rates of the fluid for solving multi-objective function to minimize and maximize the friction coefficient resistance and heat transfer rate, respectively. The present study shows that how TOPSIS method can provide the best model for finding location, thickness and PPI of a porous layer based on the priority of the thermal designer for the weight of heat transfer and friction effects. To the best of our knowledge, very few study in the Chapter 2 that considers the above complimentary circumstances for the benefit of both heat transfer and pressure drop in a meticulous and systematic approach by using TOPSIS method for wide range of the governing parameters.

5.3 GOVERNING EQUATIONS AND BOUNDARY CONDITIONS

The flow inside the pipe is assumed incompressible and steady. The gravity effect is neglected and heat transfer by thermal radiation is negligible. The aluminium foam is isotropic, homogeneous and non – deformable. There is no thermal resistance between the aluminum foam and the solid surface of the pipe. A local thermal non-equilibrium approach is used for the heat transfer between the metal foam matrix and the flowing fluid inside it. Since the flow inside the clear region is turbulent, $k-\omega$ turbulence model is employed in clear region of circular pipe (Yang and Hwang (2009)). The governing equations involved in non-foam region and porous region of pipe according to (Mahmoudi and Karimi (2014)) and (Huang et al. (2010)) discussed in Chapter 3 (Eqs (3.1) – (3.13)).

As it was mentioned before, due to low values of Re_K , the effect of thermal dispersion is neglected. The details of the boundary conditions assigned for the numerical domain (Huang et al. (2010)) are presented in Chapter 4 in Table 4.3. The interface between the solid and fluid phases assumes no slip boundary conditions as well as no fluid penetration and conjugate (aluminum wall coupled with the metallic foam) heat transport model of ANSYS FLUENT software is accomplished as reported in literature of (Imani et al. (2013 & 2012)). The governing equations and interfacial condition involved between clear and porous regions are described detailed in Chapter 4 (see Table 4.4) as per (Xu et al. (2011b)) and (Mahmoudi and Karimi (2014)).

Further, the properties of aluminium foam like specific area density (a_{sf}) and interfacial heat transfer coefficient (h_{sf}) are computed based on (Calmidi and Mahajan (2002)) and (Zukauskas (1987)) using Eqs. (3.14) – (3.16) reported in chapter 3. The specific surface area density of the aluminium foam computed and depicted in the Table 5.4. The steps involved in the numerical simulation of the present work is depicted in the form of a flowchart given in Figure 5.2.

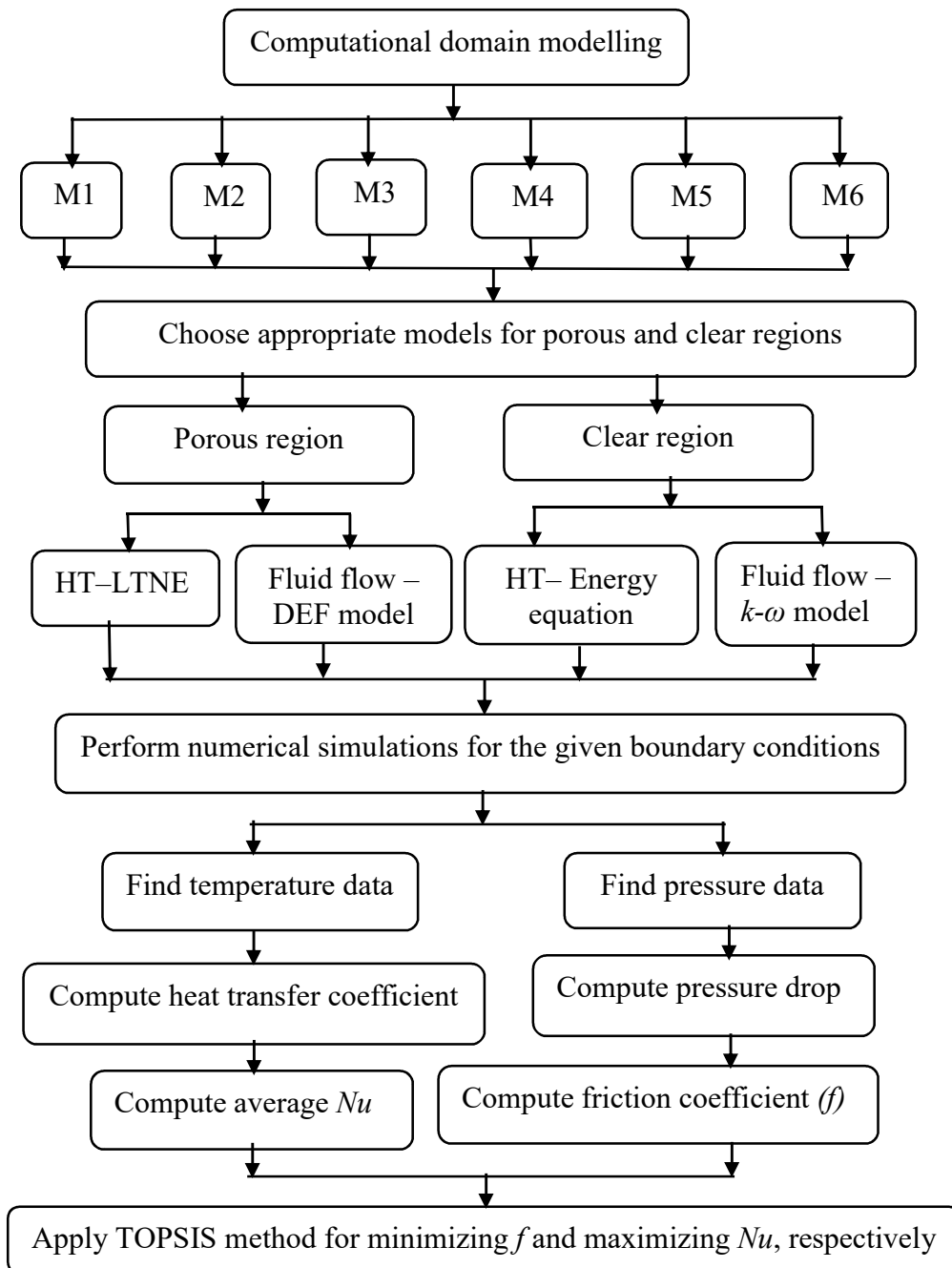


Figure 5.2 Flowchart representing the steps involved in numerical simulation.

HT = Heat transfer; DEF = Darcy extended Forchheimer flow; M1 = Model 1; M2 = Model 2; M3 = Model 3; M4 = Model 4; M5 = Model 5 and M6 = Model 6; Nu = Nusselt number; and f = Friction coefficient.

5.4 TOPSIS METHOD FOR MULTI – OBJECTIVE FUNCTIONS

TOPSIS method/technique is beneficial in dealing and making decision matrix with multiple objective functions involved in the real world problems. In the current investigation, the TOPSIS method is applied in order to minimize and maximize the friction coefficient and heat transfer parameters, respectively.

Initially, the thermo-hydrodynamic parameters are computed with the help of numerical investigation and further five different weights are assigned with different conditions/criteria's: viz; criteria I: $(f)_{\min}:(Nu)_{\max} = 0.0:1.0$, criteria II: $(f)_{\min}:(Nu)_{\max} = 0.25:0.75$, criteria III: $(f)_{\min}:(Nu)_{\max} = 0.50:0.50$, criteria IV: $(f)_{\min}:(Nu)_{\max} = 0.75:0.25$ and criteria V: $(f)_{\min}:(Nu)_{\max} = 1.0:0.0$ in order to obtain the performance score or rank of the matrix for the given multi-objective function.

As mentioned earlier, the main objective of the current study is to focus on the prominence of minimizing the friction coefficient and maximizing the heat transfer rate by considering six different models which are partially filled inside the pipe. To accomplish this, TOPSIS method is used to obtain the best possible combination of models and the foam samples that are involved based on the computed values of the performance score. The followings are the detailed conditions/criteria involved to evaluate the thermo-hydrodynamic attributes:

5.4.1 Step I: Computation of Normalized Matrix

The simulated results obtained from the numerical investigation are normalized using Eqs. (5.4) and (5.5). The results of friction coefficient and average Nusselt number values are converted into normalized magnitudes. Generate a matrix of two columns each containing Nusselt number values (Nu_{i1}) and friction coefficient (f_{i2}) respectively. Then extend the matrix with another set of two columns each containing normalized magnitudes of Nusselt number and friction coefficient (\overline{Nu}_{ij}) and (\overline{f}_{ij}) respectively using Eqs. (5.4) and (5.5).

$$\overline{Nu}_{i3} = \frac{Nu_{i1}}{\sqrt{\sum_{i=1}^m Nu_{i1}^2}} \quad (5.4)$$

$$\bar{f}_{i4} = \frac{f_{i2}}{\sqrt{\sum_{i=1}^m f_{i2}^2}} \quad (5.5)$$

where 'i' indices show the rows of the matrix and m refers to total number of foam samples.

5.4.2 Step II: Computation Weight Assigned Normalized Matrix

Additionally, in order to obtain the weighted normalized matrix using Eqs. (5.6) - (5.7); the weight is assigned or multiplied (i.e., it is varying from 0 to 1) to the hitherto computed values of normalized matrix magnitudes of friction coefficient and average Nusselt number. The assigned weight totally depends on the specific interest of the users.

$$V_{i5} = (\overline{Nu_{i3}}). W_{Nu} \quad i = 1, 2, \dots, m. \quad (5.6)$$

$$V_{i6} = (\bar{f}_{i4}). W_f \quad i = 1, 2, \dots, m. \quad (5.7)$$

where W_{Nu} and W_f are the assigned weight for average Nusselt number and friction factor. Two new columns (5th and 6th) are added into the matrix.

5.4.3 Step III: Compute Ideal Worst Values of V^- and Ideal Best Values of V^+ Among Weighted Normalized Matrix of Nu and f .

The ideal worst values and ideal best values are obtained from the previously computed weighted normalized matrix of friction coefficient and the average Nusselt number. In the present study, the friction coefficient considered as non-beneficial parameter while average Nusselt number considered as beneficial parameter. Henceforth, the highest value among the weighted normalized matrix of friction coefficient is considered as ideal worst, while the lowest value among the weighted normalized matrix of friction coefficient magnitude is treated as ideal best value. On the contrary, the highest value among the weighted normalized matrix average Nusselt number is treated as ideal best value, while the lowest value among the weighted normalized matrix of average Nusselt number is considered as ideal worst value. Evaluate the ideal best alternative V^+ and ideal worst alternative V^- is represented using the Eqs. (5.8) to (5.11).

$$V_{Nu}^+ = \max (V_{i5}) \quad (5.8)$$

$$V_f^+ = \min (V_{i6}) \quad (5.9)$$

$$V_{Nu}^- = \min (V_{i5}) \quad (5.10)$$

$$V_f^- = \max (V_{i6}) \quad (5.11)$$

5.4.4 Step IV: Compute Euclidean Distance from Weighted Resultant Ideal Best Value

The relative distance between each weighted normalized magnitudes (i.e., it may be best or worst) from a particular selected value is called Euclidean distance. Positive Euclidean distance is evaluated based on weighted normalized matrix magnitudes from resultant ideal best magnitudes given by Eq. (5.12).

$$S_i^+ = \left[(V_{i5} - V_{Nu}^+)^2 + (V_{i6} - V_f^+)^2 \right]^{0.5} \quad (5.12)$$

5.4.5 Step V: Compute Euclidean Distance from Weighted Resultant Ideal Worst Value

Further, negative Euclidean distance is evaluated based on weighted normalized matrix magnitudes from resultant optimal worst magnitudes given by Eq. (5.13).

$$S_i^- = \left[(V_{i5} - V_{Nu}^-)^2 + (V_{i6} - V_f^-)^2 \right]^{0.5} \quad (5.13)$$

5.4.6 Step VI: Compute the Performance Score

The performance score indicates the ranking of various models of metal foam configurations. The ranking of the models and the foam samples are based on the various weights assigned in minimizing and maximizing the friction coefficient and average Nusselt number, respectively. The performance score is computed using the Eq. (5.14).

$$P_i = \frac{S_i^-}{S_i^- + S_i^+} \quad i = 1, 2, \dots, m \quad (5.14)$$

The aforementioned steps involved in TOPSIS method has been represented in a flowchart for clear understanding of the solution methodology in Figure 5.3.

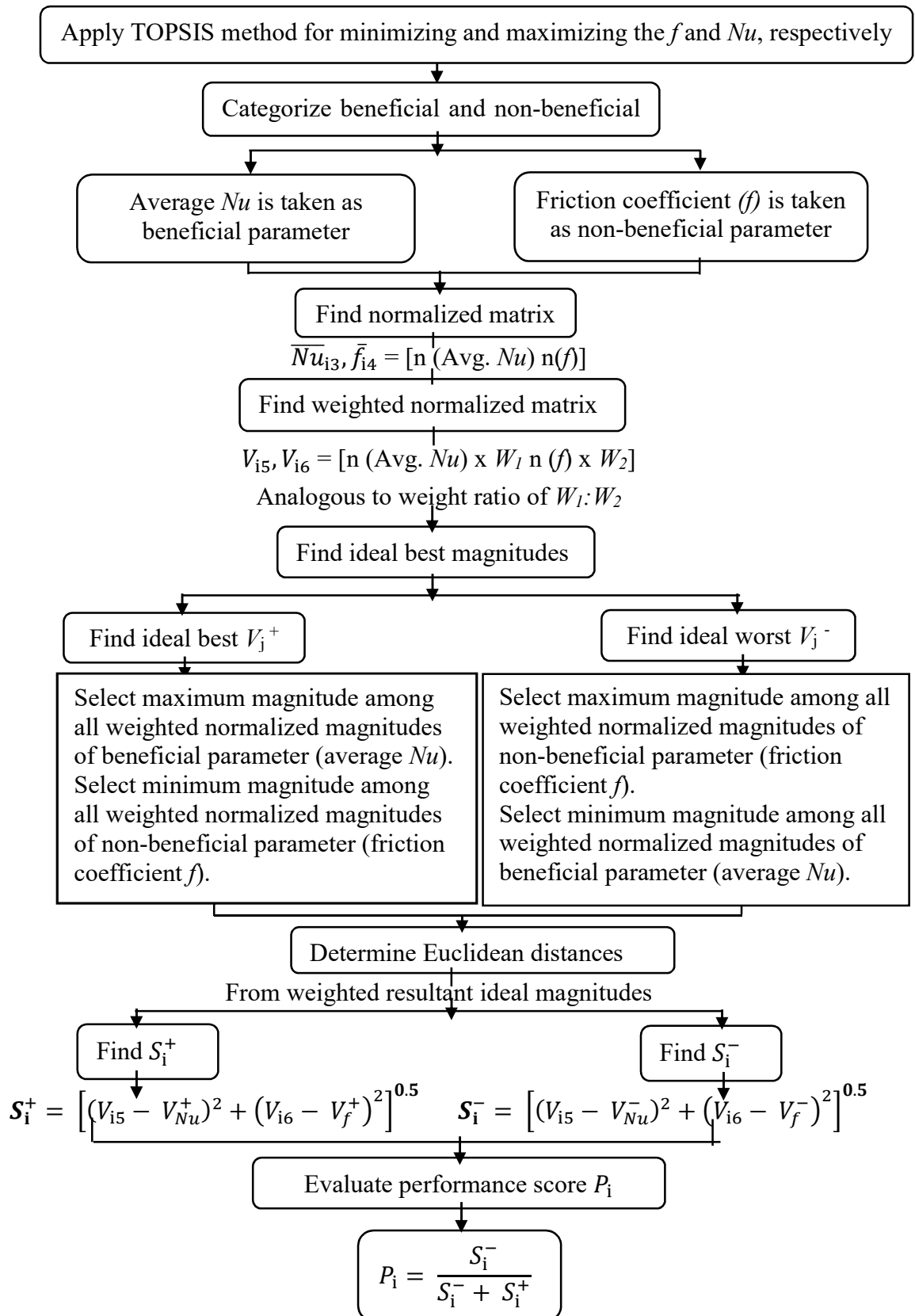


Figure 5.3 Flowchart that represents the steps involved in TOPSIS methodology.

5.5 COMPUTATIONAL DETAILS, GRID SENSITIVITY ANALYSIS AND VALIDATION STUDY

The numerical calculations are performed using software ANSYS FLUENT 19.2 (ANSYS FLUENT (2019)). The pressure-velocity coupling method is adopted for the numerical examination. A rectangular mesh is considered for the numerical simulation. The relaxation factor for the pressure and momentum equations are considered as 0.5 and turbulent kinetic energy, specific dissipation rate and the energy equation are considered as 0.75. Convergence criteria for continuity, momentum, energy and $k-\omega$ are fixed as 10^{-5} , 10^{-5} , 10^{-3} and 10^{-10} respectively. For the existing research, the grid sensitivity examination is executed for four different grid sizes of 38481, 45501, 52521 and 59541 in order to attain an advantageous size of the grid and for the aluminium foam of pore density 10 and porosity of 0.95 is filled inside the conduit with a uniform velocity of 0.7377 m/s. It was found that among four different grid sizes, the grid number of 52521 is noticed to be advantageous. Furthermore, for the present numerical approach, the results are validated with the analytical results of (Lu et al. (2016)) and Xu et al. (2011c)). The numerical investigation is accomplished for the parallel plates with 80% and 50% filling rate of the aluminum foam having the pore density of 10 with $\varepsilon = 0.9$ as per (Lu et al. (2016)). The simulated results of velocity profile obtained for the current study coincides well with the analytical results of (Xu et al. (2011c)). To check the calculation for the pressure drop, the results of simulated pressure drop are matched with the experimental work of (Kamath et al. (2013)) for 10 PPI aluminum foam partially filled inside the channel. It is found that the simulated results of pressure drop are well comparable with (Kamath et al. (2013)). The grid independence study and the validation results was reported in the previous Chapter 4.

5.6 RESULTS AND DISCUSSION

5.6.1 Velocity Distribution at Different Locations of Pipe

Figure 5.4 shows the velocity distribution for foam and non-foam filled regions at different locations of the pipe for 10 PPI and 45 PPI foam when $Re = 6500$ for model 2. The velocity of the fluid is higher at non-porous region of the channel while it

decreases at the porous region of the pipe. The increase and decrease in velocity of fluid is large in the porous and non-porous region, respectively at $Z = 0.477$ due to sudden entry of the fluid. As the fluid reaches the exit of the pipe, the variation in velocity seems to be marginally the same for foam as well as non-foam region since flow becomes fully developed. The velocity of the fluid is observed to be lesser in aluminum foam region than the non-foam region of the pipe which is very obvious. Furthermore, the velocity of the fluid in the clear region increases and in porous region decreases by increase of pore density (PPI), if Figure 5.4(a) and (b) are compared. The increase of PPI enhances flow resistance in the porous region and fluid prefers to flow in the free region with lower pressure drop. Almost the same flow configurations are observed for all studied models and different Reynolds numbers.

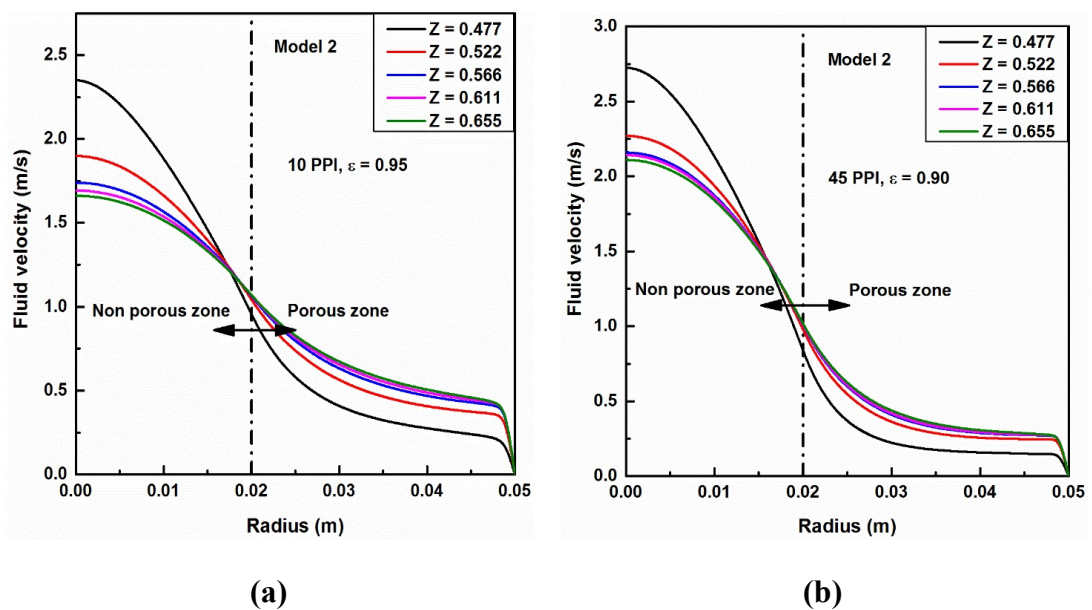


Figure 5.4 Fluid velocity variation in the pipe for model 2 when $Re = 6500$ (a) PPI = 10, $\epsilon = 0.95$ and (b) PPI = 45, $\epsilon = 0.90$.

5.6.2 Fluid-Solid Temperature Distribution at Different Locations of Pipe

The fluid-solid temperatures of the porous and clear regions of model 2 filled partially with 10 PPI and 45 PPI aluminium foam along the radius of the pipe are shown in Figure 5.5 when $Re = 6500$. From the Figure 5.5(a), the fluid temperature is observed to be small at $Z = 0.477$ and it increases at the exit of the pipe. In the porous filled

region, the fluid-solid temperature can be identified easily; and fluid temperature in the porous filled region seems to be smaller than that of solid temperature. Similar kind of fluid-solid temperature results is observed at $Z = 0.522, 0.566, 0.611$ and 0.655 . Furthermore, the fluid-solid temperature is more or less the same as it progresses towards the exit except near the wall of the pipe. In addition, the fluid-solid temperature in porous region is noticed to be constant and the same for the pore density of 45 PPI as seen in Figure 5.5(b). By increasing PPI, the specific surface area and the rate of flow mixing increases (See Table 5.4) and consequently the fluid temperature approaches to the temperature of the solid phase.

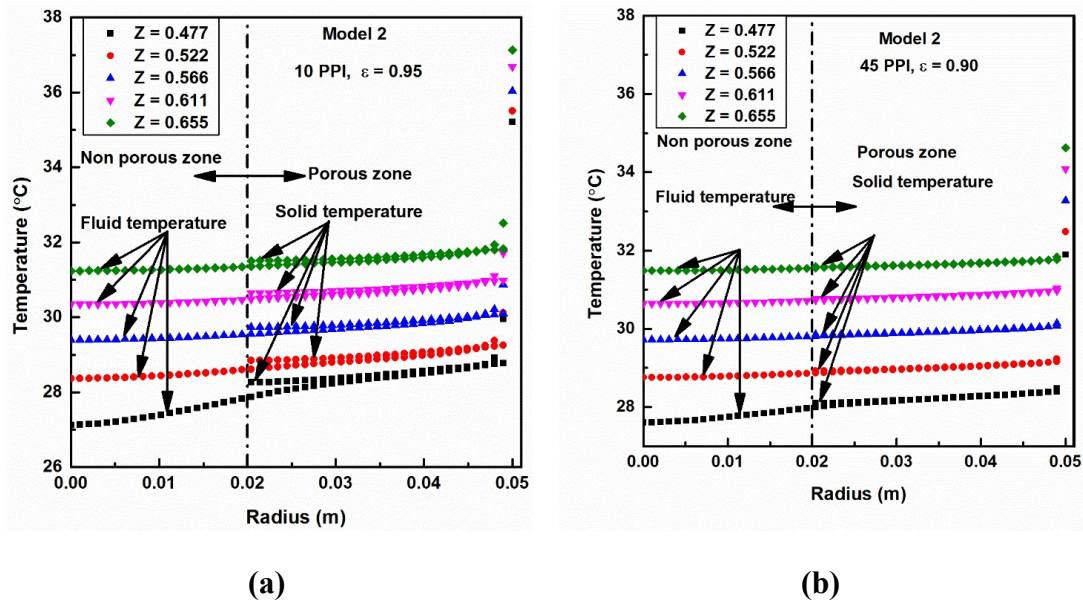


Figure 5.5 Fluid and solid temperature variation for Model 2 when $Re = 6500$ (a) PPI = 10, $\varepsilon = 0.95$ and (b) PPI = 45, $\varepsilon = 0.90$.

5.6.3 Friction Coefficient

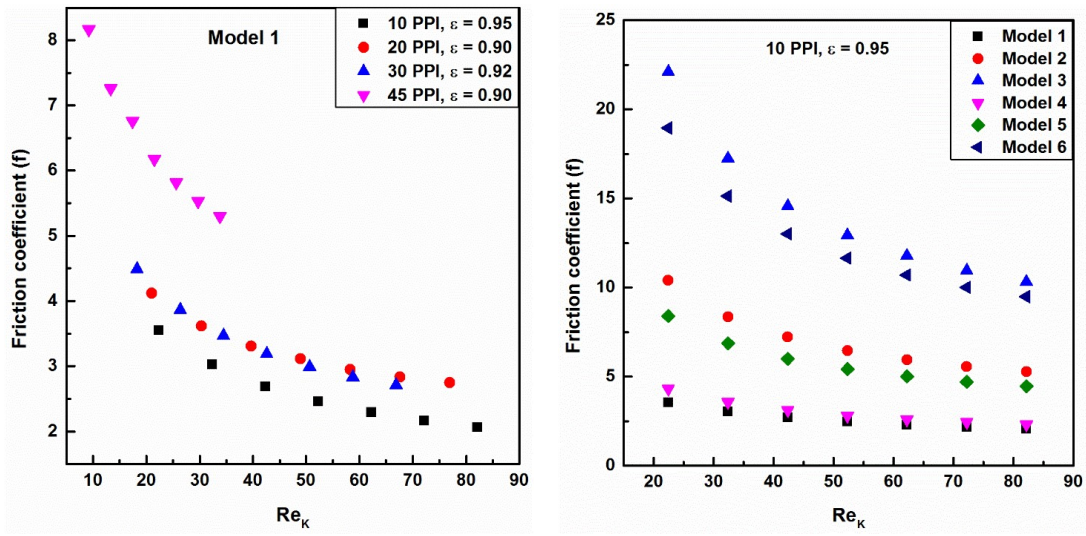
The friction coefficient is computed using the classical definition as,

$$f = \frac{2\rho_f \Delta P D_h}{u_{in}^2 L} \quad (5.15)$$

Since most of friction occurs in the aluminium foam region, the results of the friction coefficient versus Reynolds number based on permeability (Re_k) are plotted and shown in Figure 5.6. Figure 5.6(a) depicts the friction coefficient of model 1 in the presence

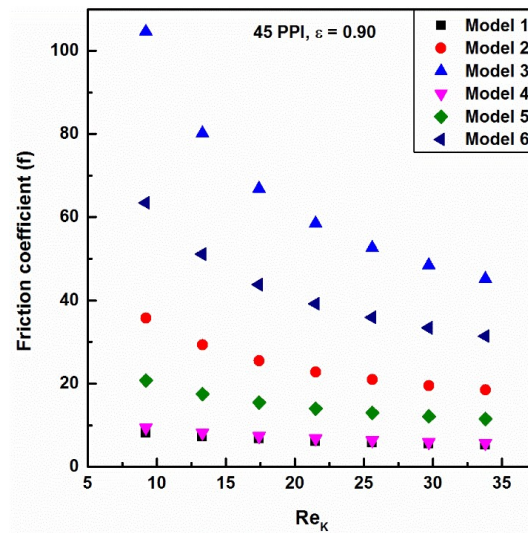
of four different foam samples of 10 PPI, 20 PPI, 30 PPI and 45 PPI. The friction coefficient decreases with the increase of Re_k for all studied PPI in this work. However, 45 PPI metal foam guaranteed the highest friction coefficient than other PPIs. Due to increase of the surface area and mixing of fluid, the flow resistance inside the pores of the aluminum foams with 45 PPI is considerably high. For instance, for $Re_k = 20$, the friction coefficient of 45 PPI is 39.53%, 50.09% and 62.16% greater than friction factor of 30 PPI, 20 PPI and 10 PPI aluminum foams, respectively. The pore density of 20 and 30 shows similar trend for the friction coefficient with respect to Re_k ; but, 10 PPI foam sample has the lowest friction coefficient than other PPI of the foam samples considered in the study as depicted in Figure 5.6(a).

Figure 5.6(b) and (c) explored the friction coefficient for 10 PPI and 45 PPI aluminium foam filled partially inside pipe for model 1 to model 6. From the obtained results, it is noticed that the model 1 and model 4 show a similar behavior of friction coefficient, and the friction factor is the lowest among other models due to the thin layer of aluminum foam for 10 PPI. A pipe filled with aluminum foam using models of 3 and 6 show a high flow resistance since the aluminum foam layer is considerably thick. The average friction factor for model 3 is 12.36% and 448.85% greater than model 6 and model 1 for 10 PPI aluminum foam, respectively in the range of Re_k simulated. The friction factor is considerably high for 45 PPI (Figure 5.6(c)) compared with 10 PPI (Figure 5.6(b)) due to high surface area and mixing of fluid. For 45 PPI, again the highest friction factor is observed for model 6 and it decreases gradually for the other models. The average friction factor for model 3 is 52.87% and 913.53% larger than those of model 6 and model 1, respectively for 45 PPI in the range of Re_k considered. As it can be seen, the thickness of the aluminum foam layer and its position (center or lateral) play an important role on the pressure drop in a pipe partially filled with aluminum foam.



(a)

(b)



(c)

Figure 5.6 The change of friction coefficient with Reynolds number based on permeability for different models and PPI (a) model 1, (b) comparative study of all models for 10 PPI and (c) comparative study of all models for 45 PPI.

5.6.4 Average Nusselt Number

The mean Nusselt number is important to compare the thermal performance of the studied models and it is defined as,

$$\overline{Nu} = \frac{\bar{h}D_h}{\lambda_{air}} \quad (5.16)$$

where \bar{h} is the average heat convective coefficient that computed using the Eq. (5.17).

$$\bar{h} = \frac{\sum_1^N h}{N} \quad (5.17)$$

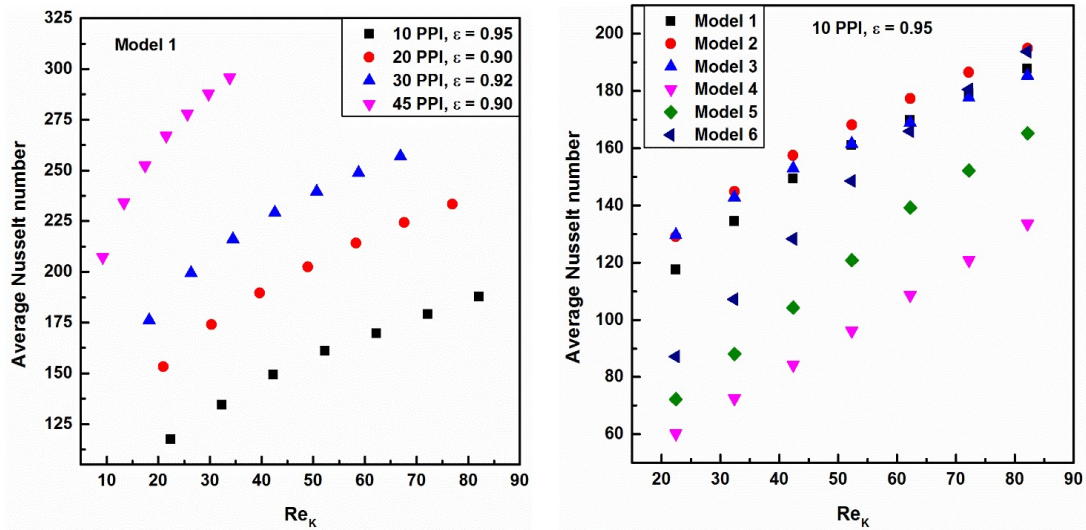
h is the local forced convection coefficient is examined using following equation.

$$h = \frac{q_w}{T_w - T_{mf}} \quad (5.18)$$

Figure 5.7(a) presents the results of average Nusselt number versus Re number based permeability (Re_k) for model 1. It is explored that the average Nusselt number in the presence of four different foam samples of 10 PPI, 20 PPI, 30 PPI and 45 PPI that are filled partially inside the pipe. The average Nusselt number augments progressively with augment in Re_k for all PPI. However, 45 PPI metal foam guaranteed the highest average Nusselt number than the other PPIs. This may be due to the fact that 45 PPI metal foam sample has the highest specific surface area and the smaller opening of the pores promotes the fluid to flow in a circuitous path causing more mixing of the fluid. 10 PPI foam sample shows the least average Nusselt number than other PPI of the aluminum foam samples considered in this study. 10 PPI foam sample has the smallest specific surface area compared to other PPIs (see Table 5.4). For $Re_k = 30$, the value of Nusselt number for 45 PPI is 38.64%, 65.52% and 116.54% higher than 30 PPI, 20 PPI and 10 PPI, respectively.

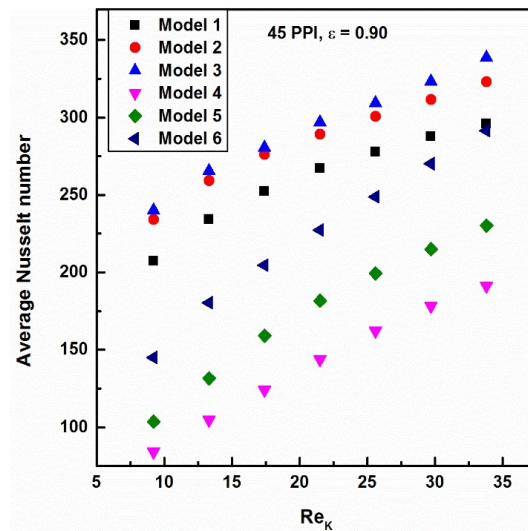
Figure 5.7(b) and (c) illustrates the change of average Nusselt number for 10 PPI and 45 PPI foam samples with respect to Re_k for all Models. From the results, it is guaranteed that the average Nusselt number increases linearly with respect to Re_k for the 6 models. In general, models 1, 2 and 3 have greater average Nusselt number compared to models 4, 5 and 6. This result shows that placing the aluminum foam layer on the solid wall provides more heat transfer compared to the location of the center of pipe. The highest Nusselt number is observed for models 2 and 3 while the lowest is seen for model 4. Models 2 and 3 have thick aluminum foam layer attached to the lateral surface while model 4 has a thin aluminum foam in the center. When $Re_k = 32$, the values of Nusselt number of model 3 and model 4 are 331.98, 185.75 and 142.72, 72.48 for 45 PPI and 10 PPI, respectively, which are 132.61% and 156.28% greater than 10

PPI, respectively. The comparison of Figure 5.7(b) and Figure 5.7(c) again shows that Nusselt number of a pipe with 45 PPI is considerably greater than 10 PPI.



(a)

(b)



(c)

Figure 5.7 The variation of average Nu with Re_k . (a) for model 1, (b) for all models when PPI = 10, (c) for all models when PPI = 45.

5.7 PERFORMANCE INVESTIGATION OF MULTI-OBJECTIVE FUNCTIONS

The performance investigation is carried out for 6 models with four different aluminium foam samples filled partially inside the pipe. The investigated performance score should meet the assigned weights so as to minimize and maximize the friction coefficient and heat transfer rate, respectively. In such cases, different units of weights are assigned and varied from 0 to 1. Here, the performance score of the aluminium foam samples which is equal to 0 implies that the given criteria is not meeting the given specified requirements. However, performance score of the foam samples is equal to 1 implies that the given condition acquires the given requirements in the current scenario. The unit weights are assigned in five different conditions/criteria's which are categorized as: $(f)_{\min}:(Nu)_{\max} = 0.0:1.0$, $(f)_{\min}:(Nu)_{\max} = 0.25:0.75$, $(f)_{\min}:(Nu)_{\max} = 0.50:0.50$, $(f)_{\min}:(Nu)_{\max} = 0.75:0.25$ and $(f)_{\min}:(Nu)_{\max} = 1.0:0.0$. Therefore, the performance score is evaluated individually with assigned unit weights in order to minimize and maximize the friction coefficient and heat transfer rate, respectively for the given foam samples.

5.7.1 Criteria I $(f)_{\min}:(Nu)_{\max} = 0.0:1.0$

The criteria I brings the scenario where no significance is given to minimize the friction coefficient (the minimum weight is assigned on $(f)_{\min}$ and is equal to 0) and the highest significance is given to maximize the heat dissipation rate of various foam samples (the maximum weight assigned on $(Nu)_{\max}$ is equal to 1) for two different Reynolds number as 6500 and 16500, as shown in Figure 5.8. From the results, the 45 PPI foam samples has the best score which is equal to 1, and 10 PPI foam sample performance is the least performance score and nearly equal to 0 irrespective of the models for both Reynolds numbers. 45 PPI aluminum foam sample performs perfectly due to the highest heat transfer specific surface area and the smaller pore size causing higher mixing of fluid in the pores (i.e., high interfacial convective heat transfer). Subsequently, 30 PPI and 20 PPI foam samples perform in between 10 PPI and 45 PPI foam samples. But, to some extent, models 1, 2 and 3 for 30 PPI foam sample meet the desired prerequisite while the other cases do not meet the desired prerequisite at lower and higher flow rate of air (i.e., $Re = 6500$ and 16500).

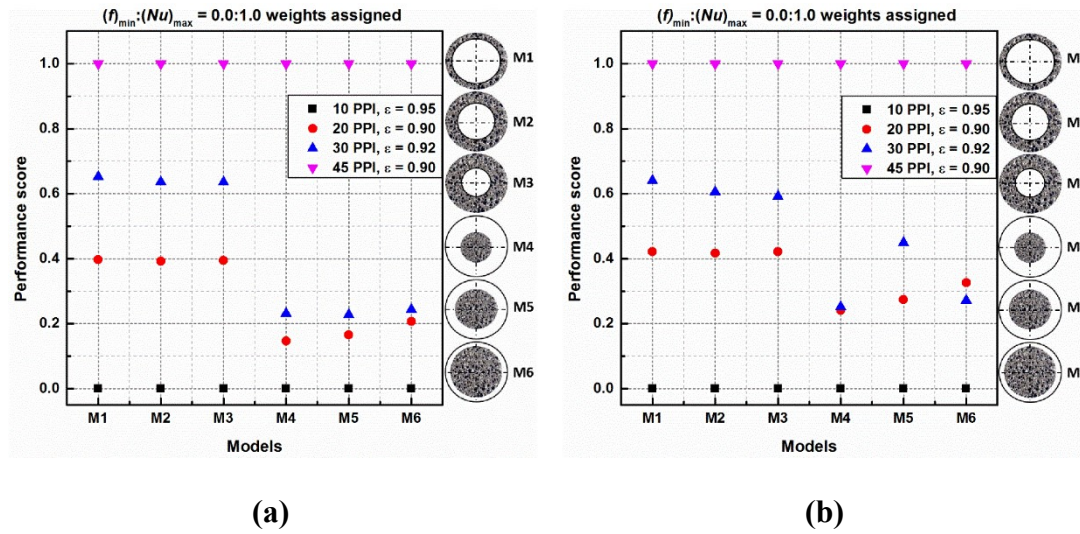


Figure 5.8 Performance score of 6 Models for *Criteria I* $(f)_{min} : (Nu)_{max} = 0.0 : 1.0$, (a) $Re = 6500$ and (b) $Re = 16500$.

5.7.2 Criteria II $(f)_{min} : (Nu)_{max} = 0.25 : 0.75$

Criteria II resembles the scenario where lesser importance is given for minimizing the friction coefficient (i.e., lesser weightage is assigned on friction coefficient $(f)_{min}$ equal to 0.25) while still higher importance is given to augmentation of heat transfer (i.e., higher weightage is assigned on $(Nu)_{max}$ and is equal to 0.75). 30 PPI with porosity of 0.92 foam sample shows the greatest performance score for the models 1, 2 and 3 at higher and lower Reynolds number as shown in Figure 5.9. The performance score increases and weakens marginally for models 1, 2 and 3 at lower and higher flow rates of fluid. The models 3 and 1 attain the highest performance score which are equal to 0.713 and 0.689 for $Re = 6500$ and 16500. The score of model 3 with 30 PPI is 25.34% and 28.60% higher than the scores of the same model with 20 PPI and 45 PPI, respectively when $Re = 6500$, and these percentages are 21.07% and 21.20% for $Re = 16500$. Although 30 PPI shows good performance for models 1, 2 and 3, the same performance is not observed for models 4, 5 and 6 since the porous layer is not attached to the lateral surface. Aluminum foam with 20 PPI and 45 PPI show also acceptable performance for models 1, 2 and 3 since their scores are greater than 0.5. Again, the smallest performance scores can be observed for 10 PPI aluminum foam due to small

heat transfer area and mixing rate.

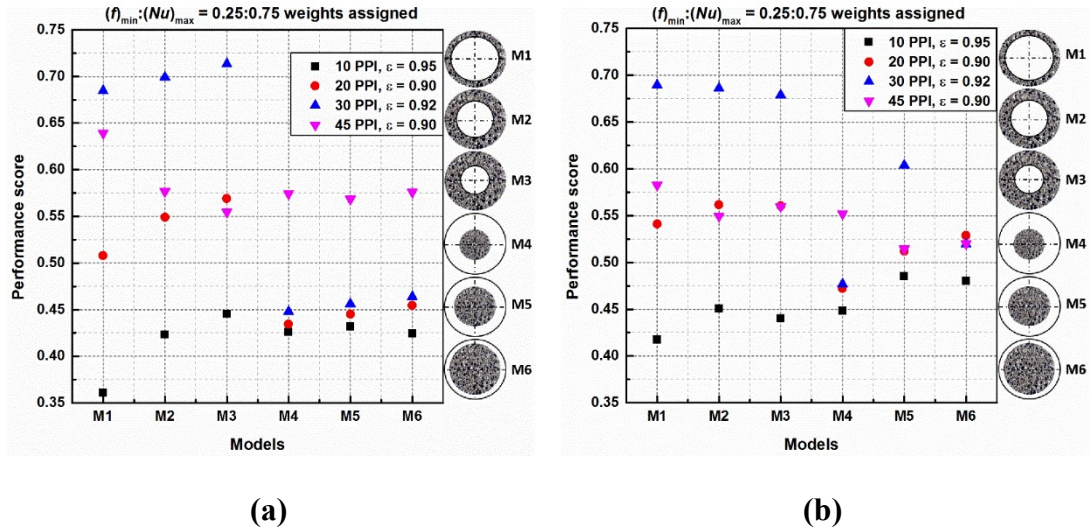


Figure 5.9 Performance score of 6 models for *Criteria II* $(f)_{min} : (Nu)_{max} = 0.25 : 0.75$, (a) $Re = 6500$ and (b) $Re = 16500$.

5.7.3 Criteria III $(f)_{min} : (Nu)_{max} = 0.50 : 0.50$

Criteria III brings the scenario where equal prominence is given for minimizing the friction coefficient (i.e., equal weightage is assigned on friction coefficient $(f)_{min}$ is equal to 0.50) and equal eminence is given to augment heat transfer (i.e., equal weightage is assigned on $(Nu)_{max}$ and is equal to 0.50) for four distinct aluminium foam samples, and the results are shown in Figure 5.10. For equal weightage assigned for condition III; aluminum foam sample of 45 PPI shows the lowest performance scores due to high flow resistance of 45 PPI. At lower flow rate (i.e., $Re = 6500$), the models 2 and 3 with 30 PPI have the highest performance scores for both $Re = 6500$ and 16500. After the highest scores of aluminum foam with 30 PPI, the foam layers with 20 PPI and 10 PPI have the second and third ranks. The score values for models 2 and 3 when PPI = 30 are 0.79, 0.81 and 0.78, 0.79 for low and high Reynolds numbers, respectively, which are 6.93%, 7.37% and 11.09%, 13.52% greater than 20 PPI and 10 PPI. Two important points attract attention in Figure 5.10.

- A considerable increase of performance scores of models 4, 5 and 6 for Criteria III compared the performance scores of Criteria I and II due to increase of

significant of pressure drop. For instance, the score of model 5 with 30 PPI for Criteria III is 0.67937 which is 49.03% and 199.40% higher than the same models and PPI of Criteria II and I, respectively at lower flow rates. From Figure 5.6(b) and (c), the low values of friction factors of model 4, 5 and 6 can be observed compared to the other models.

- b) The rank of aluminum foam with 10 PPI considerably rises for Criteria III compared Criteria I and II due to lower surface area and wide pore size causing less pressure drop. The score of model 3 with 10 PPI for Criteria III is 0.70 and it is 58.68% and 108.43% greater than the same case of Criteria II and I, respectively at lower flow rates due to the low friction factor of 10 PPI which can be observed from Figure 5.6(a).

In general, all models with 10 PPI, 20 PPI and 30 PPI provides acceptable performance score (more than 0.5) however 45 PPI fails to satisfy the required condition of Criteria III.

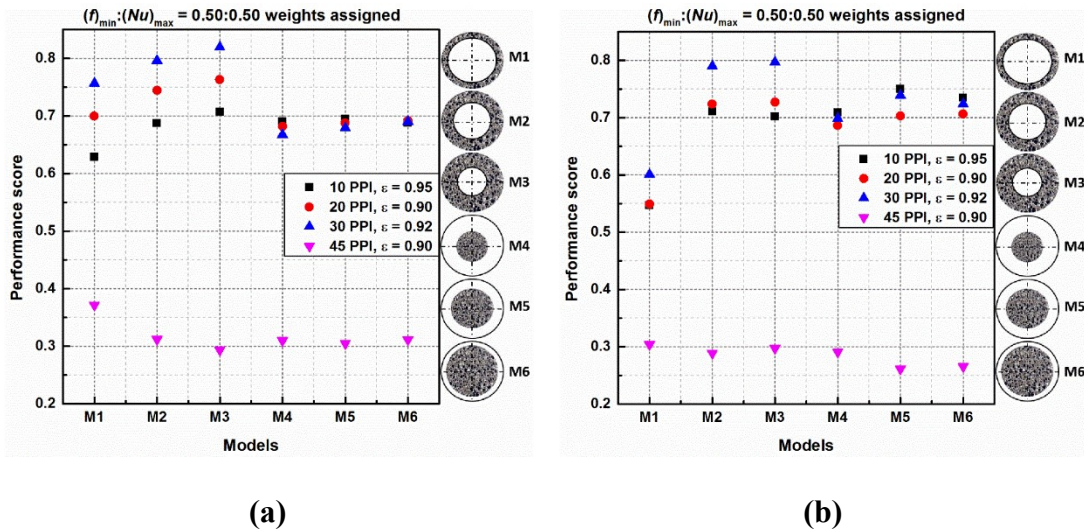


Figure 5.10 Performance score of 6 models for *Criteria III* $(f)_{min} : (Nu)_{max} = 0.50 : 0.50$, (a) $Re = 6500$ and (b) $Re = 16500$.

5.7.4 Criteria IV $(f)_{min}:(Nu)_{max} = 0.75:0.25$

Criteria IV brings the scenario where most eminence is given for minimizing the friction coefficient (i.e., higher weightage is assigned on friction coefficient $(f)_{min}$ is

equal to 0.75) while the marginally least eminence is given to augment heat transfer (i.e., less weightage is assigned on $(Nu)_{max}$ and is equal to 0.25) for four different aluminium foam samples. Figure 5.11(a) & (b) presents the results for Criteria IV in order to minimize flow resistance. Under this requirement, it is clear that a pipe containing aluminum foam with 45 PPI foam has the smallest score for all Models from 1 to 6. Therefore, definitely the foam sample of 45 PPI does not meet the required condition. The interesting point is that for the both two Reynolds numbers (6500 and 16500), the aluminum foam with 10 PPI takes the highest score and the scores of models 4, 5 and 6 becomes almost equal with models 1, 2 and 3 for both Reynolds number due to attention paid to pressure drop. Model 3 with 10 PPI shows the best performance score for $Re = 6500$ while model 5 with 10 PPI provides the best score due to high velocity and friction factor for $Re = 16500$. The scores of models 3 and 5 with 10 PPI are 22.46% and 19.11% greater than the scores of model 3 with 20 and 30 PPI, and 15.73% and 11.87% greater than the scores of model 5 with 20 PPI and 30 PPI, respectively. Similar to Criteria III, all models with 10 PPI, 20 PPI and 30 PPI satisfy the requirement of Criteria IV.

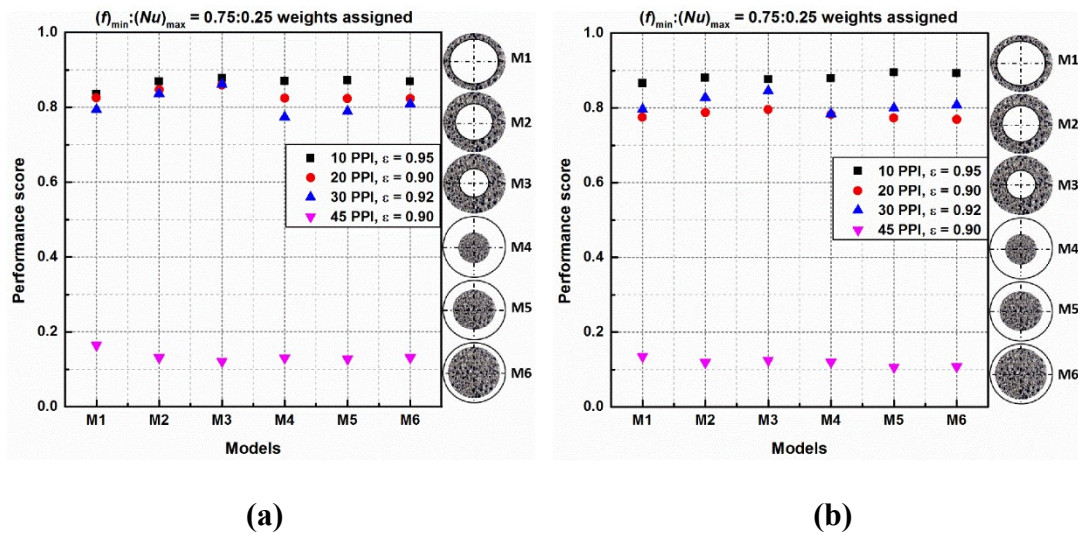


Figure 5.11 Performance score of 6 models for *Criteria III* $(f)_{min} : (Nu)_{max} = 0.75 : 0.25$, (a) $Re = 6500$ and (b) $Re = 16500$.

5.7.5 Criteria V $(f)_{min} : (Nu)_{max} = 1.0:0.0$

Criteria V brings the scenario where most prominence is given for minimizing the friction coefficient (i.e., maximum weightage is assigned on friction coefficient $(f)_{min}$ is equal to 1.0) while least prominence is given to augment of heat transfer (i.e., no weightage is assigned on $(Nu)_{max}$ and is equal to 0.0). From Figure 5.12(a) and (b) it is observed that all the models from M1 to M6 performs equally and are equal to a performance score of 1 for 10 PPI lower and higher flow rates of the fluid. However, 45 PPI presents the least performance score and is nearly equal to zero for the all models from 1 to 6. This is because the resistance between the fluid and foam is comparatively higher for 45 PPI. Henceforth, the aluminum foam sample of 45 PPI definitely does not meet the given required desire. For $Re = 6500$, the second rank for performance score belongs to 20 PPI and the third rank relates to 30 PPI, however there is no big difference between their score values. Our computational results showed that for low values of pore Reynolds number (Re_k), the friction factor of 20 PPI is a little bit less than 30 PPI for the studied aluminum foams. However, by increasing Re_k , the friction factor of 30 PPI becomes a little bit smaller than 20 PPI, as seen from Figure 5.6(a). This small changes in in friction factor causes the performance score of 30 PPI becomes a little bit above the 20 PPI for $Re = 16500$.

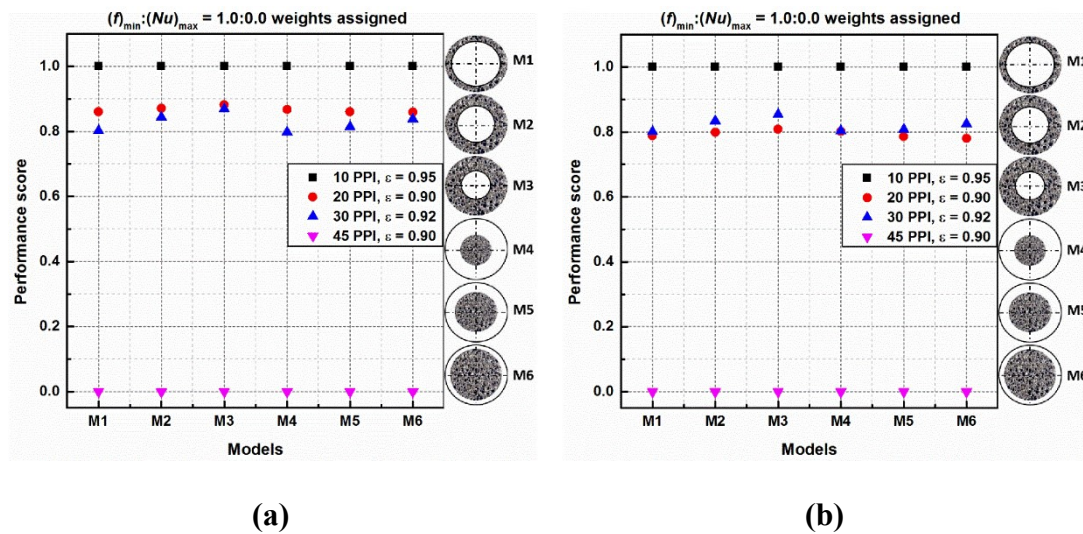


Figure 5.12 Performance score of 6 models for *Criteria III* $(f)_{min} : (Nu)_{max} = 1.0 : 0.0$, (a) $Re = 6500$ and (b) $Re = 16500$.

5.8 SUMMARY

Forced convection heat transfer was studied with the effect of partial filling high porosity metal foams in a horizontal pipe. The numerical exploration considered six different models with variation in PPI's of the aluminium metallic foams. The TOPSIS method was applied to find out the best combination of models and the foam samples involved in the study. Five different criteria have been proposed to analysis the heat transfer and pressure drop in connection with the six models. Based on the investigation, the salient points are drawn below:

- Higher PPI of the foam (such as 45 PPI) possesses more flow resistance however it increases heat transfer compared to other studied PPI metal foams. Reversely 10 PPI metal foam shows the lowest flow resistance and its contribution for heat transfer is minimum.
- According to criteria I (minimum weight is assigned on friction factor), 45PPI has the highest performance score among all the models for the Reynolds numbers 6500 and 16500. Since highest importance is given only to the heat transfer than the friction factor, irrespective of any models one can choose the above configuration for the enhancement of heat transfer.
- Based on criteria II (lesser weightage is assigned on friction coefficient as 0.25), Model 3 attains highest performance with 30 PPI for the Reynolds number of 6500 (Score = 0.713), and for Reynolds number of 16500, Model 1 attains highest performance (Score = 0.689). The aluminum foam with 45PPI with 0.9 porosity still becomes the next best possible solution for all the considered models.
- Aluminum foam with 30PPI dominates under criteria III where equal importance was given to both heat transfer and friction factor. Other PPIs compete with 30PPI however aluminum foam with 45PPI becomes under performer for all the models and Reynolds numbers because of the increased friction factor.
- For the criteria IV and V (higher weightage and maximum weightage are assigned on friction coefficient as 0.75 and 1, respectively), all the models engage themselves to go in for a better performance score, eventually 10 PPI

occupies the highest place for both Reynolds numbers due to the lowest friction factor among the studied PPI (Score = 1). Similar to criteria III, 45PPI stands last in the performance score as the mentioned criteria end up with high importance only to pressure drop.

5.9 CLOSURE

Performance score based multi-objective optimization for thermal design of partially filled high porosity metal foam pipes under forced convection was studied. The foam is aluminum with PPI varying from 10 to 45 and the porosity range is 0.90-0.95.

The TOPSIS optimization techniques with five different criteria was used. TOPSIS was an appropriate method for optimization of the partially filled porous media channels or pipes. Based on the preference between the pumping power and heat transfer enhancement, the best position, thickness and PPI was determined accurately. The next Chapter presents the overall conclusion of current research work.

CHAPTER 6

CONCLUSIONS

In the present thesis, a parametric analysis of fully, discrete and partially filled high porosity metallic foams in a horizontal pipe was performed to augment heat transfer with reasonable pressure drop. Also the optimization study was performed for the multi-objective functions for maximization and minimization of heat transfer rate and pressure drop. A two-dimensional axis symmetry physical domain was employed for the computational modelling of the porous medium. The pipe wall was coupled with heater around the circumference of the pipe and the heater was assigned with constant heat input. The air was considered as the working fluid. The current thesis commences with an introduction that covers the concepts of porous medium and fluid flow models. It also covers the thermal models available for predicting heat flow through porous medium. In **Chapter 1**, the facts on metal foam porous medium and their applications, as well as their benefits were highlighted. **Chapter 2** outlines the critical evaluation of the literature followed by the key objectives of the present work. **Chapter 3** explores the effect of fully and discrete filled metallic foam, pore density, porosity and flow Reynolds number for various flow regimes. Initially, a detailed analysis was carried out for 0.6L m fully filled foam placed exactly at center of the pipe. Later, four different numerical domains were created to perform parametric analysis such that the heat transfer and pressure drop must be increased and decreased. The details of four numerical domains were: $L_f = 0.6L$ m discrete filled foam, $L_f = 0.8L$ m fully filled foam, $L_f = 0.8L$ m discrete filled foam and $L_f = L$ m fully filled foam. From the study, for a constant flow Reynolds number, the heat transfer rate showed maximum and minimum with higher PPI and porosity of the metallic foams, respectively. However, at higher Reynolds number the heat transfer rate advanced with increment in pore density and declines with the porosity of the metallic foams. Henceforth, heat transfer rate must be enhanced by considering lower porosity and higher pore density (PPI) of the metallic foams accompanied with cost of pressure drop. Subsequently, $L_f = 0.8L$ m fully filled foam performs the higher dissipation rate than the $L_f = 0.8L$ m discrete filled

foam with the same pressure drop. Henceforth, $L_f = 0.8L$ m fully filled foam is highly recommended than the $L_f = 0.8L$ m discrete filled foam. Further, by comparing $L_f = 0.6L$ m fully and discrete filled foam, the $L_f = 0.6L$ m fully filled provides the better heat dissipation rate, heat transfer enhancement ratio as well as the performance factor accompanied with the cost of pressure drop. In addition, when $0.6L$ m discrete and $0.8L$ m discrete metallic foams are inserted, the heat transfer rate decreases the most at higher flow rates than when $0.6L$ m filled and $0.8L$ m fully filled foams are inserted. It is also noticed that, beyond $Re = 3500$; the results of performance factor showed very similar for $0.6L$ m fully filled and $0.8L$ discrete filled foam for a constant PPI as well as porosity of the metallic foam.

Chapter 4 describes the effect of partial filling metal foam layer thickness from the wall side to towards core of the pipe and from core of the tube to towards the wall of pipe (six different models) on the flow distribution, temperature distribution and thermo-hydrodynamic performance of pipe heat exchanger. For the analysis, the pore density is varied from 10 PPI to 45 PPI and their porosity ranges between 0.9 to 0.95. As foam layer thickness increases from wall side to towards the core of the pipe (i.e., model 1, model 2 and model 3), heat dissipation rate enhanced significantly when compared to foam layer thickness increases from core to towards the wall of the pipe (i.e., model 4, model 5 and model 6). However, the pressure drop was observed to be more or less the similar for models 1 and 4 and significantly higher for the models 2 and 3 comparatively to the models 5 and 6, respectively. Furthermore, with insertion of 30 PPI foam layer thickness the convection coefficient showed more or less the similar results for the models 2 and 3 accompanied with maximum pressure drop for the model 3 than the model 2. Hence, in order to minimize the pressure drop with maximum heat dissipation rate the model 2 is highly recommended over the model 3. It is also noticed that, with insertion of 10 PPI copper foam layer thickness at the core of the pipe (i.e., model 6) the heat transfer augment faster beyond $Re = 16500$; comparatively to all other models involved for the study. When compared to various PPI of metal foams in the range of Reynolds numbers studied, 30 PPI aluminium metal foam had the highest thermal performance factor for model 1. The thermal performance factor of 10 PPI aluminium foam, on the other hand, is extremely close to that of the more expensive 10

PPI copper foam. As a result, 10 PPI aluminium foam with a good performance factor, little pressure loss, and lower foam cost can be chosen.

Chapter 5 presents the performance score multi-objective optimization to minimize and maximise friction resistance and heat transfer rate, respectively. To solve multi-objective functions, the TOPSIS approach was used. TOPSIS technique incorporated to discover the best model for determining the best position, thickness, and PPI of aluminium porous layer thickness depending on the thermal designer's priority for heat transfer and friction effects. The solid-fluid temperature distribution within the foam filled region can be noticed easily for the lower pore density of the metallic foam. However, at higher pore density (45 PPI) of the metallic foam, solid-fluid temperature showed more or less the same due to higher specific surface availability. It is also observed that, heat transfer rate was found to be higher for 30 PPI aluminium foam than the 20 PPI aluminium foam accompanied with similar friction resistance with flow permeability Reynolds number. Further from the optimization study, at lower and higher Reynolds numbers, 45PPI foam sample has showed the highest performance score among all the models according to criteria I (no weight is assigned on friction factor and maximum weight is assigned on Nusselt number). Because the heat transfer factor is more important than the friction factor, the above setup can be used to improve heat transmission regardless of the model. Also, when equal importance was given for both heat transfer and structural flow resistance the 30 PPI aluminium foam sample dominates under criteria III. Further, when no weightage is assigned on Nusselt number and maximum weightage is assigned on flow resistance the 10 PPI foam samples showed the best performer (performance score = 1) under criteria V for lower and higher Reynolds number since lesser flow resistance. For criteria III and V aluminium foam sample with 45 PPI showed the under performer for the all the models and Reynolds number.

6.1 SCOPE FOR FUTURE WORK

The major goal of this numerical investigation is to obtain flow and heat transfer features through metallic porous ligaments without taking into account the influence of mixing and tortuosity in the metal porous foam. The effects of thermal dispersion through the metal porous foam were also overlooked in the investigation. Hence, for the future study the following points are suggested:

- Experimental investigation is required to validate the numerical results obtained for various problem statements.
- To optimize the pore structure of the metal foam, pore scale analysis need to be done so as to reduce the pressure drop and increase the heat transfer for a given application.
- Conventional metal foam structures need to be compared with additively manufacture metal foams in order to develop more compact heat exchangers.
- Functionally graded metal foams need to be analysed to improve the performance of the heat exchangers along with the optimization studies.

REFERENCES

- Abadi, G. B., and Kim, K. C. (2016). “Experimental Heat Transfer and Pressure Drop in a Metal-Foam-Filled.” *Exp. Therm. Fluid Sci.*, 82(April), 42–49.
- Ahammed, N., Asirvatham, L. G., and Wongwises, S. (2016). “Thermoelectric cooling of electronic devices with nanofluid in a multiport minichannel heat exchanger.” *Exp. Therm. Fluid Sci.*, 74, 81–90.
- Ahmed, H. E., Fadhil, O. T., and Salih, W. A. (2019). “Heat transfer and fluid flow characteristics of tubular channel partially filled with grooved metal foams.” *Int. Commun. Heat Mass Transf.*, 108(October), 104336.
- Alazmi, B., and Vafai, K. (2001). “Analysis of fluid flow and heat transfer interfacial conditions between a porous medium and a fluid layer.” *Int. J. Heat Mass Transf.*, 44(9), 1735–1749.
- Alkam M. K., and Al-Nimr M. A. (1999) “Solar Collectors with Tubes Partially Filled with Porous.” *J. Sol. Energy Eng.*, 121(1), 20–24.
- Alomar, O. R. (2020). “Numerical investigation of two-phase flow in a horizontal porous evaporator with localised heating using non-Darcian flow and two equations model.” *Heat Mass Transf. und Stoffuebertragung*, 56(4), 1203–1221.
- Angeline, A. A., Jayakumar, J., Asirvatham, L. G., and Wongwises, S. (2018). “Power generation from combusted ‘Syngas’ using hybrid thermoelectric generator and forecasting the performance with ANN technique.” *J. Therm. Eng.*, 4(4), 2149–2168.
- ANSYS Fluent, (2019). “ANSYSV R 19.2, Help System, User’s Guide/Theory Guide.” ANSYS 2019, Inc., Canonsburg, PA, <http://www.ansys.com/Products/Fluids/ANSYS-Fluent>.
- Arbak, A., Dukhan, N., Bağcı, Ö., and Özdemir, M. (2017). “Influence of pore density on thermal development in open-cell metal foam.” *Exp. Therm. Fluid Sci.*, 86, 180–188.
- Asirvatham, L. G., Wongwises, S., and Babu, J. (2015). “Heat transfer performance of a glass thermosyphon using graphene-acetone nanofluid.” *J. Heat Transfer*, 137, 1–9.

Ba, Ö., and Dukhan, N. (2018). "Impact of pore density on oscillating liquid flow in metal foam." *Exp. Therm. Fluid Sci.*, 97(April), 246–253.

Baloyo, J. M., and Zhao, Y. (2021). "Permeability, Form Drag Coefficient and Heat Transfer Coefficient of Porous Copper." *Heat Transf. Eng.*, 42(8), 670–682.

Bamorovat Abadi, G., and Kim, K. C. (2017). "Experimental heat transfer and pressure drop in a metal-foam-filled tube heat exchanger." *Exp. Therm. Fluid Sci.*, 82, 42–49.

Banhart, J. (2001). "Manufacture, characterisation and application of cellular metals and metal foams." *Prog. Mater. Sci.*, 46(6), 559–632.

Baragh, S., Shokouhmand, H., Ajarostaghi, S. S. M., and Nikian, M. (2018). "An experimental investigation on forced convection heat transfer of single-phase flow in a channel with different arrangements of porous media." *Int. J. Therm. Sci.*, 134(August), 370–379.

Bodade, P. R. (2013). "A study on the heat transfer enhancement for air flow through a duct with various rib inserts (Review)." *Int. J. Latest Trends Eng Technol.*, 2(4), 479–485.

Boules, D., Sharqawy, M. H., and Ahmed, W. H. (2021). "Enhancement of heat transfer from a horizontal cylinder wrapped with whole and segmented layers of metal foam." *Int. J. Heat Mass Transf.*, 165, 120675.

Boyd, B., and Hooman, K. (2012). "Air-cooled micro-porous heat exchangers for thermal management of fuel cells." *Int. Commun. Heat Mass Transf.*, 39(3), 363–367.

Brusly Solomon, A., Mathew, A., Ramachandran, K., Pillai, B. C., and Karthikeyan, V. K. (2013). "Thermal performance of anodized two phase closed thermosyphon (TPCT)." *Exp. Therm. Fluid Sci.*, 48, 49–57.

Calmidi, V. V., and Mahajan, R. L. (2002). "Forced Convection in High Porosity Metal Foams." *J. Heat Transfer*, 122(3), 557.

Celik, H., Mobedi, M., Manca, O., and Ozkol, U. (2017). "A pore scale analysis for determination of interfacial convective heat transfer coefficient for thin periodic porousmedia undermixed convection." *Int. J. Numer. Methods Heat Fluid Flow*,

27(12), 2775–2798.

Chen, K., Wang, X., Chen, P., and Wen, L. (2022). “Numerical simulation study on heat transfer enhancement of a heat exchanger wrapped with metal foam.” *Energy Reports*, 8, 103–110.

Chen, X., Sun, C., Xia, X., Liu, R., and Wang, F. (2019). “Conjugated heat transfer analysis of a foam filled double-pipe heat exchanger for high-temperature application.” *Int. J. Heat Mass Transf.*, 134, 1003–1013.

Chumpia, A., and Hooman, K. (2014). “Performance evaluation of single tubular aluminium foam heat exchangers.” *Appl. Therm. Eng.*, 66(1–2), 266–273.

Darcy, H. (1856). “Les Fontains Publiques de la Ville de Dijon.” Victor Dalmont, Paris.

Deb, S., Kaushik, L. K., Mahalingam, A. K., and Muthukumar, P. (2020). “Performance characterization of a cluster porous radiant burner for clean and efficient lpg combustion.” *Chem. Eng. Trans.*, 81(August), 361–366.

Deb, S., Satish, S. H. V, and Muthukumar, P. (2021). “Numerical Study of Combustion Modes in a Clustered Porous Radiant Burner.” *Energy proceedings*, Vol. 24, pp. 1–4.

Devi, S., Sahoo, N., and Muthukumar, P. (2023). “Comparative performance evaluation of a porous radiant burner with a conventional burner: Biogas combustion.” *Appl. Therm. Eng.*, 218(August 2022), 119338.

Dupuit, J. (1863). “Études théoriques et pratiques sur le mouvement des eaux dans les canaux découverts et à travers les terrains perméables.” Dunod, Paris.

Edrisi, S., Bidhendi, N. K., and Haghghi, M. (2017). “A new approach to modeling the effective thermal conductivity of ceramics porous media using a generalized self-consistent method.” *Heat Mass Transf. und Stoffuebertragung*, 53(1), 321–330.

Forchheimer, P. (1901). “Wasserbewegung durch Boden.” Edition, 45th. Zeitschrift des Vereins deutscher Ingenieuer Düsseldorf.

Gangapatnam, P., Kurian, R., and Venkateshan S. P. (2018). “Numerical simulation of heat transfer in metal foams.” *Heat Mass Transf.*, 54, 553–562.

- Garrity, P. T., Klausner, J. F., and Mei, R. (2015). "Performance of aluminum and carbon foams for air side heat transfer augmentation." *J. Heat Transfer*, 132(12), 1–9.
- Ge, Y., Liu, Z., and Liu, W. (2016). "Multi-objective genetic optimization of the heat transfer for tube inserted with porous media." *Int. J. Heat Mass Transf.*, 101, 981–987.
- Ghafarian, M., Mohebbi-Kalhari, D., and Sadeghi, J. (2013). "Analysis of heat transfer in oscillating flow through a channel filled with metal foam using computational fluid dynamics." *Int. J. Therm. Sci.*, 66, 42–50.
- Ghaneifar, M., Arasteh, H., Mashayekhi, R., and Rahbari, A. (2020). "Thermohydraulic analysis of hybrid nanofluid in a multilayered copper foam heat sink employing local thermal non-equilibrium condition : Optimization of layers thickness." *Appl. Therm. Eng.*, 181(June), 115961.
- Ghorab, M. G. (2015). "Forced convection analysis of discrete heated porous convergent channel." *Heat Transf. Eng.*, 36(9), 829–846.
- Godson, L., Raja, B., Mohan Lal, D., and Wongwises, S. (2010). "Enhancement of heat transfer using nanofluids-An overview." *Renew. Sustain. Energy Rev.*, 14(2), 629–641.
- Golbaghi Masouleh, S. S., Nikian, M., and Ghazi, M. (2022). "Analytical study on core flow in a novel scheme of cascade heat exchanger intensified with open foam partially filled in an annulus." *Int. J. Therm. Sci.*, 177(March), 107568.
- Gugulothu, R., Reddy, K. V. K., Somanchi, N. S., and Adithya, E. L. (2017). "A Review on Enhancement of Heat Transfer Techniques." *Mater. Today Proc.*, 4(2), 1051–1056.
- Hamadouche, A., Nebbali, R., Benahmed, H., Kouidri, A., and Bousri, A. (2015). "Experimental investigation of convective heat transfer in an open-cell aluminum foams." *Exp. Therm. Fluid Sci.*, 71, 86–94.
- Han, H. Z., Li, B. X., Wu, H., and Shao, W. (2015). "Multi-objective shape optimization of double pipe heat exchanger with inner corrugated tube using RSM method." *Int. J. Therm. Sci.*, 90, 173–186.
- Huang, Z. F., Nakayama, A., Yang, K., Yang, C., and Liu, W. (2010). "Enhancing heat transfer in the core flow by using porous medium insert in a tube." *Int. J. Heat Mass*

Transf., 53(5–6), 1164–1174.

Hunt, G., Karimi, N., and Torabi, M. (2017). “Analytical investigation of heat transfer and classical entropy generation in microreactors – The influences of exothermicity and asymmetry.” *Appl. Therm. Eng.*, 119, 403–424.

Hutter, C., Büchi, D., Zuber, V., and Rudolf von Rohr, P. (2011). “Heat transfer in metal foams and designed porous media.” *Chem. Eng. Sci.*, 66(17), 3806–3814.

Imani, G., Maerefat, M., and Hooman, K. (2013). “Pore-Scale Numerical Experiment on the Effect of the Pertinent Parameters on Heat Flux Splitting at the Boundary of a Porous Medium.” *Transp. Porous Media*, 98, 631–649.

Imani, G. R., Maerefat, M., and Hooman, K. (2012). “Estimation of heat flux bifurcation at the heated boundary of a porous medium using a pore-scale numerical simulation.” *Int. J. Therm. Sci.*, 54, 109–118.

Kamath, P. M., Balaji, C., and Venkateshan, S. P. (2011). “Experimental investigation of flow assisted mixed convection in high porosity foams in vertical channels.” *Int. J. Heat Mass Transf.*, 54(25–26), 5231–5241.

Kamath, P. M., Balaji, C., and Venkateshan, S. P. (2013). “Convection heat transfer from aluminium and copper foams in a vertical channel - An experimental study.” *Int. J. Therm. Sci.*, 64, 1–10.

Kaushik, L. K., Deb, S., and Muthukumar, P. (2018). “Energy Saving and Techno-economic Assessment of Self Aspirated Domestic LPG Stove with Porous Radiant Burner.” *IOP Conf. Ser. Mater. Sci. Eng.*, 377(1).

Kaviany, M. (1991). “Principles of Heat Transfer in Porous Media.” Edition, S. Springer-Verlag, New York.

Kopanidis, A., Theodorakakos, A., Gavaises, E., and Bouris, D. (2010). “3D numerical simulation of flow and conjugate heat transfer through a pore scale model of high porosity open cell metal foam.” *Int. J. Heat Mass Transf.*, 53(11–12), 2539–2550.

Kotresha, B., and Gnanasekaran, N. (2018). “Investigation of Mixed Convection Heat Transfer Through Metal Foams Partially Filled in a Vertical Channel by Using

Computational Fluid Dynamics.” *J. Heat Transfer*, 140(11), 112501.

Kotresha, B., and Gnanasekaran, N. (2019). “Effect of thickness and thermal conductivity of metal foams filled in a vertical channel – a numerical study.” *Int. J. Numer. Methods Heat Fluid Flow*, 29(1), 184–203.

Krohling, R. A., and Pacheco, A. G. C. (2015). “A-TOPSIS - An approach based on TOPSIS for ranking evolutionary algorithms.” *Procedia Comput. Sci.*, 55(Itqm), 308–317.

Kuwahara, F., Yang, C., Ando, K., and Nakayama, A. (2011). “Exact solutions for a thermal nonequilibrium model of fluid saturated porous media based on an effective porosity.” *J. Heat Transfer*, 133(11), 3–5.

Lai, T., Liu, X., Chu, J., He, M., and Zhang, Y. (2021). “Numerical Study of Flow and Heat Transfer in a Rectangular Channel Partially Filled with Porous Media at the Pore Scale Using Lattice Boltzmann Method.” *Heat Transf. Eng.*, 0(0), 1–19.

Leong, K. C., and Jin, L. W. (2005). “An experimental study of heat transfer in oscillating flow through a channel filled with an aluminum foam.” *Int. J. Heat Mass Transf.*, 48(2), 243–253.

Li, Y., Wang, S., and Zhao, Y. (2018a). “Experimental study on heat transfer enhancement of gas tube partially filled with metal foam.” *Exp. Therm. Fluid Sci.*, 97(April), 408–416.

Li, Y., Wang, S., Zhao, Y., and Lu, C. (2017). “Experimental study on the influence of porous foam metal filled in the core flow region on the performance of thermoelectric generators.” *Appl. Energy*, 207, 634–642.

Li, Z., Xia, X., Li, X., and Sun, C. (2018b). “Discrete vs . continuum-scale simulation of coupled radiation and convection inside rectangular channel filled with metal foam.” *Int. J. Therm. Sci.*, 132(June), 219–233.

Lin, W., Xie, G., Yuan, J., and Sundén, B. (2016). “Comparison and Analysis of Heat Transfer in Aluminum Foam Using Local Thermal Equilibrium or Nonequilibrium Model.” *Heat Transf. Eng.*, 37(3–4), 314–322.

- Long, R., Li, B., Liu, Z., and Liu, W. (2015). “Multi-objective optimization of a continuous thermally regenerative electrochemical cycle for waste heat recovery.” *Energy*, 93, 1022–1029.
- Lu, W., Zhang, T., and Yang, M. (2016). “Analytical solution of forced convective heat transfer in parallel-plate channel partially filled with metallic foams.” *Int. J. Heat Mass Transf.*, 100, 718–727.
- Lu, W., Zhao, C. Y., and Tassou, S. A. (2006). “Thermal analysis on metal-foam filled heat exchangers. Part I: Metal-foam filled pipes.” *Int. J. Heat Mass Transf.*, 49(15–16), 2751–2761.
- Lu, X., and Zhao, Y. (2019). “Effect of flow regime on convective heat transfer in porous copper manufactured by lost carbonate sintering.” *Int. J. Heat Fluid Flow*, 80(September), 108482.
- Maerefat, M., Mahmoudi, S. Y., and Mazaheri, K. (2011). “Numerical simulation of forced convection enhancement in a pipe by porous inserts.” *Heat Transf. Eng.*, 32(1), 45–56.
- Magyari, A. B. Æ. E., and Storesletten, Æ. I. P. Æ. L. (2008). “Mixed convection with viscous dissipation in an inclined porous channel with isoflux impermeable walls.” *Heat Mass Transf.*, 44, 979–988.
- Mahmoudi, Y., and Karimi, N. (2014). “Numerical investigation of heat transfer enhancement in a pipe partially filled with a porous material under local thermal non-equilibrium condition.” *Int. J. Heat Mass Transf.*, 68, 161–173.
- Mancin, S., Zilio, C., Diani, A., and Rossetto, L. (2013). “Air forced convection through metal foams : Experimental results and modeling.” *Int. J. Heat Mass Transf.*, 62, 112–123.
- Manglik R. M. (2003). “Heat Transfer Enhancement.” *Heat Transfer Handbook*, Wiley Hoboken NJ, 39, 1029–1130.
- Manova, S., Asirvatham, L. G., Nimmagadda, R., Bose, J. R., and Wongwises, S. (2020a). “Cooling of high heat flux electronic devices using ultra-thin multiport

minichannel thermosyphon.” *Appl. Therm. Eng.*, 169(November 2019), 114669.

Manova, S., Asirvatham, L. G., Nimmagadda, R., Bose, J. R., and Wongwises, S. (2020b). “Feasibility of using multiport minichannel as thermosyphon for cooling of miniaturized electronic devices.” *Heat Transf.*, 49(8), 4834–4856.

Mendes, M. A. A., Skibina, V., Talukdar, P., Wulf, R., Gross, U., Trimis, D., and Ray, S. (2014). “Experimental validation of simplified conduction-radiation models for evaluation of Effective Thermal Conductivity of open-cell metal foams at high temperatures.” *Int. J. Heat Mass Transf.*, 78, 112–120.

Mohammed, H. A., Abed, A. M., and Wahid, M. A. (2013). “The effects of geometrical parameters of a corrugated channel with in out-of-phase arrangement.” *Int. Commun. Heat Mass Transf.*, 40(1), 47–57.

Mousa, M. H., Miljkovic, N., and Nawaz, K. (2021). “Review of heat transfer enhancement techniques for single phase flows.” *Renew. Sustain. Energy Rev.*, 137(March 2021), 110566.

Nasution, M. K. M., Elveny, M., Syah, R., Behroyan, I., and Babanezhad, M. (2022). “Numerical investigation of water forced convection inside a copper metal foam tube: Genetic algorithm (GA) based fuzzy inference system (GAFIS) contribution with CFD modeling.” *Int. J. Heat Mass Transf.*, 182, 122016.

Nazari, M., Ashouri, M., Kayhani, M. H., and Tamayol, A. (2015). “Experimental study of convective heat transfer of a nanofluid through a pipe filled with metal foam.” *Int. J. Therm. Sci.*, 88, 33–39.

Neild, D. A., and Bejan, A. (2006). “Convection in Porous Media.” 3rd eds., Springer, Berlin, Germany.

Nimmagadda, R., Haustein, H. D., Godson Asirvatham, L., and Wongwises, S. (2019). “Effect of uniform/non-uniform magnetic field and jet impingement on the hydrodynamic and heat transfer performance of nanofluids.” *J. Magn. Magn. Mater.*, 479(June), 268–281.

Nimvari, M. E., and Jouybari, N. F. (2017). “Investigation of turbulence effects within

porous layer on the thermal performance of a partially filled pipe.” *Int. J. Therm. Sci.*, 118, 374–385.

Paul, A., and Ramamurty, U. (2000). “Strain rate sensitivity of a closed-cell aluminum foam.” *Mater. Sci. Eng. A*, 281(1–2), 1–7.

Pavel, B. I., and Mohamad, A. A. (2004). “An experimental and numerical study on heat transfer enhancement for gas heat exchangers fitted with porous media.” *Int. J. Heat Mass Transf.*, 47(23), 4939–4952.

Peng, C., Ming, T., and Tao, Y. (2015). “Thermal and hydraulic performances of a tube filled with various thermal conductivities of porous media.” *Int. J. Heat Mass Transf.*, 81, 784–796.

Pourfarzad, E., Behrangzade, A., Houshfar, E., and Ashjaee, M. (2021). “Thermal and Fluid-Flow Characteristics of Silver-Water Nanofluid in a Metal-Foam Filled Channel.” *Heat Transf. Eng.*, 42(21), 1827–1845.

Qu, Z. G., Xu, H. J., and Tao, W. Q. (2012). “Fully developed forced convective heat transfer in an annulus partially filled with metallic foams: An analytical solution.” *Int. J. Heat Mass Transf.*, 55(25–26), 7508–7519.

Rabbani, P., Hamzeshpour, A., Ashjaee, M., Najafi, M., and Houshfar, E. (2019). “Experimental investigation on heat transfer of MgO nanofluid in tubes partially filled with metal foam.” *Powder Technol.*, 354, 734–742.

Ranut, P., Nobile, E., and Mancini, L. (2014). “High resolution microtomography-based CFD simulation of flow and heat transfer in aluminum metal foams.” *Appl. Therm. Eng.*, 69(1–2), 230–240.

Rastogi, M., Chauhan, A., Vaish, R., and Kishan, A. (2015). “Selection and performance assessment of Phase Change Materials for heating , ventilation and air-conditioning applications.” *Energy Convers. Manag.*, 89, 260–269.

Sabatier, J., Lanusse, P., Feytout, B., and Gracia, S. (2016). “CRONE control based anti-icing/deicing system for wind turbine blades.” *Control Eng. Pract.*, 56, 200–209.

Saedodin, S., Zamzamian, S. A. H., Nimvari, M. E., Wongwises, S., and Jouybari, H.

- J. (2017). "Performance evaluation of a flat-plate solar collector filled with porous metal foam: Experimental and numerical analysis." *Energy Convers. Manag.*, 153(August), 278–287.
- Samudre, P., and Kailas, S. V. (2022). "Thermal performance enhancement in open-pore metal foam and foam-fin heat sinks for electronics cooling." *Appl. Therm. Eng.*, 205(July 2021), 117885.
- Sener, M., Yataganbaba, A., and Kurtbas I. (2016). "Forchheimer forced convection in a rectangular channel partially filled with aluminum foam." *Exp. Therm. Fluid Sci.*, 75, 162–172.
- Sheikhnejad, Y., Hosseini, R., and Saffar Avval, M. (2017). "Experimental study on heat transfer enhancement of laminar ferrofluid flow in horizontal tube partially filled porous media under fixed parallel magnet bars." *J. Magn. Magn. Mater.*, 424, 16–25.
- Shen, L., Xu, S., Bai, Z., Wang, Y., and Xie, J. (2021). "Experimental study on thermal and flow characteristics of metal foam heat pipe radiator." *Int. J. Therm. Sci.*, 159(April 2020), 106572.
- Shi, C., Wang, M., Yang, J., Liu, W., and Liu, Z. (2021). "Performance analysis and multi-objective optimization for tubes partially filled with gradient porous media." *Appl. Therm. Eng.*, 188(January), 116530.
- Shirvan, K. M., Mirzakhani, S., Kalogirou, S. A., Oztop, H. F., and Mamourian, M. (2017). "Heat transfer and sensitivity analysis in a double pipe heat exchanger filled with porous medium." *Int. J. Therm. Sci.*, 121, 124–137.
- Shokouhmand, H., Jam, F., and Salimpour, M. R. (2009). "Simulation of laminar flow and convective heat transfer in conduits filled with porous media using Lattice Boltzmann Method." *Int. Commun. Heat Mass Transf.*, 36(4), 378–384.
- Shokouhmand, H., Jam, F., and Salimpour, M. R. (2011). "The effect of porous insert position on the enhanced heat transfer in partially filled channels." *Int. Commun. Heat Mass Transf.*, 38(8), 1162–1167.
- Siavashi, M., Talesh Bahrami, H. R., and Aminian, E. (2018). "Optimization of heat

transfer enhancement and pumping power of a heat exchanger tube using nanofluid with gradient and multi-layered porous foams.” *Appl. Therm. Eng.*, 138(April), 465–474.

Solórzano, E., Reglero, J. A., Rodríguez-Pérez, M. A., Lehmkus, D., Wichmann, M., and Saja, J. A. de. (2008). “An experimental study on the thermal conductivity of aluminium foams by using the transient plane source method.” *Int. J. Heat Mass Transf.*, 51(25–26), 6259–6267.

Sunden, B. (2012). “Introduction to Heat Transfer.” WIT Press, Ashurst, UK.

Tharayil, T., Asirvatham, L. G., Ravindran, V., and Wongwises, S. (2016). “Thermal performance of miniature loop heat pipe with graphene-water nanofluid.” *Int. J. Heat Mass Transf.*, 93, 957–968.

Tharayil, T., Godson Asirvatham, L., Rajesh, S., and Wongwises, S. (2018). “Effect of Nanoparticle Coating on the Performance of a Miniature Loop Heat Pipe for Electronics Cooling Applications.” *J. Heat Transfer*, 140(2), 1–9.

Tian, H., Zhao, T., Shi, L., Chen, T., Ma, X., Zhang, H., and Shu, G. (2020). “Assessment and optimization of exhaust gas heat exchanger with porous baffles and porous fins.” *Appl. Therm. Eng.*, 178(May), 115446.

Tian, J., Kim, T., Lu, T., Hodson, H., Queheillalt, D., Sybeck, D., and Wadley, H. (2004). “The effects of topology upon fluid flow and heat transfer within cellular copper structures.” *Int. J. Heat Mass Transf.*, 47(14–16), 3171–3186.

Tio, K., Liu, C. Y., and Toh, K. C. (2000). “Thermal analysis of micro heat pipes using a porous-medium model.” *Heat Mass Transf.*, 36, 21–28.

Tomy, A. M., Ahammed, N., Subathra, M. S. P., and Asirvatham, L. G. (2016). “Analysing the Performance of a Flat Plate Solar Collector with Silver/Water Nanofluid Using Artificial Neural Network.” *Procedia Comput. Sci.*, 93(September), 33–40.

Torabi, M., Dickson, C., and Karimi, N. (2016). “Theoretical investigation of entropy generation and heat transfer by forced convection of copper-water nanofluid in a porous channel - Local thermal non-equilibrium and partial filling effects.” *Powder Technol.*,

301, 234–254.

Tsolas, N., and Chandra, S. (2012). “Forced Convection Heat Transfer in Spray Formed Copper and Nickel Foam Heat Exchanger Tubes.” *J. Heat Transfer*, 134(6), 062602.

Vafai, K. (2005). “Handbook of Porous Media.” Edition, S. CRC Press, Taylor and Francis.

Walters, D. K. (2019). “A Three-Equation Eddy-Viscosity Model for Reynolds-Averaged Navier – Stokes Simulations of.” *J. Fluids Eng.* 130(12), 1–14.

Wang, H., and Guo, L. (2019). “Volumetric Convective Heat Transfer Coefficient Model for Metal Foams.” *Heat Transf. Eng.*, 40(5–6), 464–475.

Wakao, N., Kaguei, S., and Funazkri, T. (1979). “Effects of Fluid Dispersion Coefficients on Particle-to-Fluid Heat Transfer Coefficients in packed beds.” *Chem. Eng. Sci.*, 34, 325–336.

Wang, Y., Tian, H., Shu, G., Yu, G., Ma, X., and Li, X. (2017). “Simulation and Optimization of Metal-foam Tube Banks for Heat Transfer Enhancement of Exhaust Heat Exchangers.” *Energy Procedia*, 142, 3863–3869.

Xu, H. J., Gong, L., Zhao, C. Y., Yang, Y. H., and Xu, Z. G. (2015). “Analytical considerations of local thermal non-equilibrium conditions for thermal transport in metal foams.” *Int. J. Therm. Sci.*, 95, 73–87.

Xu, H. J., Qu, Z. G., Lu, T. J., He, Y. L., and Tao, W. Q. (2011a). “Thermal modeling of forced convection in a parallel-plate channel partially filled with metallic foams.” *J. Heat Transfer*, 133(9), 20–22.

Xu, H. J., Qu, Z. G., and Tao, W. Q. (2011b). “Analytical solution of forced convective heat transfer in tubes partially filled with metallic foam using the two-equation model.” *Int. J. Heat Mass Transf.*, 54(17–18), 3846–3855.

Xu, H. J., Qu, Z. G., and Tao, W. Q. (2011c). “Thermal transport analysis in parallel-plate channel filled with open-celled metallic foams.” *Int. Commun. Heat Mass Transf.*, 38(7), 868–873.

Xu, Z. G., and Gong, Q. (2018). “Numerical investigation on forced convection of tubes

partially filled with composite metal foams under local thermal non-equilibrium condition.” *Int. J. Therm. Sci.*, 133(June), 1–12.

Xu, Z. G., Qin, J., Zhou, X., and Xu, H. J. (2018). “Forced convective heat transfer of tubes sintered with partially-filled gradient metal foams (GMFs) considering local thermal non-equilibrium effect.” *Appl. Therm. Eng.*, 137(March), 101–111.

Yang, C., Kuwahara, F., Liu, W., and Nakayama, A. (2015). “Thermal Non-Equilibrium Forced Convective Flow in an Annulus Filled with a Porous Medium.” *The Open Transp. Phenomenon J.* 3(1), 31–39.

Yang, C., Ando K., and Nakayama A. (2011). “A Local Thermal Non-Equilibrium Analysis of Fully Developed Forced Convective Flow in a Tube Filled with a Porous Medium.” *Transp. Porous Media*, 89, 237–249.

Yang, K., Li, X., Liu, K., and Wang, J. (2022a). “Coupling effect of heat transfer in plate heat exchanger filled with porous media.” *Int. J. Heat Mass Transf.*, 182, 121966.

Yang, W., Zhu, W. C., Li, Y., Zhang, L., Zhao, B., Xie, C., Yan, Y., and Huang, L. (2022b). “Annular thermoelectric generator performance optimization analysis based on concentric annular heat exchanger.” *Energy*, 239, 122127.

Yang, Y. T., and Hwang, M. L. (2009). “Numerical simulation of turbulent fluid flow and heat transfer characteristics in heat exchangers fitted with porous media.” *Int. J. Heat Mass Transf.*, 52(13–14), 2956–2965.

Zhao, C. Y. (2012). “Review on thermal transport in high porosity cellular metal foams with open cells.” *Int. J. Heat Mass Transf.*, 55(13–14), 3618–3632.

Zhao, C. Y., Kim, T., Lu, T. J., and Hodson, H. P. (2001). “Thermal Transport Phenomena in Porvair Metal Foams and Sintered Beds Department of Engineering University of Cambridge.” *Engineering*, (August).

Zhao, C. Y., Lu, W., and Tassou, S. A. (2006). “Thermal analysis on metal-foam filled heat exchangers. Part II: Tube heat exchangers.” *Int. J. Heat Mass Transf.*, 49(15–16), 2762–2770.

Zhao, N., Li, S., and Yang, J. (2016). “A review on nanofluids: Data-driven modeling

of thermalphysical properties and the application in automotive radiator.” *Renew. Sustain. Energy Rev.*, 66, 596–616.

Zheng, Z. J., Li, M. J., and He, Y. L. (2015a). “Optimization of porous insert configurations for heat transfer enhancement in tubes based on genetic algorithm and CFD.” *Int. J. Heat Mass Transf.*, 87, 376–379.

Zheng, Z. J., Li, M. J., and He, Y. L. (2015b). “Optimization of Porous Insert Configuration in a Central Receiver Tube for Heat Transfer Enhancement.” *Energy Procedia*, 75, 502–507.

Zukauskas, A. A. (1987). “Convective heat transfer in cross-flow.” in: S. Kakac, R. K. Shah, W. Aung (Eds.), *Handbook of Single-Phase Convective Heat Transfer*, Wiley, New York.

LIST OF PUBLICATIONS

LIST OF INTERNATIONAL JOURNALS

1. **Prakash H. Jadhav**, N Gnanasekaran and D Arumuga Perumal (2021). “Numerical consideration of LTNE and Darcy Extended Forchheimer Models for the analysis of forced convection in a horizontal pipe in the presence of metal foam”, ASME Journal of Heat Transfer, Vol. 143, Issue 1, pp. 012702 (1-16), [SCIE Indexed].
DOI: <https://doi.org/10.1115/1.4048622>
2. **Prakash H. Jadhav**, N. Gnanasekaran, D. Arumuga Perumal and Moghtada Mobedi (2021). “Performance evaluation of partially filled high porosity metal foam configurations in a pipe”, Applied Thermal Engineering, Vol. 194, pp. 117081, [SCIE Indexed].
DOI: <https://doi.org/10.1016/j.applthermaleng.2021.117081>
3. **Prakash H. Jadhav**, G. Trilok, N. Gnanasekaran and Moghtada Mobedi (2022). “Performance score based multi-objective optimization for thermal design of partially filled high porosity metal foam pipes under forced convection”, International Journal of Heat and Mass Transfer, Vol. 186, pp. 121911, [SCIE Indexed].
DOI: <https://doi.org/10.1016/j.ijheatmasstransfer.2021.121911>
4. **Prakash H. Jadhav**, N Gnanasekaran and D Arumuga Perumal (2021). “Conjugate heat transfer study comprising the effect of thermal conductivity and irreversibility in a pipe filled with metallic foams”, Heat and Mass Transfer, Vol. 57; Issue 6: pp. 911-930, [SCI Indexed].
DOI: <https://doi.org/10.1007/s00231-020-03000-x>
5. **Prakash H. Jadhav** and N Gnanasekaran (2021). “Optimum design of heat exchanging device for efficient heat absorption using high porosity metal foams”, International Communication in Heat and Mass Transfer, Vol. 126, pp. 105475, [SCI Indexed].
DOI: <https://doi.org/10.1016/j.icheatmasstransfer.2021.105475>

6. **Prakash H. Jadhav**, N Gnanasekaran and D Arumuga Perumal (2022). Thermodynamic analysis of entropy generation in a horizontal pipe filled with high porosity metal foams, *Materials Today: Proceedings*, Vol. 51, pp. 1598-1603, [Scopus Indexed].
DOI: <https://doi.org/10.1016/j.matpr.2021.10.451>
7. Athith B, G. Trilok, **Prakash H. Jadhav** and N. Gnanasekaran (2022). “Heat transfer optimization using genetic algorithm and artificial neural network in a heat exchanger with partially filled different high porosity metal foam”, *Materials Today: Proceedings*, Vol. 51, pp. 1642-1648, [Scopus Indexed].
DOI: <https://doi.org/10.1016/j.matpr.2021.11.248>
8. **Prakash H. Jadhav**, N. Gnanasekaran, Moghatada Mobedi, “Analysis of functionally graded metal foams for the accomplishment of heat transfer enhancement under partially filled condition in a heat exchanger”, *Energy*, Vol. 263, Part A, pp. 125691, [SCI Indexed].
DOI: <https://doi.org/10.1016/j.energy.2022.125691>

BOOK CHAPTER

1. **Prakash H. Jadhav**, Banjara Kotresha, N Gnanasekaran and D Arumuga Perumal (2021). “Forced Convection Analysis in a Horizontal Pipe in the Presence of Aluminium Metal Foam—A Numerical Study”, *Fluid Mechanics and Fluid Power (FMFP), Lecture Notes in Mechanical Engineering*, pp. 491-498, Springer Singapore.
DOI: https://doi.org/10.1007/978-981-16-0698-4_53.
2. Banjara Kotresha, **Prakash H. Jadhav** and N Gnanasekaran (2021). “Natural Convection Through High Porosity Metal Foams—A Numerical Study”, *Fluid Mechanics and Fluid Power (FMFP), Lecture Notes in Mechanical Engineering*, pp. 727-735, Springer Singapore.
DOI: https://doi.org/10.1007/978-981-16-0698-4_80

CONFERENCES PROCEEDINGS

1. **Prakash H. Jadhav**, N Gnanasekaran and D Arumuga Perumal (2019). “Forced Convection Analysis in a Horizontal Pipe in the Presence of Aluminium Metal Foam—A Numerical Study”, 46TH National conference on “Fluid Mechanics and Fluid Power” (FMFP - 2019) Dec 09-11, 2019 at PSG College of Technology Coimbatore, India.
2. **Prakash H. Jadhav**, N Gnanasekaran and D Arumuga Perumal (2020). “Entropy generation analysis in a horizontal pipe filled with high porosity metal foam”, Proceedings of the International conference on Numerical Heat Transfer and Fluid Flow (NHTFF-2020) NIT Warangal, India – Jan 17-19, 2020.
3. **Prakash H. Jadhav**, N Gnanasekaran and D Arumuga Perumal (2021). “Thermodynamic analysis of entropy generation in a horizontal pipe filled with high porosity metal foams”, 2nd International Conference on Sustainable Energy Solutions for a Better Tomorrow (SESBT 2021), July 23-24, 2021, VIT Chennai, India.
4. Athith B, G. Trilok, **Prakash H. Jadhav** and N Gnanasekaran (2021). “Heat transfer optimization using genetic algorithm and artificial neural network in a heat exchanger with partially filled different high porosity metal foam”, 2nd International Conference on Sustainable Energy Solutions for a Better Tomorrow (SESBT 2021), July 23-24, 2021, VIT Chennai, India.

BIODATA

PRAKASH HEERASING JADHAV

Mobile: +918073237043; +917774873889

Email Id: jdvprakash@gmail.com

prakashheerasingjadhav.187me011@nitk.edu.in



EDUCATION

- 2008 – 2010 M. Tech, Thermal Engineering, NITK Surthkal, Karnataka, India.
- 2002 – 2006 B.E, Mechanical Engineering, Poojya Doddappa Appa College of Engineering (PDACE), Gulbarga, Karnataka, India.

WORK EXPERIENCE

- Worked as Asst. Professor in Late Narayan Das Bhavan Das Chabada Engineering Institute of Technology (LNBCIET), Satara, Maharashtra, from 19 Jan. 2011 to 06 May 2011.
- Worked as Asst. Professor in Walchand Institute of Technology (WIT), Solapur, Maharashtra, from 1st July 2011 to 20 June 2014.
- Worked as Asst. Professor in KJ's Educational Institute, Trinity Academy of Engineering (KJ's TAE), Pisoli Pune, Maharashtra, 27 June 2104 to 31 June 2018.

ACHIEVEMENTS

- Qualified Gate Exams during the Year of 2007, 2008 and 2017.

COMPUTER SKILLS

Meshing Software: Gambit 2.4.2, ANSYS Meshing.

CFD Analysis Software: ANSYS Fluent.

Coding Software: MATLAB

Graph Tools: Origin Software 9.0, Techplot and Excel.

Office Tools: Microsoft office.

PROFESSIONAL TRAINING

- Two-week ISTE workshop on “**Engineering Thermodynamics**” conducted by Indian Institute of Technology Bombay from 11th to 21st December, 2012 under National Mission on Education through ICT (MHRD).
- Two-week ISTE workshop on “**Engineering Mechanics**” conducted by Indian Institute of Technology Bombay from 6th to 16th December, 2013 under National Mission on Education through ICT (MHRD).
- Two-week ISTE workshop on “**Fluid Mechanics**” conducted by Indian Institute of Technology Kharagpur from 20th to 30th May, 2014 under National Mission on Education through ICT (MHRD).
- Two –Week Industrial Training at “**Laxmi Oil Pumps and Systems Pvt. Ltd.**” Solapur-413003.
- TEQIP – III Sponsored Five Day National Workshop on “**Frontiers in Design, Manufacturing and Energy Sustainability**”, organized by Department of Mechanical Engineering, National Institute of Technology, Karnataka (NITK) Surathkal, conducted from 3 – 7, 2018.
- TEQIP – III Three Day National Workshop on “**Intelligent Optimization Techniques for Engineering Problems**”, organized by Department of Mechanical Engineering, National Institute of Technology, Karnataka (NITK) Surathkal, conducted from 19 – 21, 2019.
- One-Week Student Development Program in “**Engineering Analysis for Thermo-Fluids Research Challenges using ANSYS**” conducted at VTU Department of Mechanical Engineering Kalburgi from 27-07-2020 – 31-07-2020.
- Five days SERB online International workshop on “**Recent Advancements in Modelling Analysis of Porous material (RAMAPM 2022)**”, organized by Department of Mechanical Engineering, National Institute of Technology, Karnataka Surathkal, conducted from 28-02-2022 to 04-03-2022.

RESEARCH INTEREST

Computational Fluid Dynamics (CFD), Fluid Flow and Heat Transfer in Porous Media, Fluid flow (Incompressible, Laminar and Turbulent Flows), Heat and Mass Transfer Systems, Bio-Diesel, IC Engines.

POST GRADUATION RESEARCH WORK

Performance and Emission Analysis of a C.I. Engine Fuelled with WCO Biodiesel with EGR Technique and DEE as Additive.

Organization: NITK Surathkal, Karnataka, India

PERSONAL DETAILS

Date of Birth	4 th June 1982
Marital Status	Married
Languages Known	Kannada, English and Hindi
Nationality	Indian

I certify that the forgoing information is correct and complete to the best of my knowledge and belief and nothing has been concealed / distorted

PRAKASH HEERASING JADHAV
NITK, SURATHKAL